The Astrophysical Journal, 776:71 (38pp), 2013 October 20 doi:10.1088/0004-637X/776/2/71

THE ZURICH ENVIRONMENTAL STUDY OF GALAXIES IN GROUPS ALONG THE COSMIC WEB. I. WHICH ENVIRONMENT AFFECTS GALAXY EVOLUTION?*

C. Marcella Carollo[1], Anna Cibinel[1], Simon J. Lilly[1], Francesco Miniati[1], Peder Norberg[2], John D. Silverman[3], Jacqueline van Gorkom[4], Ewan Cameron[1], Alexis Finoguenov[5], Yingjie Peng[1], Antonio Pipino[1], and Craig S. Rudick[1]
[1] Institute for Astronomy, ETH Zurich, CH-8093 Zurich, Switzerland; marcella@phys.ethz.ch
[2] Department of Physics, Institute for Computational Cosmology, Durham University, South Road, Durham DH1 3LE, UK
[3] Kavli Institute for the Physics and Mathematics of the Universe (WPI), Todai Institutes for Advanced Study, The University of Tokyo, Chiba 277-8583, Japan
[4] Department of Astronomy, Columbia University, New York, NY 10027, USA
[5] Max-Planck-Institut für extraterrestrische Physik, D-84571 Garching, Germany
Received 2012 June 14; accepted 2013 July 18; published 2013 September 27

ABSTRACT

The Zurich Environmental Study (ZENS) is based on a sample of ∼1500 galaxy members of 141 groups in the mass range $\sim 10^{12.5-14.5}\,M_{\odot}$ within the narrow redshift range $0.05 < z < 0.0585$. ZENS adopts novel approaches, described here, to quantify four different galactic environments, namely: (1) the mass of the host group halo; (2) the projected halo-centric distance; (3) the rank of galaxies as central or satellites within their group halos; and (4) the filamentary large-scale structure density. No self-consistent identification of a central galaxy is found in ∼40% of $<10^{13.5}\,M_{\odot}$ groups, from which we estimate that ∼15% of groups at these masses are dynamically unrelaxed systems. Central galaxies in relaxed and unrelaxed groups generally have similar properties, suggesting that centrals are regulated by their mass and not by their environment. Centrals in relaxed groups have, however, ∼30% larger sizes than in unrelaxed groups, possibly due to accretion of small satellites in virialized group halos. At $M > 10^{10}\,M_{\odot}$, satellite galaxies in relaxed and unrelaxed groups have similar size, color, and (specific) star formation rate distributions; at lower galaxy masses, satellites are marginally redder in relaxed relative to unrelaxed groups, suggesting quenching of star formation in low-mass satellites by physical processes active in relaxed halos. Overall, relaxed and unrelaxed groups show similar stellar mass populations, likely indicating similar stellar mass conversion efficiencies. In the enclosed ZENS catalog, we publish all environmental diagnostics as well as the galaxy structural and photometric measurements described in companion ZENS papers II and III.

Key words: galaxies: evolution – galaxies: formation – galaxies: groups: general – galaxies: star formation – galaxies: stellar content – galaxies: structure

Online-only material: machine-readable table

1. INTRODUCTION

The study of environmental effects on the evolution of galaxies is beset by a number of difficulties that have made it hard to define a single coherent picture and to isolate the main physical processes. It has been clear for many years that both the mass and the environment of a galaxy affect its evolution and its appearance today. Since the pioneering work of, e.g., Oemler (1974), Dressler (1980), and Postman & Geller (1984), many studies have highlighted clear trends between different observational diagnostics of evolution such as stellar absorption line strengths, color or morphology, and either galactic mass or environment or both (e.g., Carollo et al. 1993; Balogh et al. 1999; Goto et al. 2003; Blanton et al. 2005; Zehavi et al. 2002; Weinmann et al. 2006b, 2009; Croton et al. 2005; Park et al. 2007; Kovač et al. 2010b; Peng et al. 2010, 2012; Cooper et al. 2010; Wetzel et al. 2012; Calvi et al. 2012; Woo et al. 2013), but the detailed phenomenology, as well as a physical understanding, remains unclear. This fact can be traced to several complicating factors and difficulties.

First, there are a number of galactic properties that are relevant to defining a galaxy's evolutionary state. Galaxy evolution may be traced by changes in the star-formation rates (SFRs) of galaxies (e.g., Lilly et al. 1996; Madau et al. 1996; Chary & Elbaz 2001; Rodighiero et al. 2010; Wetzel et al. 2012; Woo et al. 2013), leading to differences in the integrated stellar populations and therefore the spectral properties and colors of galaxies (e.g., Carollo & Danziger 1994; Carollo et al. 1997; Masters et al. 2010; Bundy et al. 2010; perhaps modified by the effects of dust; e.g., Labbé et al. 2005; Williams et al. 2009; Wolf et al. 2009). Galaxy evolution may also be manifested by changes in the morphologies of galaxies, both in terms of the overall structural morphology of bulge-to-disk ratios and the structural properties of each component (Carollo et al. 1998, 2007; Carollo 1999; Brinchmann & Ellis 2000; Kovač et al. 2010b; Oesch et al. 2010; Feldmann et al. 2011; Skibba et al. 2012; Calvi et al. 2012; Cooper et al. 2012; Raichoor et al. 2012, among others) and also in the appearance of features such as spiral arms or bars. Color and morphology clearly broadly correlate within the nearby galaxy population, but with a significant and poorly understood scatter (Strateva et al. 2001). Morphology and color may reflect different aspects of a single evolutionary sequence, or may reflect the outcome of quite different physical processes that may conceivably occur either synchronously or asynchronously. Many previous studies have focused on just one parameter of this color–morphology duality. A comprehensive picture is likely to require the simultaneous treatment of all such physically relevant properties.

Second, in regards to mass and environment, it is not clear exactly *which* mass or environment is likely to be the most relevant for centrals, i.e., galaxies that appear to dominate their halos, and satellites, i.e., galaxies that orbit another more massive galaxy within a single dark matter halo (e.g., Cooper

* Based on observations collected at the European Southern Observatory, La Silla Chile. Program ID 177.A-0680.

et al. 2005; De Lucia et al. 2012; Haas et al. 2012; Muldrew et al. 2012). Observationally, the existing stellar mass of a galaxy is the most easily accessible, but the physical driver of the evolution could be the mass of the dark matter halo of a galaxy or, in the case of satellite galaxies, the mass of the dark matter halo in which the galaxy resides, leading to an environment-like measure of mass. Similarly, the environment that could influence the evolution of a galaxy could reflect either very local effects, e.g., the location of a galaxy in a dark matter halo or the interaction with nearby neighbors through the mass of the dark matter halo (as above) or the broader environment beyond the halo, as defined by the cosmic web of filaments and voids. Clearly some of the definitions of environment are closely linked to the mass of a galaxy, especially for galaxies that dominate their dark matter halos. Even for galaxy stellar mass, we could imagine some direct crosstalk between this property and environment if the stellar mass function of galaxies was itself dependent on environment (Bundy et al. 2006; Baldry et al. 2006; Bolzonella et al. 2010; Kovač et al. 2010b), necessitating the careful isolation of these two variables.

A recent analysis in the Sloan Digital Sky Survey (SDSS; York et al. 2000) of the three-way relationships between color, stellar mass, and environment, where the last term is defined simply in terms of a fifth-nearest galaxy-neighbor density, reveals some interesting simplicities within the galaxy population (Peng et al. 2010). Not least, the effects of environment and stellar mass on the fraction of galaxies that are observed to be red (the red fraction) are straightforwardly separable in the sense that the chance that a given galaxy is red is the product of two functions, a mass function independent of environment and an environment function independent of mass. This result led Peng et al. to identify two separate physical processes, termed mass-quenching and environment-quenching. A conclusion of this analysis was that the effects of the environment dominate for galaxy stellar masses below $\sim 10^{10}\ M_{\odot}$, while above $\sim 10^{11}\ M_{\odot}$, the galaxy population is dominated by the effects of merging, which again are environmentally determined. The differential effects of galactic stellar mass and environment can be most clearly seen in the $\sim 10^{10-11}\ M_{\odot}$ galaxy population. Peng et al. (2012) extended their original formalism to the central-satellite dichotomy of galaxies using a large group catalog (Yang et al. 2005, 2007). Although the characteristics of mass- and environment-quenching were identified, their physical origin remains uncertain.

Also, it unclear remains whether morphological transformations are causally connected with, and whether they anticipate or lag behind, the spectrophotometric transformations that shift blue, star-forming galaxies onto the red sequence of bulge-dominated systems (e.g., Arnouts et al. 2007; Faber et al. 2007; Pozzetti et al. 2010; Feldmann et al. 2010, 2011). Many processes can lead to the disruption of disks and the quenching of star formation, e.g., galaxy mergers or tidal interactions (e.g., Park et al. 2007 and references therein), ram pressure stripping of cold gas (Gunn & Gott 1972; Feldmann et al. 2011, but see also Rasmussen et al. 2008), or strangulation of the galactic system by removal of hot and warm gas necessary to fuel star formation (Larson 1980; Balogh & Morris 2000; Font et al. 2008; Rasmussen et al. 2012). In a hierarchical picture, a gaseous disk can be re-accreted around pre-made spheroids at relatively late epochs. This evolutionary path is observed to happen in high-resolution cosmological hydrodynamical simulations (Springel & Hernquist 2005; Feldmann et al. 2010).

The intermediate-mass scales of galaxy groups, which are the most common environments of $\sim L^*$ galaxies in the local universe (Eke et al. 2004a), have a reputation for being the place where environmental drivers of galaxy evolution should be at their peak efficiency. With an in-spiral timescale of dynamical friction that varies in proportion to σ^3/ρ, where σ and ρ are the dark matter halo velocity dispersion and density, respectively, galaxy tidal interactions and mergers should take place on a cosmologically short timescale in group potentials with relatively low velocity dispersions, unlike the most massive galaxy clusters where the velocity dispersions are much higher. Also, with ram pressure efficiency varying as $\rho_{\rm igm} v^2$, where $\rho_{\rm igm}$ and v are the density of the intergalactic/intragroup medium (IGM) and relative velocity of the galaxy toward the IGM, respectively, galaxies may well begin to lose their gas already at the intermediate environmental densities typical of galaxy groups (Rasmussen et al. 2006; Rasmussen et al. 2008). The resulting internal dynamical instabilities may also contribute to galaxy evolution, e.g., by fuelling star formation and supermassive black holes in the centers of galaxies (see, e.g., Di Matteo et al. 2007; Hopkins et al. 2008 for a theoretical perspective; and Genzel et al. 1998; Kewley et al. 2006; Smith et al. 2007; Silverman et al. 2011 for observational evidence) and establishing feedback loops that affect entire galaxies (Croton et al. 2006).

These considerations motivate the present study, termed the Zurich Environmental Study (ZENS), where we use a statistically complete sample of 1627 galaxies brighter than $b_J = 19.45$, known to be members of 141 nearby groups spanning a mass range between $\sim 10^{12.5}\ M_{\odot}$ and $\sim 10^{14.5}\ M_{\odot}$. The ZENS sample is complete at stellar masses above $10^{10}\ M_{\odot}$ for passively evolving galaxies with old stellar populations and above $10^{9.2}\ M_{\odot}$ for star-forming galaxies. In ZENS, we aim at simultaneously (1) characterizing the present evolutionary state of galaxies in as broad a way as possible, using both diagnostics based on stellar populations and structural morphology and (2) studying as broad a range of environments as possible and characterizing the environments in a number of ways that sample different physical scales, where we include a careful distinction between central and satellite galaxies. Specifically, in our study, we directly compare, at fixed galaxy stellar mass, the dependence of key galactic populations diagnostics on the large-scale environmental (over)density ($\delta_{\rm LSS}$), the mass of the host group halo ($M_{\rm GROUP}$), and the location of galaxies within their group halos (expressed in terms of projected distance from the halo center, R/R_{200}, with R_{200} being the characteristic size of the group), while maintaining a central-satellite distinction when possible and relevant.

The ZENS sample is extracted from the two-degree Field Galaxy Redshift Survey (2dFGRS; Colless et al. 2001), which contains nearly 225,000 redshifts for galaxies with $14 < b_J < 19.45$ at a median redshift $z \sim 0.11$, with a redshift completeness of $85\% \pm 5\%$. In combination with a dynamic range of 5 mag at each redshift, the 2dFGRS is the ideal basis for constructing a homogeneous catalog of nearby galaxies in a wide range of environments. We have followed up the ZENS sample with B and I deep Wide Field Imaging (WFI) at the ESO/2.2 m to derive, for all galaxies in the sample, detailed properties of substructure such as bulges, disks, bars, and tidal tails. The wealth of data on the ZENS groups enables us to define very carefully the nature of groups, including their likely dynamical states (relaxed or unrelaxed). We can also do a careful group-by-group identification of the most likely dominant member and derive accurate photometric and structural

measurements for galactic subcomponents (disks, bulges, and bars); all analyses unaffected by distance, size, magnitude, mass, type, and other biases, which often complicate the interpretation of comparisons of independent studies published in the literature.

In this first paper in the ZENS series:

(1) We describe the ZENS design and database (Section 2);

(2) We present our definitions and calculations of the four environmental parameters $\delta_{\rm LSS}$, $M_{\rm GROUP}$, and R/R_{200}, plus the central-satellite distinction (Section 3). Specifically, in this section, we detail the approaches that we adopt to identify central and satellite galaxies and thus the centers of the groups. We also measure a large-scale structure (LSS) (over)density proxy, which, at relatively low group masses, provides a measurement that is independent of the richness and mass of the host group halos. This independence is in contrast with the often-used *N*th-neighbor-galaxies estimators. We furthermore quantify how random and systematic errors in the computation of each environmental parameters affect the trends of galaxy properties with such environments;

(3) We publish the ZENS catalog (Section 4), which lists, for every galaxy in the sample, the environmental parameters derived in this paper, as well as structural (from Cibinel et al. 2013a, hereafter Paper II) and spectrophotometric measurements (from Cibinel et al. 2013b, hereafter Paper III). The structural measurements are corrected for magnitude-, size-, concentration-, ellipticity-, and point spread function (PSF)-dependent biases;

(4) We discuss our classification of groups in dynamically "relaxed" and "unrelaxed" systems (Section 5) and briefly investigate whether their galaxy members, both central and satellites, differ in fundamental structural (size), star formation (specific star formation rate, sSFR), SFR surface density ($\Sigma_{\rm SFR}$), and optical ($B-I$) properties (see also Appendix D). Finally,

(5) we summarize our main points in Section 6.

In Appendices A, B, C, and E we present details of (1) the impact on our study of the 2dFGRS magnitude limits in the ZENS fields, (2) the impact of "missed" galaxies, either by the 2dFGRS, or by the new B and I ESO 2.2 m/WFI imaging for the ZENS sample, (3) 2dFGRS Percolation-Inferred Galaxy Group (2PIGG) incompleteness in group membership, (4) additional tests on the robustness of our fiducial LSS density estimates and the comparison with traditional *N*th-neighbor-galaxies estimators and, finally, (5) the *Readme* file of the published ZENS catalog.

For the relevant cosmological parameters, we assume the following values: $\Omega_m = 0.3$, $\Omega_\Lambda = 0.7$, and $h = 0.7$. Unless otherwise stated, group masses and luminosities are given in units of $M_\odot$ and $L_\odot$, i.e., we incorporate the value $h = 0.7$ in the presentation of our results. All magnitudes are in the AB system. These choices are also adopted in Cibinel et al. (2013a, 2013b); these papers present the structural and photometric measurements, respectively, included in the catalog associated with this paper.

2. THE ZURICH ENVIRONMENTAL STUDY (ZENS)

2.1. Design and Sample Specifications

The entire ZENS sample of 141 galaxy groups was selected from the 2PIGG catalog (Eke et al. 2004a), which is based on a friends-of-friends (FOF; Huchra & Geller 1982) percolation algorithm thoroughly tested on realistic mock galaxy catalogs generated from cosmological *N*-body simulations. We refer the reader to Eke et al. (2004a) for the details of the group-finding algorithm and the procedures adopted for the identification of the groups. The 2PIGG catalog covers 1500 deg^2 of the 2dFGRS and provides one of the largest homogeneous samples of galaxy groups currently available, with around 7000 groups with $\geqslant$4 cataloged members. The members span a wide range in both luminosity, from $\sim 10^{10}\,L_\odot$ up to $\sim 10^{12}\,L_\odot$, and dynamical mass, from a few $10^{12}\,M_\odot$ up to clusters of mass $10^{15}\,M_\odot$ (Eke et al. 2004b). The catalog is selected from a volume of $\sim$250,000 (Mpc h^{-1})^3 and it is so large that one not only has information on the groups themselves from the 2dFGRS data (e.g., velocity dispersions, spatial positions of members, mass, density, compactness, etc.), but also on the proximity of groups to large clusters, filaments, and voids of the LSS web. The 2PIGG catalog is representative of the universe as a whole and contains a large number of groups that are close enough to allow detailed studies of the galaxy members. This catalog is thus ideal for undertaking the study of nearby galaxy properties as a function of the environment and, in particular, for directly comparing how galaxy properties and key galaxy population diagnostics depend on group mass, the location of galaxies within their host groups, and the location of the host groups relative to the large-scale filamentary structure (i.e., on the local density of the cosmic web). The 2dFGRS fields are located well above the Milky Way disk, minimizing the effect of extinction from Galactic dust (typically 0.1 mag in the B-band).

The ZENS groups were randomly extracted from the complete sample of 185 2PIGG groups (excluding a few groups falling in very incomplete fields of the survey) falling in the narrow redshift bin $0.05 < z < 0.0585$ and having at least five spectroscopically confirmed galaxy members in the 2dFGRS. Note that, by construction, ZENS excludes both field galaxies or groups with fewer than five galaxy members. The motivation for this selection was to increase the probability that the associated members are truly linked within a common halo. Within these selection boundaries, the ZENS sample provides a statistically complete and representative census of the nearby galaxy population inhabiting the group environment.

The very narrow redshift range of the ZENS sample was chosen to optimize several issues: (1) the 2dFGRS magnitude limits translate at this redshift to luminosities between $[M^* - 2]$ to $[M^* + 3]$ (Norberg et al. 2002), meaning that the existing redshift catalog already samples all of the luminosity function of massive galaxies and does a good job straddling the break or bimodality in galaxy properties around M^* (Kauffmann et al. 2003). (2) This redshift range is located just below the peak in $N(z)$ in 2PIGG, and thus ideally samples the targeted range of group mass $\sim 10^{12.5-14.5}\,M_\odot$. (3) Likewise, the groups fully cover the entire range of LSS environments, with some groups residing in very dense regions and others residing in much lower density environments, allowing us to study the effects of the LSS on group and galaxy evolution. (4) At this redshift, the group selection is robust and less affected by the peculiar velocities of the galaxies than is the case at lower redshifts. (5) Finally, deep, ground-based imaging with typical seeing $\sim 1''$ is well suited for the determination of morphologies, substructure units such as bars, bulges, and disks, and the presence and properties of faint structures. This imaging is also directly relatable to *Hubble Space Telescope* (*HST*) $\ll 1''$ resolution images of the $z > 0.5$ universe (with a relative angular diameter distance of a factor $\sim$8) and therefore provides an ideal benchmark for a

Table 1
Coordinates, Properties, and LSS Environment of the ZENS Groups

Name	R.A. (B1950)	Decl. (B1950)	z	$r_{\rm rms}$ (Mpc)	$\hat{R}_{200}$ (Mpc)	σ (km s^{-1})	$L_{\rm GROUP}$ ($10^{10} L_{\odot}$)	N_m	$M_{\rm GROUP}$ ($10^{12} M_{\odot}$)	$\log(1+\delta_{\rm LSS})$	Env.
[2] 2PIGG-s1248	23:41:34.53	−26:44:18.8	0.05188	0.362	0.340	600.7	4.990	8	4.683	0.78	4
[2] 2PIGG-s1272	23:37:55.83	−30:07:02.9	0.05079	0.784	0.465	247.6	8.602	9	11.98	0.03	2
[2] 2PIGG-s1282	23:43:44.24	−27:40:01.7	0.05038	0.446	0.356	148.8	5.414	8	5.363	0.65	4
[2] 2PIGG-s1308	23:59:16.70	−35:45:24.3	0.05143	0.338	0.328	287.4	4.678	5	4.211	0.34	3
[2] 2PIGG-s1313	23:43:59.64	−28:17:42.9	0.05020	0.454	0.445	57.2	7.976	6	10.49	0.40	3
[5] 2PIGG-s1325	22:28:47.25	−27:04:44.6	0.05066	0.222	0.363	42.0	5.624	5	5.719	−0.00	2
[5] 2PIGG-s1334	23:31:22.74	−30:08:48.2	0.05157	0.785	0.840	301.9	26.53	23	70.70	0.92	4
[2] 2PIGG-s1349	23:53:45.32	−25:48:25.1	0.05122	0.272	0.236	132.0	2.378	6	1.564	−0.38	1
[2] 2PIGG-s1390	22:11:20.62	−26:12:44.0	0.05192	0.481	0.449	261.7	8.102	5	10.78	0.73	4
[2] 2PIGG-s1418	02:29:19.43	−25:23:58.9	0.05275	0.349	0.271	264.8	3.218	5	2.374	0.00	2
[5] 2PIGG-s1454	01:16:41.52	−31:21:13.0	0.05270	0.373	0.288	161.5	3.653	5	2.861	0.15	2
[5] 2PIGG-s1459	22:39:44.52	−25:22:48.2	0.05294	0.380	0.283	58.3	3.529	5	2.717	0.57	3
[5] 2PIGG-s1471	23:42:25.65	−26:54:06.7	0.05276	0.721	0.689	255.4	17.49	15	39.06	0.97	4
[2] 2PIGG-s1476	00:38:10.18	−28:16:13.4	0.05366	0.395	0.325	172.1	4.610	5	4.116	0.29	3
[5] 2PIGG-s1481	23:18:56.30	−30:30:23.4	0.05360	0.243	0.410	24.9	6.969	7	8.280	−0.26	1
[2] 2PIGG-s1520	23:59:28.18	−35:09:38.0	0.05434	0.603	0.505	219.3	9.951	9	15.46	0.48	3
[5] 2PIGG-s1538[a]	00:33:27.53	−31:31:14.4	0.05447	0.254	0.366	43.4	5.724	5	5.894	0.37	3
[2] 2PIGG-s1554	22:05:41.02	−24:16:55.8	0.05610	0.448	0.598	286.9	13.41	6	25.64	0.90	4
[2] 2PIGG-s1571	02:34:50.63	−25:36:33.5	0.05676	0.286	0.501	330.8	9.835	10	15.14	0.95	4
[2] 2PIGG-s1572	01:36:09.86	−26:20:05.3	0.05534	0.312	0.308	160.8	4.173	5	3.510	−0.24	1
[1] 2PIGG-s1600	02:44:28.07	−28:15:32.1	0.05561	0.208	0.438	90.8	7.810	6	10.11	−0.04	2
[5] 2PIGG-s1601	22:41:13.88	−32:54:00.8	0.05634	0.650	0.466	169.7	8.653	10	12.11	0.00	2
[2] 2PIGG-s1606[a]	02:10:42.52	−26:56:25.8	0.05700	0.353	0.515	405.0	10.29	7	16.37	0.81	4
[5] 2PIGG-s1609	23:01:09.93	−33:24:56.6	0.05461	0.636	0.849	171.4	27.29	12	73.36	0.77	4
[5] 2PIGG-s1613	22:50:31.74	−33:19:03.5	0.05552	0.306	0.279	52.3	3.433	5	2.607	−0.10	2
[4] 2PIGG-s1614	22:22:29.12	−25:38:30.9	0.05676	0.658	0.746	447.0	20.59	18	49.80	0.60	4
[5] 2PIGG-s1632	02:36:41.35	−27:09:22.1	0.05704	0.367	0.538	335.3	11.10	9	18.69	0.89	4
[5] 2PIGG-s1635[a]	00:14:10.01	−27:25:22.2	0.05578	0.549	0.579	189.1	12.64	11	23.27	0.45	3
[2] 2PIGG-s1641	22:25:29.09	−30:31:27.6	0.05515	0.679	0.675	644.6	16.85	12	36.91	1.89	4
[2] 2PIGG-s1654	22:26:06.85	−25:32:23.8	0.05568	0.558	0.425	116.5	7.408	7	9.214	0.31	3
[3] 2PIGG-s1659	22:29:12.65	−25:39:07.8	0.05655	0.510	0.244	279.0	2.580	5	1.743	0.15	2
[5] 2PIGG-s1661	01:55:37.94	−27:40:31.3	0.05650	0.393	0.253	211.3	2.802	5	1.951	0.46	3
[2] 2PIGG-s1662	22:05:07.47	−29:11:55.6	0.05616	0.667	0.492	206.0	9.512	6	14.30	1.35	4
[2] 2PIGG-s1665	02:35:48.88	−26:54:17.1	0.05701	0.900	0.885	284.2	30.06	13	83.24	0.80	4
[2] 2PIGG-s1666	23:56:22.08	−34:08:53.4	0.05649	0.752	0.415	150.1	7.100	8	8.551	0.78	4
[5] 2PIGG-s1670	01:03:41.10	−34:29:55.1	0.05708	0.323	0.379	289.6	6.092	5	6.554	0.23	3
[2] 2PIGG-s1671	22:21:10.37	−30:15:31.1	0.05671	0.469	0.618	210.1	14.26	10	28.34	0.51	3
[2] 2PIGG-s1673	02:31:18.64	−26:40:47.4	0.05619	0.500	0.302	−70	4.008	5	3.296	0.75	4
[2] 2PIGG-s1677	22:15:49.09	−26:48:48.5	0.05630	0.392	0.630	99.6	14.78	6	30.03	1.04	4
[2] 2PIGG-s1688	22:03:50.60	−24:22:35.0	0.05510	1.163	0.665	398.0	16.34	13	35.19	0.83	4
[2] 2PIGG-s1691	23:49:42.16	−34:05:28.6	0.05635	0.570	0.616	175.1	14.16	9	28.04	0.48	3
[5] 2PIGG-s1696[a]	01:52:32.06	−28:23:38.3	0.05780	0.305	0.384	423.0	6.227	5	6.804	0.04	2
[2] 2PIGG-s1708[a]	22:17:33.50	−32:56:16.8	0.05675	0.441	0.667	90.6	16.47	7	35.61	0.47	3
[5] 2PIGG-s1721	23:57:13.34	−33:46:02.4	0.05754	0.775	0.450	169.4	8.188	6	10.99	0.94	4
[5] 2PIGG-s1729	01:37:38.25	−28:12:32.3	0.05662	0.689	0.601	52.2	13.54	5	26.07	0.01	2
[2] 2PIGG-s1730	02:09:44.75	−25:58:15.7	0.05746	0.371	0.399	215.4	6.659	5	7.646	−0.14	1
[2] 2PIGG-s1735	23:57:15.26	−34:44:59.1	0.05663	0.770	0.670	185.6	16.60	13	36.04	0.88	4
[2] 2PIGG-s1744	22:05:50.68	−24:52:57.9	0.05664	0.642	0.439	216.4	7.829	7	10.15	1.20	4
[5] 2PIGG-s1749	01:49:55.62	−28:45:38.2	0.05692	0.377	0.285	60.0	3.578	6	2.773	−0.07	2
[2] 2PIGG-s1752	22:18:23.02	−26:15:32.7	0.05773	0.351	0.775	194.4	22.37	11	56.01	0.72	4
[5] 2PIGG-s1762[a]	01:56:00.40	−30:49:20.9	0.05711	0.358	0.343	−70	5.094	5	4.846	−0.57	1
[2] 2PIGG-s1767	02:10:38.51	−26:39:21.3	0.05735	0.855	0.511	242.0	10.16	11	16.03	0.60	4
[2] 2PIGG-s1783	22:14:30.38	−37:14:49.1	0.05833	0.256	0.741	208.9	20.37	8	49.00	0.79	4
[5] 2PIGG-s1786	00:59:46.79	−28:41:06.9	0.05758	0.301	0.482	109.6	9.180	8	13.43	0.03	2
[2] 2PIGG-s1793	23:46:48.92	−31:03:35.2	0.05728	0.717	0.339	−70	4.998	5	4.694	0.05	2
[5] 2PIGG-s1798	00:56:46.93	−26:44:43.0	0.05761	0.459	0.510	142.8	10.12	6	15.93	−0.44	1
[5] 2PIGG-s1799	01:12:14.90	−34:12:01.3	0.05819	0.438	0.653	199.5	15.83	13	33.50	1.47	4
[5] 2PIGG-s1802	23:38:30.06	−31:22:09.2	0.05794	0.335	0.578	136.4	12.60	7	23.16	0.76	4
[2] 2PIGG-s1807	03:27:32.73	−31:44:00.3	0.05814	0.681	0.377	121.0	6.020	5	6.423	0.67	4
[2] 2PIGG-s1840	22:20:27.71	−29:21:01.2	0.05825	0.799	0.583	132.0	12.81	10	23.79	0.63	4
[3] 2PIGG-s1863	22:20:57.32	−29:48:30.4	0.05806	0.410	0.422	114.2	7.333	6	9.047	0.63	4
[2] 2PIGG-s1886	03:16:48.81	−30:35:18.7	0.05805	0.481	0.456	87.0	8.349	5	11.37	0.52	3
[5] 2PIGG-s1889	01:53:24.18	−05:02:28.0	0.05214	0.362	0.227	355.8	2.186	5	1.40	0.21	3
[4] 2PIGG-s1935	22:25:04.97	−30:49:51.5	0.05802	1.867	1.770	554.6	200.9	159	667.0	1.76	4
[3] 2PIGG-n1267	13:55:38.14	−04:26:56.6	0.05024	0.264	0.410	371.2	6.951	5	8.241	−0.58	1

Table 1
(Continued)

Name	R.A. (B1950)	Decl. (B1950)	z	$r_{\rm rms}$ (Mpc)	$\hat{R}_{200}$ (Mpc)	σ (km s^{-1})	$L_{\rm GROUP}$ ($10^{10} L_{\odot}$)	N_m	$M_{\rm GROUP}$ ($10^{12} M_{\odot}$)	$\log(1+\delta_{\rm LSS})$	Env.
[1] 2PIGG-n1320	10:15:21.93	−01:07:51.4	0.05076	0.497	0.631	157.6	14.78	10	30.04	0.97	4
[1] 2PIGG-n1330	10:25:04.34	−02:48:39.1	0.05044	0.287	0.440	−70	7.843	5	10.19	1.38	4
[1] 2PIGG-n1345	10:06:15.29	−04:15:10.6	0.05140	0.367	0.545	61.2	11.32	8	19.33	0.83	4
[1] 2PIGG-n1347	09:57:13.93	−05:02:28.0	0.05214	0.534	0.624	167.7	14.46	10	29.00	0.78	4
[3] 2PIGG-n1363	12:03:15.25	−02:41:48.6	0.05207	0.289	0.402	221.0	6.727	8	7.781	−0.28	1
[1] 2PIGG-n1365	10:26:06.57	−00:53:25.5	0.05153	0.483	0.510	170.8	10.08	8	15.81	0.47	3
[1] 2PIGG-n1377	11:30:08.88	−03:33:45.5	0.05154	1.330	0.856	222.3	27.76	23	75.06	0.92	4
[3] 2PIGG-n1381	14:25:37.08	−02:17:49.1	0.05215	0.426	0.468	140.0	8.704	10	12.23	1.25	4
[3] 2PIGG-n1382	14:06:07.75	00:04:00.8	0.05237	0.673	0.418	255.8	7.173	7	8.709	0.26	3
[6] 2PIGG-n1384	14:19:07.38	−00:08:18.9	0.05305	0.812	0.785	308.3	22.92	11	57.96	1.44	4
[1] 2PIGG-n1385	10:17:28.19	−04:46:24.7	0.05106	0.784	0.705	275.5	18.28	17	41.77	1.45	4
[1] 2PIGG-n1394	10:21:34.44	−01:48:32.7	0.05210	0.583	0.760	75.1	21.35	8	52.44	0.82	4
[1] 2PIGG-n1398	10:52:36.36	−02:26:58.4	0.05255	0.416	0.412	115.0	6.998	5	8.339	0.27	3
[3] 2PIGG-n1403	11:30:37.40	−02:34:04.5	0.05130	0.366	0.406	219.3	6.837	7	8.003	−0.13	2
[4] 2PIGG-n1404[a]	13:43:09.95	−05:15:13.1	0.05211	0.446	0.777	218.7	22.37	7	56.01	0.29	3
[3] 2PIGG-n1413	11:21:18.46	−03:58:43.0	0.05295	0.694	0.800	395.5	23.86	13	61.23	1.08	4
[1] 2PIGG-n1416	10:23:21.85	−02:43:11.3	0.05151	0.547	0.348	401.2	5.218	7	5.043	1.57	4
[4] 2PIGG-n1418	11:38:49.88	−02:18:59.3	0.05364	0.349	0.417	355.6	7.151	5	8.660	0.89	4
[4] 2PIGG-n1423	13:40:34.33	−04:45:17.2	0.05278	0.317	0.280	106.2	3.447	5	2.623	−0.21	1
[1] 2PIGG-n1440	10:15:00.48	−05:46:28.7	0.05390	0.948	0.753	294.5	20.98	20	51.10	0.86	4
[3] 2PIGG-n1441	11:15:37.87	−04:11:11.5	0.05313	0.600	0.658	241.8	16.01	15	34.10	0.50	3
[3] 2PIGG-n1445	11:22:24.09	−03:41:09.3	0.05283	0.737	0.548	106.6	11.46	8	19.73	1.03	4
[4] 2PIGG-n1449	13:32:37.51	−02:45:17.1	0.05318	0.593	0.370	79.7	5.806	5	6.039	−0.14	1
[4] 2PIGG-n1454	13:37:43.48	−04:32:33.8	0.05366	0.252	0.640	188.1	15.17	5	31.31	0.16	2
[6] 2PIGG-n1457	14:15:17.75	00:32:59.4	0.05194	0.812	1.134	552.8	55.92	30	174.1	1.87	4
[1] 2PIGG-n1461	10:16:13.64	−04:21:26.4	0.05415	0.657	0.394	253.5	6.488	10	7.306	0.45	3
[3] 2PIGG-n1466	14:01:26.94	−01:25:45.0	0.05292	0.906	0.747	331.9	20.59	17	49.79	0.59	3
[2] 2PIGG-n1467	11:08:52.83	−04:11:27.5	0.05414	0.327	0.385	151.9	6.245	5	6.840	0.63	4
[3] 2PIGG-n1469[a]	11:39:06.31	−01:58:08.3	0.05429	0.406	0.555	155.1	11.73	6	20.51	0.76	4
[4] 2PIGG-n1472	14:03:23.30	−00:59:32.7	0.05370	0.430	0.589	176.7	13.03	5	24.46	0.70	4
[1] 2PIGG-n1475	10:19:33.68	−01:14:46.9	0.05405	0.295	0.583	252.3	12.81	5	23.79	0.66	4
[3] 2PIGG-n1476	11:19:51.61	−03:59:41.7	0.05292	0.888	0.828	204.8	25.76	14	67.93	1.03	4
[1] 2PIGG-n1480	10:13:01.02	−05:22:09.4	0.05368	0.521	0.574	258.9	12.43	13	22.61	0.62	4
[3] 2PIGG-n1484	13:15:52.05	01:09:57.2	0.05401	0.464	0.314	84.9	4.314	5	3.700	−0.29	1
[6] 2PIGG-n1486	14:05:16.34	−00:42:48.7	0.05393	0.826	0.905	388.5	31.59	23	88.69	1.09	4
[6] 2PIGG-n1488	14:09:19.73	00:11:00.9	0.05398	0.810	0.636	190.5	15.03	9	30.86	0.49	3
[2] 2PIGG-n1491	10:07:43.43	−04:44:52.6	0.05618	1.136	1.138	444.2	56.73	48	177.0	1.17	4
[6] 2PIGG-n1494	14:20:27.82	01:01:16.1	0.05389	0.291	0.376	98.1	5.998	5	6.383	0.11	2
[1] 2PIGG-n1503	11:04:23.33	−04:29:00.8	0.05419	0.432	0.400	225.5	6.678	6	7.684	0.38	3
[1] 2PIGG-n1510	10:15:35.24	−05:10:41.2	0.05475	1.003	0.767	253.6	21.84	14	54.13	0.79	4
[1] 2PIGG-n1514	10:18:30.19	−04:13:03.4	0.05433	0.688	0.733	235.7	19.87	17	47.27	1.18	4
[6] 2PIGG-n1522	14:09:21.21	00:43:55.4	0.05450	0.558	0.643	240.6	15.34	10	31.89	0.80	4
[3] 2PIGG-n1523	14:04:38.91	−02:29:22.8	0.05533	0.412	0.442	289.6	7.916	5	10.35	0.16	2
[6] 2PIGG-n1525	14:05:46.98	−00:21:17.1	0.05295	0.677	0.487	265.6	9.327	11	13.81	1.23	4
[6] 2PIGG-n1528	14:06:45.08	00:09:26.6	0.05363	0.921	0.425	183.8	7.384	9	9.160	0.29	3
[3] 2PIGG-n1532	13:34:06.07	−03:17:04.2	0.05344	1.133	0.864	127.0	28.33	15	77.10	0.86	4
[6] 2PIGG-n1533[a]	14:07:31.39	−00:04:29.3	0.05399	0.504	0.324	257.5	4.590	5	4.086	0.88	4
[3] 2PIGG-n1534	11:39:08.71	−02:34:53.7	0.05501	0.360	0.497	273.8	9.673	5	14.71	0.67	4
[3] 2PIGG-n1540	14:27:03.55	00:35:26.4	0.05489	1.023	1.138	275.7	56.61	32	176.6	0.79	4
[3] 2PIGG-n1543	13:23:17.84	−00:25:09.4	0.05493	0.136	0.413	133.9	7.051	6	8.449	0.07	2
[1] 2PIGG-n1556	10:09:00.67	−05:38:24.9	0.05485	0.478	0.512	128.0	10.17	8	16.06	0.56	3
[6] 2PIGG-n1558	14:07:47.65	−00:52:47.0	0.05426	0.571	0.547	90.7	11.42	7	19.60	0.47	3
[6] 2PIGG-n1572	14:22:58.68	−01:16:30.3	0.05501	0.899	0.733	190.0	19.84	19	47.17	0.87	4
[4] 2PIGG-n1574	14:04:12.43	−03:27:19.1	0.05485	1.017	0.979	269.3	38.31	28	112.4	0.67	4
[3] 2PIGG-n1584	14:34:02.76	00:54:18.5	0.05583	0.323	0.421	150.0	7.280	6	8.936	0.70	4
[4] 2PIGG-n1587	11:40:04.46	−02:50:06.3	0.05555	0.406	0.373	92.0	5.924	5	6.249	0.30	3
[1] 2PIGG-n1588	10:19:01.37	−04:42:04.2	0.05444	1.094	1.271	454.4	76.80	71	246.1	1.16	4
[2] 2PIGG-n1593	10:17:17.68	−03:39:05.8	0.05635	0.675	0.511	231.2	10.17	9	16.04	0.67	4
[6] 2PIGG-n1597	14:25:07.25	−01:31:58.2	0.05468	1.007	0.883	351.6	29.82	16	82.37	1.07	4
[3] 2PIGG-n1598	14:33:19.46	−01:03:40.0	0.05600	0.569	0.606	114.2	13.75	9	26.71	0.55	3
[2] 2PIGG-n1606	10:36:15.34	02:04:02.8	0.05612	0.262	0.505	106.4	9.953	7	15.47	0.21	2
[2] 2PIGG-n1610	09:51:07.59	−04:54:10.5	0.05615	0.251	0.495	145.1	9.608	10	14.54	0.63	4
[6] 2PIGG-n1622	14:28:45.22	−01:31:48.8	0.05458	0.970	1.017	524.5	42.18	27	126.1	1.22	4
[2] 2PIGG-n1623	10:15:52.23	−03:41:41.9	0.05702	0.552	0.367	253.8	5.745	5	5.930	0.86	4
[4] 2PIGG-n1626	11:35:34.50	−05:10:26.9	0.05620	0.238	0.270	190.1	3.196	5	2.350	0.54	3

Table 1
(Continued)

Name	R.A. (B1950)	Decl. (B1950)	z	$r_{\rm rms}$ (Mpc)	$\hat{R}_{200}$ (Mpc)	σ (km s^{-1})	$L_{\rm GROUP}$ ($10^{10} L_{\odot}$)	N_m	$M_{\rm GROUP}$ ($10^{12} M_{\odot}$)	$\log(1+\delta_{\rm LSS})$	Env.
[2] 2PIGG-n1630[a]	14:44:22.06	−03:19:29.5	0.05846	0.538	1.042	370.3	45.02	18	136.1	1.64	4
[2] 2PIGG-n1637	09:56:42.39	−04:26:00.7	0.05646	0.379	0.338	112.8	4.951	5	4.621	0.20	2
[2] 2PIGG-n1648	11:02:12.89	−03:39:25.1	0.05645	0.387	0.232	37.9	2.304	5	1.500	−0.06	2
[4] 2PIGG-n1671	11:36:30.38	−04:02:25.5	0.05542	1.031	1.299	368.7	81.61	41	262.7	1.29	4
[2] 2PIGG-n1672	11:03:57.41	−03:42:14.1	0.05686	0.419	0.321	177.7	4.520	5	3.987	0.16	2
[2] 2PIGG-n1702	09:51:59.37	−03:51:50.5	0.05738	0.451	0.573	69.7	12.42	9	22.60	0.72	4
[2] 2PIGG-n1706	14:47:04.10	−03:25:40.7	0.05781	0.490	0.747	275.3	20.69	7	50.14	1.44	4
[2] 2PIGG-n1714	10:33:34.48	−03:46:37.9	0.05760	0.652	0.550	−70	11.57	7	20.04	0.78	4
[3] 2PIGG-n1721	12:35:48.75	−04:16:47.8	0.05844	0.881	0.488	128.8	9.400	8	14.00	0.66	4
[2] 2PIGG-n1746	14:37:43.57	−03:33:05.7	0.05849	0.520	0.516	191.4	10.34	9	16.53	0.24	3
[2] 2PIGG-n1829	10:04:21.96	−05:20:25.4	0.05718	0.905	1.483	691.3	119.5	67	392.0	1.62	4

Notes. Properties of the ZENS groups. The first column lists the group ID. The superscripts prefixing the IDs identify the observing run during which the WFI *B*- and *I*-band imaging was acquired for a given group; see Paper II. From left to the right, the other columns list right ascension and declination of the group, 2dFGRS redshift, 2PIGG rms radius in Mpc, our computation of group size $\hat{r}_{200}$ in Mpc, 2PIGG velocity dispersion σ in km s^{-1}, total group luminosity $L_{\rm GROUP}$, number of members above the magnitude limit of the survey, total group mass $M_{\rm GROUP}$, and the value of LSS overdensity calculated with our fifth-nearest-*group* algorithm. The last column lists the overdensity quartile to which the groups belong relative to the global distribution of overdensities in the redshift window $0.035 < z < 0.075$ (with the first and fourth quartile indicating regions of the lowest and highest environmental density, respectively). Definitions for all quantities are given in the text (if not self-explanatory). The IDs follow the original 2PIGG nomenclature: an "n" (2PIGG-nXXXX) identifies groups located in the Northern Galactic Hemisphere; an "s" identifies groups in the Southern Hemisphere. Groups that have a velocity dispersion derived with the gapper estimator that is smaller than the typical 2dFGRS redshift error (∼70–85km s^{-1}) have null σ values in the original 2PIGG catalog (see Equation (4.6) in Eke et al. 2004a). For these groups, the entry in the column for σ lists "−70," i.e., the velocity dispersion is set equal to the 2dFGRS redshift error of 70 km s^{-1} at $z \sim 0.05$ and the minus sign is used as a flag to identify the groups in question. With the symbol "a", we indicate groups that satisfy the criterion for being "fossil" according to the definition presented in Section 2.4.

direct comparison with *HST* images of galaxies in high-z groups (e.g., Knobel et al. 2009; Kovač et al. 2010b; Gerke et al. 2012). A summary of the properties of the ZENS groups is given in Table 1 and Figure 1.

2.2. Impact of the 2dFGRS Selection Function on ZENS

2.2.1. Impact of the 2dFGRS Redshift Incompleteness and Field-to-field Scatter in the 2dFGRS Magnitude Limits

The depth and completeness of the 2dFGRS are not uniform over the sky for a number of reasons (Colless et al. 2001): the 2dFGRS parent catalog (Automatic Plate Measuring (APM) survey; Maddox et al. 1990) was recalibrated and the extinction corrections were revised after the survey limit of $b_j = 19.45$ was originally set; moreover, the number of successful or repeated observations varies with position on the sky. We quantify in Appendix A the impact of the original 2dFGRS magnitude limits on our targeted fields. These limits translate into a minimum mass at which ZENS is complete; this mass corresponds to $10^{10}\,M_{\odot}$ for "quenched" red-and-dead galaxies with old stellar populations and $10^{9.2}\,M_{\odot}$ for galaxies with star-forming spectral energy distributions (SEDs). A detailed description of the derivation of galaxy stellar masses and the mass completeness limits of ZENS is given in Paper III.

We also note that, unless explicitly stated otherwise, all statistical analyses that we present in this paper and in following ZENS papers refer to quantities corrected for spectroscopic incompleteness of the 2dFGRS.

2.2.2. Sample Completeness Tested on the SDSS

We investigated the resulting incompleteness in the ZENS group sample originating from the catalog limitations described above. To this end, we searched the SDSS DR7 spectroscopic catalog (Abazajian et al. 2009) for galaxies within up to ±30% of the redshift distribution of a given ZENS group, not present however in the parent 2dFGRS catalog. The details of this comparison are given in Appendix B.1. There are many aspects of our analyses that could in principle be affected by any such incompleteness, i.e., the estimates of the group masses, the determination of the central galaxy and thus of the group centers, and, consequently, the radial trends with group-centric distance. Our tests, presented in Appendix B.1, indicate, however, that our main results are not severely affected by significant biases due to incompleteness in the parent 2dFGRS catalog.

2.3. New B- and I-band Data with the ESO/2.2 m Wide Field Imaging Camera

ZENS capitalizes on the wealth of data and measurements already available from the original 2dFGRS analyses and other surveys (e.g., the *Galaxy Evolution Explorer* (*GALEX*), the Two Micron All Sky Survey (2MASS), and SDSS). In particular, for all ZENS galaxies, b_j and r_F photometry is available from the 2dFGRS catalog. However, pixel data for the original APM scans of the photographic plates are not provided. The digitalized versions of the SuperCOSMOS Survey plates (Hambly et al. 2001), which have also been used in the definition of the 2dFGRS photometric catalog, are available online but with no photometric calibration information. Furthermore, the resolution of these images (∼2″–2.″5) is not suited for detailed structural analyses of typical galaxies in the sample.

In order to obtain accurate measurements of the structural (Cibinel et al. 2013a) and stellar population properties (Cibinel et al. 2013b) of galactic subcomponents, we thus acquired new deep *B*- ($BB\#B/123\_ESO878$) and *I*-band ($BB\#I/203\_ESO879$) images with the WFI at the MPG/ESO 2.2 m telescope. The WFI observations reach limiting magnitudes, defined as the magnitude of an uniform area of 2″ having a signal five times higher than the typical noise, of $B_{\rm AB} = 25$ mag and $I_{\rm AB} = 23.4$ mag (compared with the corresponding depth of the $b_{J,\rm AB}$ and $r_{F,\rm AB}$ plates, which are ∼22.5 mag and

~21.7 mag, respectively). Note, however, that our new deeper photometry was not utilized to extend the group membership in order to maintain consistency with the original 2dFGRS/2PIGG catalogs for which the spectroscopic information is available.

The data were taken in several observing runs over the period 2005–2009. Following a pilot-project time allocation in 2005, most of the observations were carried out as service-mode observations in the context of the ESO Large Program 177.A-0680. Due to a combination of weather and technical issues, the service-mode observations were distributed over several runs during the period 2006–2008. The last two observing runs were carried out in visitor mode at the end of 2008 and 2009, achieving a final sample of 141 groups randomly extracted from the original complete sample of 185 targets.

These 141 ZENS groups host a total of 1627 cataloged galaxy members brighter than the magnitude limit of the 2dFGRS survey, 1484 of which are within our WFI pointings (see Appendix B; note that the vast majority of galaxies outside our WFI pointings have stellar masses below our completeness limits discussed above and would thus not be included in the majority of our analyses). For these 1484 galaxies,[6] we have derived accurate structural measurements (sizes, bulge-disk decompositions, bar sizes and strengths, non-parametric diagnostics such as concentration, Gini, asymmetry, etc., as well as a quantitative, robust morphological classification that corrects for seeing, inclination effects, and dust effects; see Paper II) and photometric measurements (e.g., colors, specific and total SFRs, and stellar masses for the whole galaxies, as well as for bulges and disks, including corrections for inclination, dust effects, and fiber-area effects; see Paper III).

In Paper II, we provide details of the observing runs, the raw data properties, the data reduction procedures, and the photometric calibration for WFI data of the ZENS groups.

2.4. Fossil Groups in the ZENS Sample

The ZENS sample includes groups whose luminosity budget is dominated by a single bright central galaxy, highlighting peculiar halo occupation properties and thus formation or evolution histories. A widely used definition for such "fossil" groups is that they show an absolute magnitude gap between the most luminous galaxy and the second brightest member of $\Delta m_{12} > 2$ mag in the R band (Jones et al. 2003).

We adopt this optical criterion using the r_F magnitudes that are available for the 2dFGRS galaxies from the SuperCOSMOS Survey (Hambly et al. 2001). To derive the k-correction from the galaxy $C = b_j - r_F$ color provided by the 2dFGRS and thus compute r-band absolute magnitudes, we use Equation (3) of Cole et al. 2005: $k_{r_F} = (-0.08 + 1.45C)(z/z+1) + (-2.88 - 0.48C)(z/z+1)^2$. About 7% of ZENS groups (i.e., a total of 10 groups) satisfy the fossil selection criterion above. These fossil groups are marked with an asterisk symbol in Table 1.

Only in three out of the 10 ZENS fossil groups is the dominant galaxy a giant E/S0 galaxy. These groups' masses span a wide range, from $\sim 6 \times 10^{12}\ M_\odot$ up to $\sim 1.5 \times 10^{14}\ M_\odot$, similar to fossil groups that are found to host an early-type central galaxy in other studies (e.g., Ponman et al. 1994; Romer et al. 2000; Khosroshahi et al. 2004). The mass range of the remaining seven fossil groups in our sample that host morphological late-type centrals overlaps at the low end with the range above, extending down to $\sim 4 \times 10^{12}\ M_\odot$, but remains confined to generally lower masses $< 2 \times 10^{13}\ M_\odot$. Interestingly, in seven of the 10 fossil-like groups, including two with E/S0 centrals, the central galaxy is either undergoing a merger, in a close pair with a satellite, or shows a disturbed morphology. Only three ZENS fossil groups, one of which hosts a central elliptical, are "unrelaxed" systems according to the definition that we describe in Sections 3.2.1 and 5. No fossil groups show sub-clustering according to the Dressler and Shectman test (Dressler & Shectman 1988) that we present in Section 5.1.

The small fraction of compact groups that we find in our sample echoes other previous studies showing that such groups are, at any mass scale, a small fraction of the population (e.g., van den Bosch et al. 2007; see however Yang et al. 2008 for larger estimates toward lower halo masses). Unless explicitly stated, we will therefore include these groups in our ZENS analysis.

2.5. The Strength of ZENS

Relative to previous work, the ZENS database offers additional power in several aspects for studying environmental effects on galaxy properties. Previous detailed analyses have often focused on biased group samples, e.g., X-ray selected, "compact," or "fossil" groups (e.g., Lee et al. 2004; McConnachie et al. 2009; Harrison et al. 2012). While understanding these systems is important, a comprehensive study of the role of environment on different scales necessitates a less biased selection of the sample and a definition of a "group" that is as general as possible. As discussed in Section 2.1, ZENS is fully representative of the local population of galaxy groups.

Other studies have adopted similarly general identification and selection criteria as those employed in 2PIGG, from which ZENS is extracted, to produce large group catalogs for the major surveys (e.g., Merchán & Zandivarez 2002; Yang et al. 2005, 2007; Berlind et al. 2006; Tago et al. 2008, 2010; Calvi et al. 2011; Robotham et al. 2011; Tempel et al. 2012). Relative to these efforts, ZENS trades off sample size with measurement accuracy. The relatively smaller size of the ZENS sample enables us to analyze and measure properties for each of the galaxies individually, rather than relying on automatic algorithms that introduce a substantial "impurity" in the measurements and thus classifications of larger galaxy samples. Furthermore, in ZENS, we have attempted to identify problems inherent in standard definitions of the different environments and to implement solutions that minimize or at least flag such potential causes for signal contamination. Finally, all environmental and galactic estimates performed on the ZENS sample have been accurately calibrated against several intrinsic and observational biases, as discussed below (see also Papers II and III for details on the derivation of the structural and morphological galaxy parameters, respectively). The sum of the above calibrations minimizes or, when possible, eliminates uncertainties, often of order ~30%–40%, which affect statistically handled measurements in the larger samples, giving ZENS a unique niche to study aspects of galaxy evolution in group halos that are complementary to those enabled by larger but less detailed samples.

3. FOUR ENVIRONMENTS IN COMPARISON WITH ONE ANOTHER

With the goal of identifying *which* environment affects galactic evolution at different galaxy mass scales, we quantify

[6] Note that there are only 1455 galaxy entries in the 2dFGRS catalog corresponding to our 141 2PIGG groups. However, 29 of these entries correspond to galaxy pairs, for which we measure all quantities individually.

four environmental diagnostics that will enable us to search for differential trends with these environments in different galactic populations. The four environments are: (1) the mass of the host group halo, (2) the distance of a galaxy from the center of its group halo, (3) the average LSS density at the position of the host group, determined by the underlying filamentary structure of the cosmic web, and (4) the central versus satellite dichotomy, considered here to be also an environmental condition that galaxies experience in their life within a bound common halo.

3.1. Environment Number One: The Mass of the Host Group Halo

The 2PIGG catalog from which we have extracted the ZENS sample lists the velocity dispersions σ returned by the FOF algorithm that was used to construct the catalog and the radii of the groups (reported in Table 1), defined as the weighted rms of the projected separations between the nominal 2PIGG center and the remaining group members. Eke et al. (2004a) and Eke et al. (2004b) discuss in detail the tests performed to ascertain the robustness of these estimates, which were optimized to best reproduce the global properties of the 2dFGRS mock catalogs (Eke et al. 2004a). Dynamical halo masses computed as $M_{\rm dyn} = 5(\sigma^2 r_{\rm rms}/G)$ are however affected by large uncertainties, especially for groups with a relatively low number of members (redshift errors in the 2dFGRS are typically $\sim$70 km s^{-1} at $z \sim 0.05$). In contrast, group total (stellar) luminosities can be measured with a higher accuracy even in poor groups. Using mock catalogs, Eke et al. (2004b) calibrated the observed group total luminosities into total group masses, providing robust estimates for the halo mass-to-light ratios (Υ_{b_j}) needed to convert the b_j luminosities into total halo masses $M_{\rm GROUP}$. We adopt such b_j luminosity-based halo masses as our fiducial estimates for the matter content of the ZENS groups.[7]

Specifically, following the prescription of Eke et al. (2004b), we computed the observed group luminosity as the weighted sum of the luminosities of the individual galaxy members L_{i,b_j}, i.e., $L_{\rm GROUP,OBS} = \sum_i^N w_i L_{i,b_j}$, where N is the number of member galaxies in the group, w_i are the weights used in the construction of the 2PIGG catalog that account for the 2dFGRS redshift incompleteness, and b_j are the original apparent (Vega) 2dFGRS magnitudes. The magnitudes were converted to absolute magnitudes by applying the mean $k+e$ correction as given in Equation (2.4) of Eke et al. (2004b), $k+e = (z + 6z^2/1 + 8.9z^{5/2})$. This observed luminosity was corrected into a total luminosity ($L_{\rm GROUP}$) by integrating a Schechter function to zero luminosity, namely, by dividing $L_{\rm GROUP,OBS}$ by the incomplete gamma function $\Gamma(\alpha+2, L_{\rm min}/L_*)/\Gamma(\alpha+2)$. In the above formula, (α, L_*) are the slope and cut-off luminosity of the Schechter function, respectively, and $L_{\rm min}$ is the luminosity corresponding to the magnitude limit of the 2dFGRS survey at the considered position in the sky. The correction was done by keeping α and L_* fixed for all groups and assuming the values $\alpha = -1.18$ and $M_* = -19.725$, obtained by Eke et al. (2004b) from a global Schechter function for the 2dFGRS galaxies. Our fiducial total halo masses $M_{\rm GROUP}$ were finally obtained using Equation (4.4) in Eke et al. (2004b) for the mass-to-light ratio: $\log_{10}\Upsilon_{b_j} = 2.28 + 0.4\tanh[1.9(\log L_{\rm GROUP} - 10.6)]$.

[7] Note that although an expression for $\log_{10}\Upsilon_{r_F}$ is also provided by Eke et al. (their Equation (4.5)), we chose to use b_j luminosities for our estimates, since the overall shape of the mass-to-light ratio vs. luminosity relations is very similar in both passbands, as discussed by Eke et al. (2004b), and the $\log_{10}\Upsilon_{r_F}$ estimates are regardless based on the total b_j luminosity.

As expected, the comparison of the obtained masses for the ZENS groups with the dynamical $M_{\rm dyn}$ estimates defined above shows that the mass difference decreases with increasing $M_{\rm GROUP}$, from $\Delta(\log M) \equiv \log_{10} M_{\rm dyn} - \log_{10} M_{\rm GROUP} = 0.40 \pm 0.12$ at $M_{\rm GROUP} < 10^{12.7}\,M_\odot$ down to $\Delta(\log M) = -0.01 \pm 0.06$ at $M_{\rm GROUP} > 10^{13.5}\,M_\odot$. The median difference for the total ZENS sample is $\Delta(\log M) = 0.12 \pm 0.05$. In our future ZENS analyses, we will systematically test and report whether any of our results will significantly change if the dynamical mass estimates were to be used instead of our adopted definition of $M_{\rm GROUP}$; this situation is not the case for any of the analyses of Paper I, II, and III.

3.1.1. Sources and Effect of Errors on Our Fiducial Group Masses

The conversion of group luminosity into dark matter halo mass outlined above is affected by several factors, in addition to errors in the relevant galactic measurements (such as redshifts and luminosities). The most important additional contributions to the uncertainty in the conversion come from (1) errors in group membership, either by "missing" group members above the galaxy luminosity completeness cut in the survey, or by including interloper galaxies that are not physically associated with the given group; (2) peculiarities in the groups' luminosity functions; and (3) the intrinsic uncertainty/scatter in the group mass-to-light ratio relation, partly due to uncertainties in the physics underlying this conversion. These sources of error on the group masses are not easy to eliminate and thus we try to assess their impact on our analyses.

3.1.1.1. Erroneous group membership assignments: interlopers and "missing" galaxies. How sensitive are our halo mass estimates to the spurious inclusion or exclusion of member galaxies from a given group? The most obvious source of such kinds of error is a non-optimal performance of the FOF algorithm used to generate the 2PIGG catalog.

We start by assessing the impact of interlopers. At the typical redshift and mass scale of the ZENS groups, the level of contamination from such interlopers ranges between 20%–40%, depending on the mass of the group; this result is clear from Figure 2 of Eke et al. (2004a), which shows the fraction of interlopers as a function of halo mass for the parent 2PIGG sample. Note that similar levels of interloper fractions are found in other studies (see, e.g., the Yang et al. 2005 compilation, further discussed in Section 3.1.1.2). Interlopers are thus a substantial source of error in the estimate of the group masses and may also affect estimates of global properties of galaxies in groups. Since we have no a priori knowledge of which galaxies could be false members, we need to approach this problem in a statistical manner.

To specifically estimate the impact of interlopers on the group mass estimates, we removed from each group, in 3000 bootstrap realizations, a random 20%–40% of the member galaxies (both including and, in a separate set of tests, excluding the possible extra candidates discussed below in this section). For each realization, we recalculated the mass of the groups from the luminosity function, as outlined in Section 3.1. Note that for groups with low numbers of galaxies, this methodology is equivalent to spanning all the possible combination of rejected galaxies. For groups with $N_{\rm gal} > 15$, this technique is not the case anymore; however, given the large number of bootstrap samples we employ in the analysis, the derived distributions will be representative of the complete mass range. This bootstrap approach provides us, for each group, with a distribution of masses for each configuration and a median of this distribution.

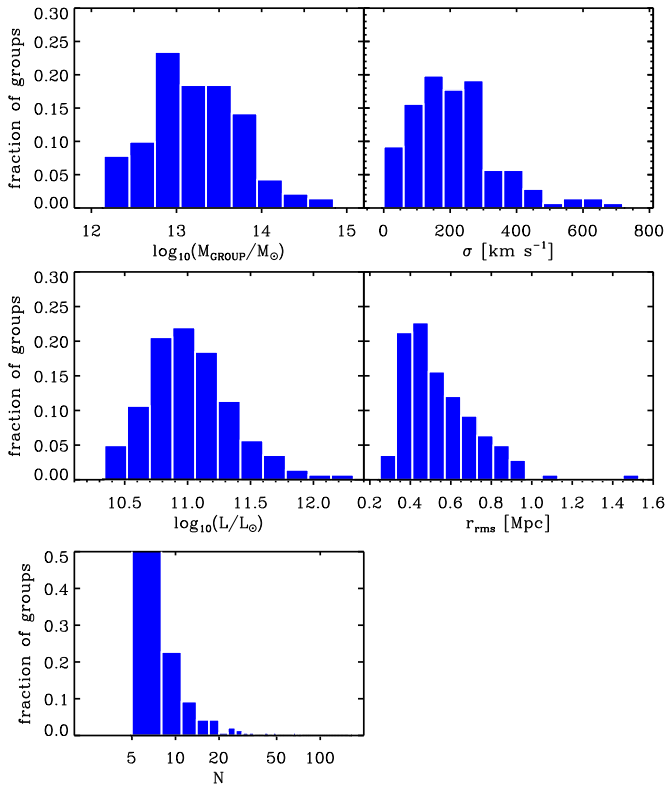

Figure 1. Distributions of main properties for the 141 ZENS groups. From left to right and top to bottom, we plot the distributions of ZENS group masses (derived as described in Section 3.1), velocity dispersions and luminosities, the distributions of projected rms galaxy separations within the groups, and the number of group member galaxies.

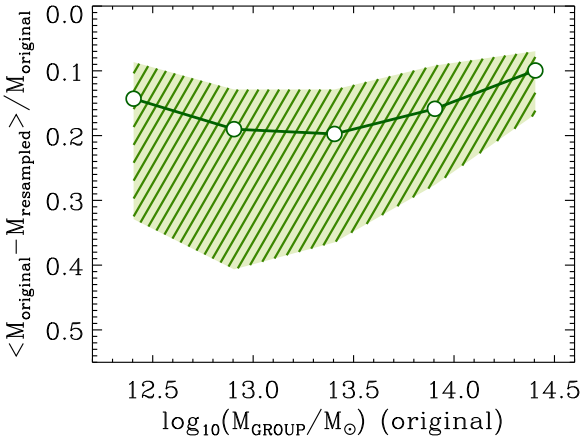

Figure 2. Quantification of the effect of interloper galaxies on group halo mass estimates. The global effect is an overestimate of typically ∼20% and up to ∼40% at low masses. The solid line shows the median of the distributions of differences, normalized to the fiducial mass of a group as determined in Section 3.1, between the fiducial mass ("original") and the mass in a given bootstrap realization ("resampled") obtained by removing, for each group, between 20% and 40% of the member galaxies (also including potential extra galaxies, as discussed in Section 3.1.1.1). The points are the corresponding averages within bins of group mass of width 0.5 dex; the shaded area shows the typical scatter around the median value.

The results are shown in Figure 2. The symbols in the plot are the medians, in different bins of group mass, of the distributions of differences, normalized to the fiducial mass of a group (as determined in Section 3.1), between the fiducial mass of that group ("original") and that in a given bootstrap realization ("resampled"). The shaded area shows the 1σ scatter around the plotted medians.

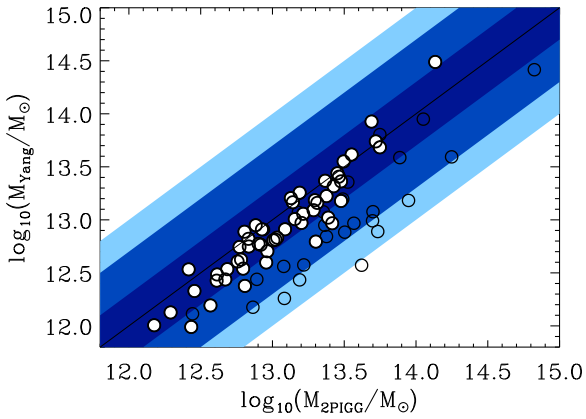

Figure 3. Comparison between the ZENS group masses as originally defined by the 2PIGG catalog and the mass of the cross-matched groups in the Yang et al. (2005) catalog. The latter are defined as the most massive groups in this catalog that are associated with each ZENS group. The shaded areas show a factor of two (dark-color strip), five (intermediate), and 10 (light-color strip) difference in mass. Groups that are fragmented into more than one group in the Yang et al. catalog are shown with empty points. Note that not all galaxies in ZENS groups are necessarily associated with groups in the Yang et al. catalog. ZENS groups that are associated with a single galaxy in the Yang et al. group catalog or are fragmented into sub-groups containing fewer than 40% of the 2PIGG members are not shown in this figure.

The uncertainty on the mass estimates driven by the presence of the interlopers is between 15% at the highest masses and 40% at and below $\sim 10^{13} M_{\odot}$; this trend with halo mass is a direct consequence of the trend with halo mass of the fraction of interlopers already assessed by Eke et al. We also note that the uncertainty on the group mass reported in Figure 2 is in the direction of an overestimate relative to the true value. This fact is the result of interlopers adding to the real group members and, by contrast, of a negligible number of galaxies having been "missed" by the FOF algorithm that was used to generate the parent 2PIGG sample.

To quantitatively assess this latter issue, we searched the parent 2dFGRS catalog for galaxies that in principle could have been physically associated with a 2PIGG group but were not included in that group by the 2PIGG algorithm. In particular, using similar criteria to those used to search for missed galaxies in the SDSS (Section 2.2.2 and Appendix B.1), we searched the 2dFGRS catalog for galaxies within ±30% of the redshift window of our ZENS groups, lying within a circular projected area, centered on the central galaxy, of radius equal to 1.5 times the rms radius of the group. We required that these galaxies were not associated with the given group by the 2PIGG algorithm. For those groups for which our centers differed from the original 2PIGG centers, the choice of using our own definition for the centers also enabled us to simultaneously test the impact of this definition on the resulting group membership.

Following these criteria, we found a total of 52 "extra" 2dFGRS candidate galaxy members for 24 of the ZENS groups. We present in Appendix B.3 details of the spatial and velocity distributions of these new candidates in relation to the galaxies that are identified as group members in the 2PIGG catalog, as well as the distributions of fiducial halo masses for the groups that may miss these extra candidates.

These potential extra members are found for relatively massive ZENS groups with $M_{\rm GROUP} \gtrsim 10^{13}\ M_{\odot}$. Including these potential galaxy members in the computation of the group masses has therefore a small effect at these mass scales, typically within 0.1 dex. Only for two groups is the difference between the fiducial group mass and the recalculated mass larger than this

value (of order 0.2–0.3 dex). We therefore conclude that missing 2dFGRS galaxies in the 2PIGG associations is not a dominant source of error in the computation of the fiducial ZENS group masses.

We conclude that interlopers are a ∼20% (at high group masses) up to ∼40% (at low group masses) source of overestimation of halo mass. Note also that interlopers may affect the identification of the central galaxies and thus the determination of the dynamical state of a group; again, the impact is expected to be larger at lower group masses, since the latter suffer from a higher fraction of interlopers (see discussions in Sections 3.2.2 and 5). Finally, as mentioned above, interlopers may also contaminate estimates of properties of galaxies in groups. To monitor the impact of interlopers on our ZENS analyses, we will systematically take into account the uncertainty on possible trends with halo mass that they introduce, as outlined in Section 3.1.1.4, and we will establish through statistical simulations the impact of their contamination on the global properties of group member galaxies.

3.1.1.2. Comparison with independent group catalogs for the 2dFGRS. Another question we ask is how sensitive are the halo mass estimates, as inferred in Section 3.1, to the details of the algorithm adopted for identification of the groups. To learn about this issue in a "post-processing" approach, we cross-matched the ZENS sample, extracted from the 2PIGG catalog, with the independent 2dFGRS group catalog, of Yang et al. (2005). In this catalog, the basic identification of potential groups also follows a FOF algorithm, but the final group membership—and hence properties—are iteratively refined, starting from the initial FOF estimates, by assuming that groups at any redshift are described by a Navarro–Frenk–White density profile (Navarro et al. 1997) and that the phase space distribution of galaxies is similar to that of dark matter particles. The membership assignment is made by comparing the local density contrast, calculated following the above halo occupation recipe, with a background level that is comparable to the density in the outskirts of a halo and that is chosen to minimize the contamination while maximizing the completeness of the groups.

Furthermore, the Yang et al. 2dFGRS catalog imposes a minimum redshift completeness of 80%. The parent 2dFGRS catalog adopted by Yang et al. hence excludes galaxies (the sample used is 25% smaller than the one in 2PIGG), which means that 128 of our 141 ZENS sample groups can be compared with the group catalog of these authors. Note that not all galaxies in a ZENS group are necessarily associated with a group in the Yang et al. catalog. In 21 of the 128 groups in common, only one galaxy is found in the Yang et al. catalog.

In practice, for any given group in the ZENS sample, we searched the Yang et al. catalog to determine in which of its groups the ZENS member galaxies were assigned. We associated the most massive of the Yang et al. groups so identified to the given ZENS group. We show in Figure 3 the comparison between the corresponding group masses in the two catalogs, for ZENS groups that are associated with Yan et al. groups that contain at least 40% of the original galaxy members.

The masses of the Yang et al. groups matching the ZENS groups are typically smaller than the fiducial ZENS masses, as estimated in Section 3.1. An inspection of the two cross-matched catalogs shows that, in most cases, the ZENS groups are fragmented into smaller subgroups in the Yang et al. catalog. This result is shown in Figure 4, which plots, for each of the 128 groups that appear in both catalogs, the position of the nominal 2PIGG member galaxies relative to their "central galaxy" (see Section 3.2.1), where the highlighting in different colors shows galaxies associated with different groups in the Yang et al. catalog. Note that some of the 2PIGG/ZENS groups are fragmented in this catalog into single galaxies. Factors that contribute to these differences include the attempt to take into account, in the Yang et al. catalog, of the effects of interlopers discussed above and also missing galaxies in the input 2dFGRS catalog that these authors adopt, as discussed above.

Indeed, in tests performed by Yang et al. (2005), these authors show that their grouping algorithm performs slightly better in terms of reducing the interlopers fraction with respect to the standard FOF algorithm used in 2PIGG, especially for the case of flux-limited samples (see their Figure 7). Overall, their fraction of interloper galaxies remains, however, at the ∼20% level, i.e., roughly comparable with the ∼20%–30% fraction estimated by Eke et al. (2004a) in their mock 2dFGRS catalogs for groups with $M \lesssim 10^{14}\ M_{\odot}$ (see their Figure 2). At the same time, the fragmentation of the 2PIGG groups in the Yang et al. compilation does not necessarily lead to a cleaner definition of the bound structures. This fact is illustrated in Figure 5, where we plot the velocities of the galaxies in the Yang et al. catalog with respect to the group mean redshift and the velocity of the nominal 2PIGG group members. Galaxies that are assigned to distinct groups in the Yang et al. catalog often have positions and velocities within the extremes in these quantities shown by the galaxies that are assigned to a single group by the 2PIGG algorithm.

The different group identification methods and treatments of interloper galaxies used in the two studies may furthermore affect the division into dynamically "relaxed" and "unrelaxed" groups, as well as the central versus satellite distinction. We discuss these topics in Section 5 and Section 3.2.1, respectively. Assuming that, ideally, fully virialized groups should be equally well identified in both catalogs, we can use mismatches in the identification of the state of a group ("relaxed" and "unrelaxed"; see Section 5) to assess how much this latter classification, as well as the identification of the central galaxies, is affected by the different algorithmic choices. To make a sensible comparison, we use ZENS groups for which at least 50% of the 2PIGG members fall in the Yang et al. galaxy selection, for a total of 121—67 and 54 of our "relaxed" and "unrelaxed"—groups, respectively, i.e., 86% of the ZENS catalog.

Reassuringly, the ZENS "relaxed" groups are well-identifiable structures with similar properties also in the Yang et al. catalog. A fraction ∼60% of our relaxed groups are matched by a single Yang et al. group with >50% of the original galaxy members, and in all but four of these groups (89%) the identification of the central galaxy is confirmed also in the Yang et al. counterparts. On the other hand, for "unrelaxed" groups, the fraction of 2PIGG systems that are matched by a single Yang et al. group with >50% of the original galaxy members decreases to ∼25%. This result supports the picture in which groups that are classified as relaxed are genuinely bound structures, coherently detected by both algorithms, while groups classified as unrelaxed are likely a more heterogeneous class, including both structures that are genuinely dynamically young as well as systems whose identification and characterization is affected by observational limitations. This fact suggests that only about a quarter of the nominally unrelaxed groups, i.e., about 10%–15% of all ZENS groups, are genuinely dynamically young systems in an early stage of assembly. This estimate is also supported by comparisons with the SDSS catalog; we performed these comparisons to quantify the impact of spectroscopic

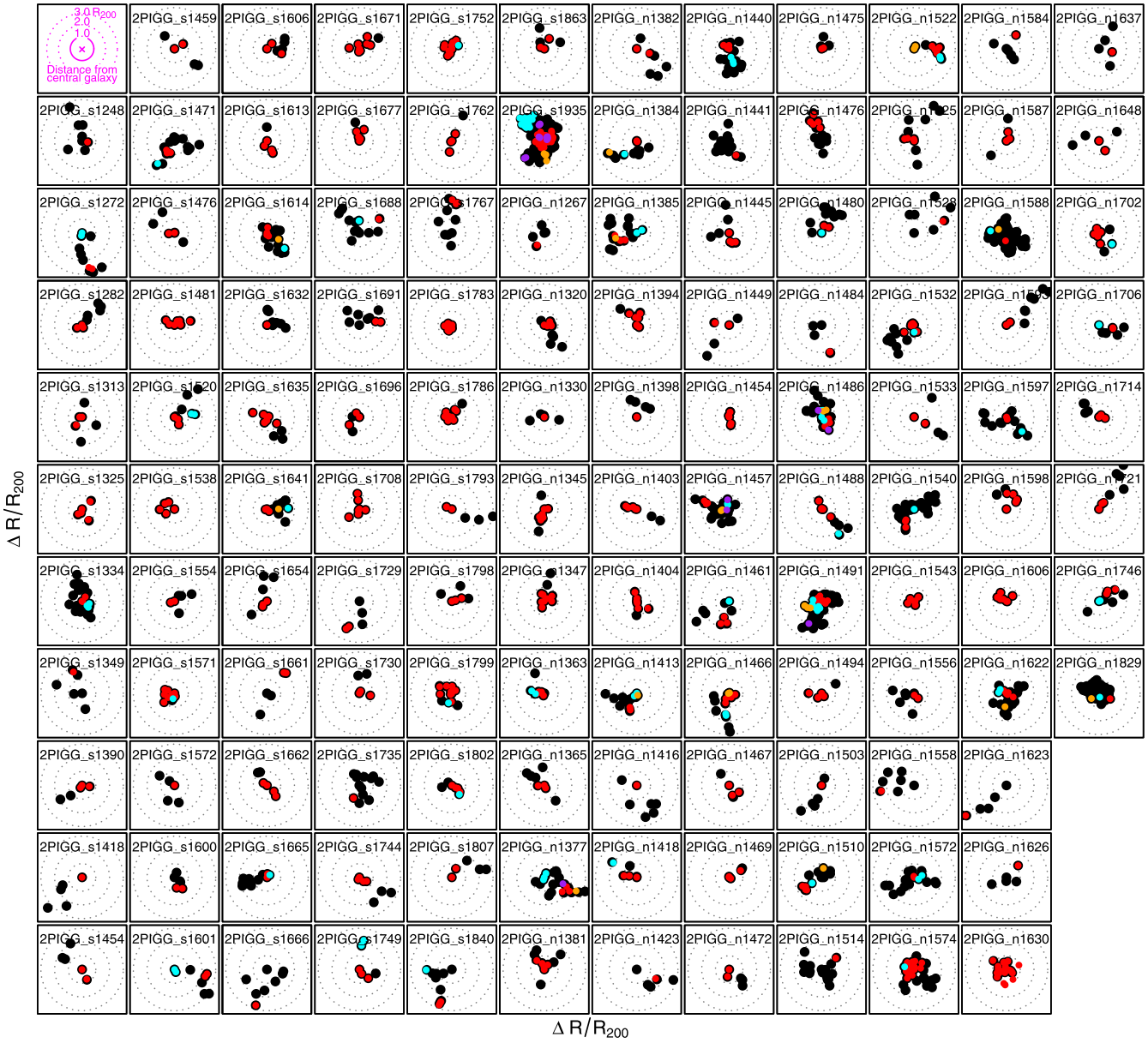

Figure 4. For each of the 128 ZENS groups that have at least one of the nominal 2PIGG members matching group in the Yang et al. (2005) group catalog, the spatial distribution is shown (black dots) with respect to the identified central galaxy. Highlighted with different colors are galaxies that are identified as members of different groups in the Yang et al. catalog (the same color identifies galaxies linked into the same group in the Yang et al. catalog; black symbols are galaxies that do not belong to any group in the Yang et al. compilation). Circles centered on the central galaxy mark halo-centric distances of $R/R_{200} = 1$, 2, and 3.

incompleteness in the 2dFGRS on the relaxed/unrelaxed classification. We also performed a group sub-clustering analysis (see Section 5).

In summary, it is important to keep in mind that different parent sample selections and grouping methods, e.g., those adopted in the Yang et al. and in the 2PIGG catalogs, can undoubtedly result in individual cross-matched groups with different properties (in particular, as already discussed, the Yang et al. sample has a systematically lower number of member galaxies and thus systematically lower group masses than the 2PIGG sample). Nevertheless, (1) for 75% of the ZENS groups, the difference in their mass estimates remains smaller than a factor of two. This uncertainty is comparable with the error in the total group mass that we estimated in Section 3.1.1.3 and does not affect our study of galaxy properties as a function of (also) group mass over about two orders of magnitudes in the latter; (2) the determination of the (apparent) "dynamical state" of the groups remains stable in the majority of cases, independent of the specific choices for the group identification algorithm; and (3) the identification of the central galaxies in relaxed groups is very robust.

3.1.1.3. How well do group halo masses inferred from the integration of luminosity functions approximate the true halo masses? Existing physical trends in galaxy properties with group mass may be smeared across different group mass bins and even washed out by the relatively large random and systematic errors in the estimates of the group masses. To quantify the uncertainties introduced by the specific algorithm of Section 3.1 that we adopted for computing the group masses, we used the Millennium simulation (Lemson & Virgo Consortium 2006)

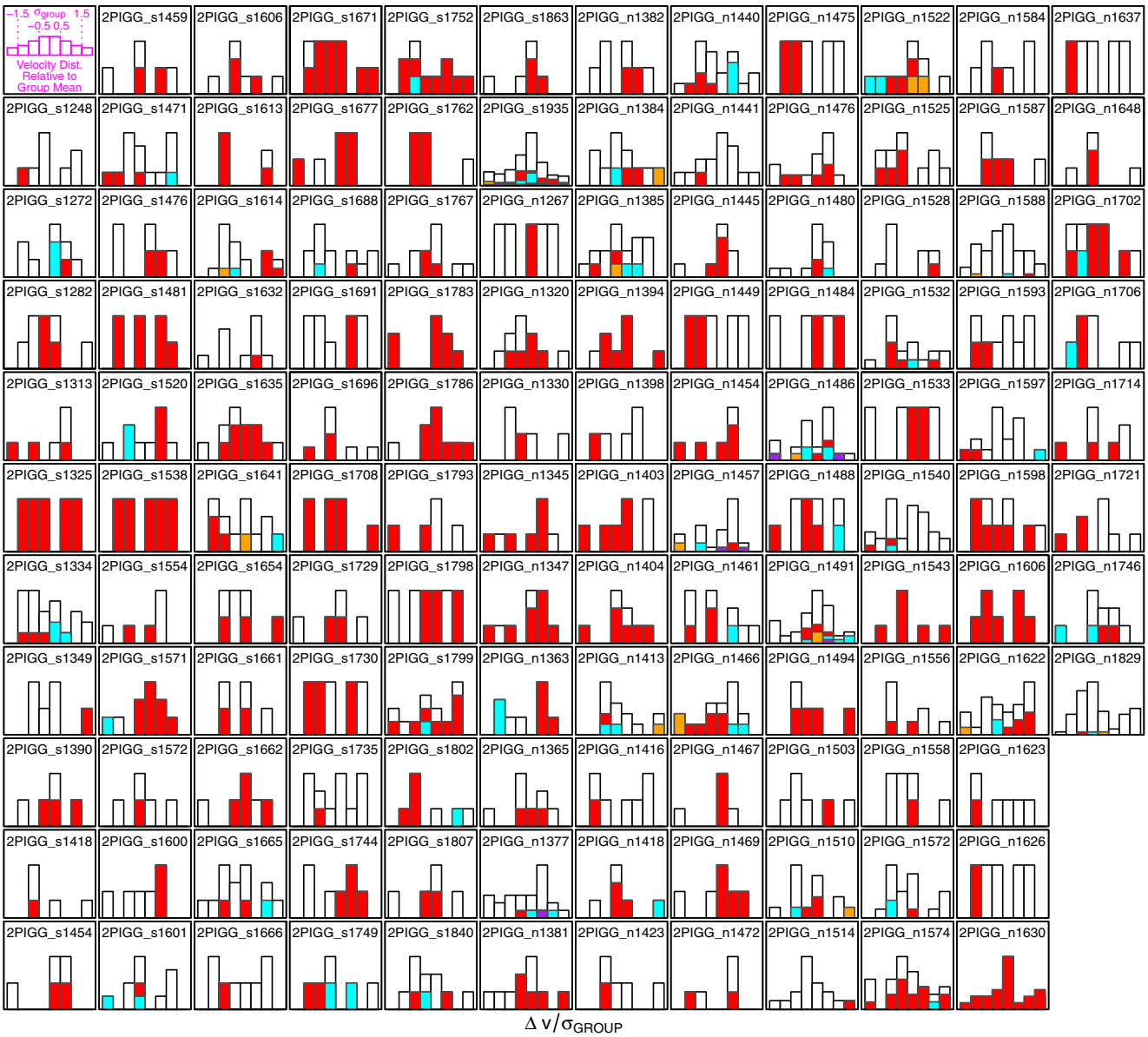

Figure 5. As in Figure 4, but for the distribution of velocities of 2PIGG group member galaxies relative to their group redshift (black histograms). Superimposed in a different color, using the identical color scheme as in Figure 4, are the corresponding histograms for galaxies that are identified as members of different groups in the Yang et al. (2005) catalog (same color for galaxies that are linked into the same group in the Yang et al. catalog).

with the semi-analytic model of De Lucia & Blaizot (2007). The model is not specifically designed to match the 2dFGRS properties and selection function; nonetheless, it allows us to gain useful insight of the limitations of our analysis.

Details of the model are given in the original reference. The dark matter component is taken from the Millennium simulation (Springel et al. 2005b); details of the baryon physics are added in the fashion that is customary in semi-analytic modeling of galaxy evolution. Recipes for gas cooling, star-formation, and active galactic nuclei and supernovae feedback are included. The typical baryonic resolution of the adopted models corresponds to a galaxy mass of $\sim 3 \times 10^9\ M_\odot$, comparable with the limiting mass of completeness for ZENS galaxies.

For each halo of mass above $10^{12.2}\ M_\odot$ in the volume, we computed the total 2dFGRS b_j luminosity of the host galaxies above the survey limit of $b_j = 19.45$. A thousand random realizations were obtained, sampling each halo with 80% of the galaxies, to simulate the spectroscopic completeness of our sample. The "inferred" halo mass was obtained by adopting the same approach that we used for the ZENS groups (see Section 3.1).

The comparison between the "true" dark matter halo masses and the halo masses inferred from the extrapolation of the group luminosity function is shown in Figure 6. The shaded area in Figure 6 shows the scatter around the median relation in 1000 realizations. The average trend tracks the 1:1 relation above $M_{\rm GROUP} \sim 10^{13.5}\ M_\odot$ with a modest scatter <10%. At lower group masses, the data tend to underestimate the true values on average at the ∼20% level, with a scatter up to 40%–50%. Not surprisingly, the scatter in the relation decreases with increasing mass of the group.

These uncertainties are comparable with the errors in the inferred group total luminosities as a function of number of member galaxies shown in Figure 3 of Eke et al. (2004b).

3.1.1.4. Summary: impact of the uncertainties on group masses on trends of galaxy properties with halo mass. The tests

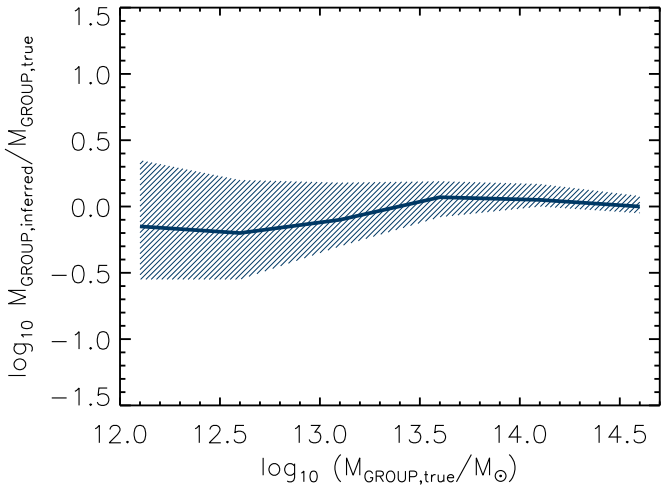

Figure 6. Relation between inferred halo mass, estimated from the total group luminosity as discussed in Section 3.1, and input ("true") dark matter halo mass from the De Lucia & Blaizot (2007) semi-analytic model applied to the Millennium simulation (Lemson & Virgo Consortium 2006). The shaded area shows the scatter around the median relation (solid line) obtained in 1000 random realizations.

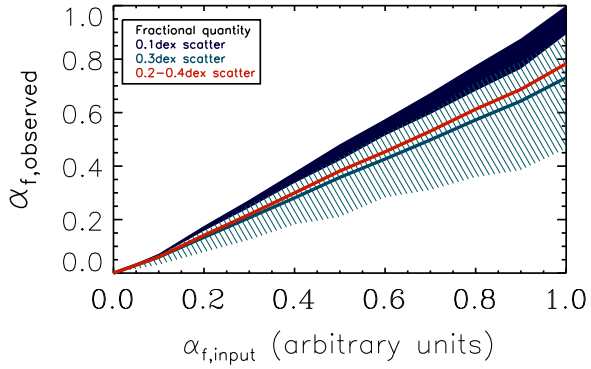

Figure 7. Effect of errors in the group masses on the measured slope $\alpha_{f,\rm observed}$ of the relationship with group mass of a given fractional property (e.g., fraction of quenched galaxies, etc.). Plotted are the effects of a 0.1 dex error (dark area) and 0.3 dex error (dashed area), assuming Gaussian errors for the group masses. The median relation for the typical case of a 0.3 dex error is highlighted as a solid line. The red solid line is the median $\alpha_{\rm observed}$-$\alpha_{\rm input}$ relation calculated assuming a 0.4 dex uncertainty in group mass at low group masses below $10^{13}\,M_{\odot}$ and an uncertainty decreasing to 0.2 dex at the highest group masses. Either considering an average 0.3 dex scatter or an increase in the error with decreasing halo mass returns similar results, namely (1) a correction factor of order ∼1.3 to recover the intrinsic slope $\alpha_{f,\rm input}$ of a trend with group mass, from the slope $\alpha_{f,\rm observed}$ that is measured using the full ZENS dataset; (2) an uncertainty of ∼0.05 on a flat relationship, i.e., for $\alpha_{f,\rm observed} = 0$.

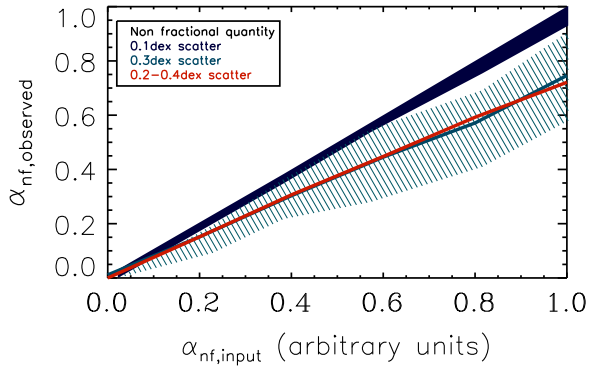

Figure 8. As in Figure 7, but for the case in which the studied property is not a fractional quantity. In this case, the errors on the group masses flatten the intrinsic slope of the relationship of this quantity with halo mass of a factor of order ∼1.4. The uncertainty on a flat relationship, i.e., $\alpha_{nf,\rm observed} = 0$, is ∼0.1. Symbols and colors are as in Figure 7.

above indicate that our fiducial group mass estimates suffer from a global uncertainty of about 0.3 dex, ranging from 0.2 dex at high group mass up to 0.4 dex at low group mass, which thus we consider to be the typical error on these estimates. We therefore ask what maximum trends in galaxy properties with group mass could remain undetected in our sample due to this level of uncertainty in the measurements of group masses. In other words, how strong a dependence of a given quantity on halo mass could disappear in our data due to the uncertainty in our practical realization of the group masses? We address this question by computing how much the observed slope of a measured trend can change with respect to the "true" one, given the statistical size of the total ZENS sample.

We consider the two cases in which the observed property is either a fractional quantity (for example, the fraction of "quenched" satellite galaxies of a given morphology in any of the environmental conditions that we study in ZENS that we present in C. M. Carollo et al. 2013b, in preparation, Paper IV), or a non-fractional quantity (for example, the colors of the bulge and disk components of these satellite galaxies)—see Figures 7 and 8. We split the simulated sample into two bins of group mass separated at $10^{13.5}\,M_{\odot}$. The $10^{13.5}\,M_{\odot}$ value is chosen because (1) it roughly divides our ZENS galaxy sample in two sub-samples of comparable sizes and it is also close to the median group mass in the ZENS sample (see Figure 1) and (2) it roughly represents the separation between typical "group" and "cluster" environments. We stress, however, that the results of the tests reported below are largely independent of the precise separating group-mass value that is used to define a low and a high group mass bin in our sample.

We impose as an initial condition for our test a similar number of galaxies in the low and high group mass bins as we have in our ZENS sample. For the case of a fractional quantity, we assume that each group has a total number of galaxies n_i of which k_i have a given property, producing a fraction f_i of galaxies in that group with this characteristic. As a starting point, we assume that the mass of the group is known without errors and that all groups in the low (high) group mass bin have initially the same $f_{i,\rm Low}$ ($f_{i,\rm High} = f_{i,\rm Low} + \delta_f$, where δ_f is the "intrinsic" difference in the two group mass bins). This methodology determines the slope $\alpha_f = \delta_f / \Delta \log_{10} M$ of the relationship between the fractional quantity under study and the group mass. For simplicity, in the analysis, we set $\Delta \log_{10} M = 1$ so the values of α_f vary between zero and one. We calculate the global input fractions $f_{\rm Low}$ and $f_{\rm High}$ of all galaxies in the low- and high-mass bins, which give the assumed "input" (i.e., true) slope of the relation. A thousand realizations of the sample are then obtained by perturbing the initial group masses with logarithmic random Gaussian errors, for several initial $f_{i,\rm Low}$ values spanning the range [0, 0.9]. Due to the errors, groups in the high group mass bin will move into the low group mass bin and vice versa. The observed fractions $\tilde{f}_{\rm Low}$ and $\tilde{f}_{\rm High}$ are computed for each realization of the error-perturbed sample and the resulting new slopes are estimated.

In Figure 7, we show the comparison between the input (true) slope $\alpha_{f,\rm input}$ with the output, error-affected slopes $\alpha_{f,\rm observed}$. This comparison enables us to assess the impact of the group mass errors on our capability to measure the input, true slope of any trend with group mass that we seek to measure. In the figure, the two shaded areas bracket the minimum and maximum resulting slopes resulting from 0.1 dex (dark color) and 0.3 dex (dashed area) perturbation amplitudes, respectively, around a

given value of the input slope. The solid line is the median relation for the typical 0.3 dex uncertainty in ZENS group masses; the red line shows the result obtained by varying the uncertainty with halo mass between 0.2 dex (at high group masses) and 0.4 dex (at low group masses), as determined above.

As expected, the effect of the errors on the group masses leads to an underestimation of the slope of any relationship of fractional galaxy properties with this environmental quantity. Nevertheless, the ZENS data enable us to detect even moderate trends with group mass. A median "correction factor" can be estimated from this test, i.e., $\alpha_{f,\mathrm{input}} \sim 1.3 \times \alpha_{f,\mathrm{observed}}$, with an uncertainty of order $\sim$0.05 for a flat relationship with $\alpha_{f,\mathrm{observed}} \sim 0$.

To establish the error on trends with group mass for non-fractional quantities, we assumed that all groups in the low group mass bins have an initial distribution of such a quantity with a certain mean value, equal to $\langle q_{nf,\mathrm{Low}} \rangle$, and a standard deviation equal to $\sigma_{nf} = 0.2$. The groups in the high group mass bin have an initial distribution of values with the same dispersion as the low-mass groups, but centered at $\langle q_{nf,\mathrm{High}} \rangle = \delta_{nf} + \langle q_{nf,\mathrm{Low}} \rangle$, where $\alpha_{nf} = \delta_n f / \Delta \log_{10} M$ is the slope of the relationship between the non-fractional quantity under study and the group halo mass. We exemplify this case in Figure 8 by setting $\langle q_{nf,\mathrm{Low}} \rangle = 0$ and exploring a range of $\langle q_{nf,\mathrm{High}} \rangle$ from zero to one in arbitrary units. Again, we set $\Delta \log_{10} M = 1$, so that the slope will vary between zero and one as well. Starting from the given initial condition, we perturb the group masses with 0.1 and 0.3 dex Gaussian errors, as before, and also with an increasing error with decreasing group mass from 0.2 dex at the highest masses to 0.4 dex at masses below $10^{13}\ M_{\odot}$, and recalculate the average values, deviations, and difference of the measurements between the low and high groups mass bins, as above. Figure 8 shows that the observed slope $\alpha_{nf,\mathrm{observed}}$ is typically $\sim$1.4 times flatter than the true slope $\alpha_{nf,\mathrm{input}}$ (both considering an average 0.3 dex scatter and an increase in the error with decreasing halo mass, as both these cases again return similar results). Also, an observed $\alpha_{nf,\mathrm{observed}} \sim 0$ may hide an intrinsic slope of $\sim$10%.

These tests give us a benchmark for interpreting correctly the trends with group mass that we explore in ZENS.

3.2. Environments Number Two and Number Three: Galaxy Distance from the Group Center and The Central/Satellite Dichotomy

Galaxies may suffer environmental effects as they enter or orbit the dark matter halos of their host groups. Also, central and satellite galaxies are expected to experience different physical conditions as they evolve with cosmic time (Somerville & Primack 1999; Simha et al. 2009). Ideally, we would want to know the precise location and velocity vector of each galaxy within the three-dimensional potential of its host group halo, relative to the characteristic size of the halo, e.g., taken here to be the R_{200} radius at which the density in the halo is a factor 200 higher than the density of the universe at the redshift of the structure. A valuable proxy for this size is given by the projected distance of the galaxy from the assumed center of the group; this quantity is what we use in our studies to explore the dependence of galaxy properties on the location of galaxies within their host groups.

While simulations easily assign the rank of central or satellite to a galaxy in a common halo, with real data determining which is the central galaxy and which are its satellites is not without challenges. Likewise, it is difficult to establish group centers. We therefore adopt an operational definition, and subsequently establish the impact on the final results of our choice.

To separate central galaxies, assumed to sit on the center of the groups, from satellite galaxies, assumed to orbit the central galaxies within the group potentials, previous works have typically adopted galaxy luminosity (e.g., Weinmann et al. 2006b; Skibba 2009; Hansen et al. 2009) or stellar mass (e.g., van den Bosch et al. 2008; Guo et al. 2009; Kimm et al. 2009). In some cases, stellar mass has been adopted in addition to luminosity (e.g., Peng et al. 2012). For our sample, the 2PIGG catalog (Eke et al. 2004a) provides a group center determined with an iterative approach: the weighted mean position of the member galaxies is calculated and the most distant galaxy is subsequently rejected until only two galaxies are left, at which point the center of the given group is associated with the galaxy with either the larger "weight" that models the local incompleteness of the 2dFGRS data, or, in the case of identical weights, the galaxy with the larger flux is adopted as the central.

In our work, we scrutinized three different definitions for the center of a group, i.e., the 2PIGG centers, the geometric center of stellar mass, and the (center of the) galaxy with the largest stellar mass. Ultimately, we opted for the last definition as our fiducial estimate for the group center and central galaxy of a group; however, we imposed that the resulting central galaxy should satisfy a consistency requirement for it being also at the spatial and velocity center of the group. Furthermore, in determining which galaxy had the highest mass, we considered not only the mass estimates provided by the "best-fit" templates to the observed galactic SEDs, but also the errors in these estimates. We discuss in detail below (Section 3.2.1) our procedure for identifying the central galaxies and the centers of the groups.

In order to derive an estimate for the characteristic projected radii, given the uncertainties in the group velocity dispersions mentioned above, we used our fiducial total group masses and derived $\hat{R}_{200} = (GM_{\mathrm{GROUP}}/[10H(z)]^2)^{1/3}$, where $H(z) = H_0\sqrt{\Omega_M(1+z)^3 + \Omega_\Lambda}$ is the Hubble constant at a given redshift. Note that we use the measured values of M_{GROUP}, which are assumed to be proportional to the M_{200} values; for this reason, we have distinguished $\hat{R}_{200} \neq R_{200}$. For simplicity, however, we will drop the $\hat{R}_{200}$ notation, but it should be kept in mind that a conversion factor is needed to rescale our size measurements to the formal R_{200} values.

3.2.1. A Non-trivial Challenge: Which is the Central and Which are the Satellites?

If we used solely luminosities or nominal best-fit stellar masses for the identification of centrals and satellites, an inspection of the properties of our ZENS groups and their central galaxies highlights some shortfalls in all those definitions. For example, Peng et al. (2012) combine a luminosity requirement with a stellar mass requirement to determine the central galaxies in their SDSS group sample so as to minimize the effects of recent star formation or dust reddening in the identification of the centrals; these effects can be substantial in a luminosity-based approach, especially when stellar mass dependent biases are introduced. It is clear, however, that the identification of "the most massive galaxy" is affected by random and systematic errors in the derivation of galaxy stellar masses; these errors are not customarily included in the identification of the central galaxies.

A result of these shortfalls is that the alleged central galaxies that are identified based on a luminosity or even a best-fit stellar mass criterion often lie at the projected spatial or kinematic outskirts of the groups, while they are supposed to be at the centers. We have tested that this fact holds in both two most currently used clustering-based group catalogs of Yang et al. (2007; for the SDSS) and Eke et al. (2004a; for the 2dFGRS). For example, identifying the group center with the nominal most massive galaxies, we find that roughly 50% of the ZENS groups suffer from this unphysical "displacement" of their own alleged centers. Other authors have addressed the issue of contamination and/or incompleteness in samples of central versus satellite galaxies, at least in terms of establishing global statistical effects (without, however, applying an active correction to their final analysis). For example, Weinmann et al. (2009) tested their grouping algorithm against SDSS mock catalogs and found a contamination of ∼30% of centrals in their sample of satellites and vice versa. Skibba et al. (2011) find that the brightest halo galaxy is often a satellite and not the central one; the probability that a satellite galaxy is more luminous than the central galaxy appears to increase with halo mass (reaching ∼40% at $\sim 10^{14}\ M_{\odot}$).

In our study we implemented a procedure for improving the identification of the central galaxies. This procedure also gives insight into the origin of central versus satellite contaminations. In detail, we scrutinized the properties of the nominal most massive galaxies for each group in our sample and we retained these objects as "centrals" only if they were compatible, within the errors on the stellar mass estimates, with being the most massive galaxies in their groups. Furthermore, we required that these objects result in self-consistent solutions in the (projected) spatial and (line-of-sight) velocity domains. That is to say, for a galaxy to be a good central in a group halo, it must be its most massive inhabitant *and* it must be compatible with the inferred spatial and velocity centroids of the halo. For cases in which the galaxy with the highest formal best-fit stellar mass did not satisfy simultaneously these criteria, we either found an alternative galaxy within the group that provided such a self-consistent solution or we flagged the group as "unrelaxed," in order to keep in our analyses the information that, for this system, none of the member galaxies satisfied all conditions for being genuine "central" galaxies.

Quantitatively, we implemented these criteria by requiring that not only (1) the central galaxy be the most massive member of the group "within the errors" of our stellar mass estimates, but also that (2) its projected location lies within the inner circular area centered on the stellar mass-weighted geometric center of the group and enclosed within a radius 0.5 R_{200}. Furthermore, we required that (3) its inferred line-of-sight velocity lies within one standard deviation of the median of the velocity distribution for that group.

We started the procedure highlighted above by assuming the best-fit (i.e., minimum χ^2) masses that result from fitting for the fiducial stellar masses of ZENS galaxies. We used the code *ZEBRA+* (Feldmann et al. 2006; Oesch et al. 2010), a large library of synthetic models of galaxy SEDs.[8] The adoption of these fiducial stellar masses leads to the identification of a nominal central galaxy, i.e., the galaxy member in a group that has the largest fiducial best-fit stellar mass. We then checked the spatial and velocity location of these nominal centrals. For each of the 141 ZENS groups, we show in Figure 9 the location of the member galaxies relative to the mass-weighted geometric group centers; in each panel, the radial scale is set by our estimate of R_{200} for the given halo. The nominal most massive member of each group is indicated with a yellow point. Light and dark blue points represent galaxies with masses within a factor of two and four of the nominal most massive galaxy, respectively. Less massive group members are shown as black dots. For each of the groups, the corresponding velocity distributions are shown in Figure 10. Here, each panel presents the relative line-of-sight velocity distribution about the median of the distribution, with the scale set by the distribution's dispersion. The position in velocity of each individual galaxy is indicated with an arrow, using the same color coding as in Figure 9 for the nominal most massive member of each group, galaxies with nominal stellar masses within a factor of two and four from the nominal most massive galaxy, and lower mass galaxies (yellow, light and dark blue, and black arrows, respectively).

In about 50% of the ZENS groups, the nominal centrals were confirmed to be fully consistent, both spatially and in terms of velocity, with lying at the bottom of the potential well of their host groups. We thus confirmed these galaxies to be genuine centrals and identified with them the centers of the groups. The yellow points/curves identifying these central galaxies in Figures 9 and 10 (and Figure 11; see below) are highlighted in green for these groups. In the remaining ∼50% of groups, however, the nominal centrals were either at the spatial periphery of their group halos or appeared to be "shooting away" from the halos in terms of relative velocities within their host groups. We thus investigated whether these results could be due to uncertainties in our galaxy stellar mass estimates (see Paper III).

To address this issue, we capitalized on the availability of the entire posterior probability distributions (PPDs) for the stellar masses. These PPDs are presented in Figure 11. Specifically, each panel in this figure shows the PPDs of the stellar masses for the few most massive galaxies in each of the ZENS groups. For each of the plotted galaxies, the PPDs are obtained by connecting 21 sampling points spanning the 1 to 99% quantiles. In each panel, the horizontal scale is logarithmic in mass and covers the range between one-tenth (leftmost value) to three times (rightmost value) the nominal highest mass; the PPD for this nominal highest mass galaxy is highlighted again in yellow. Also, the remaining colors are as in Figures 9 and 10, i.e., light and dark blue curves indicate galaxies with nominal (best-fit) stellar masses within a factor of two and four, respectively, of the nominal highest mass for that group. Note that in several groups there are galaxies, with nominal masses within a factor ∼2–4 from the nominal highest mass that would thus be classified as "satellites," which however have, according to their PPDs, a substantial probability that their stellar masses are actually larger than the nominal largest stellar mass of the nominal central.

For the groups in which the nominal (best fit) most massive galaxy failed to pass the projected-spatial criterion and/or the line-of-sight velocity criterion to be a genuine central galaxy, we thus searched for an alternative viable central that (1) satisfies both the spatial and velocity criteria, (2) has a nominal stellar mass within a factor of four of the nominal highest mass for that group, and (3) has a $\geqslant$10% probability, as defined

[8] The stellar masses for the ZENS galaxies were derived by combining the *B*- and *I*-band WFI photometry with the available multi-wavelength archival photometry (SDSS *u*, *g*, *r*, *i*, *z* (Abazajian et al. 2009), the 2MASS *J*, *H*, *K* (Skrutskie et al. 2006), and the *GALEX* NUV and FUV magnitudes; see Paper III for details on the procedure adopted to derive and calibrate the stellar masses). Note that, in our ZENS analyses, we adopt for the definition of galaxy stellar mass the integral of the star formation rate, i.e., we do not subtract the mass "returned" to the gas through stellar evolution processes.

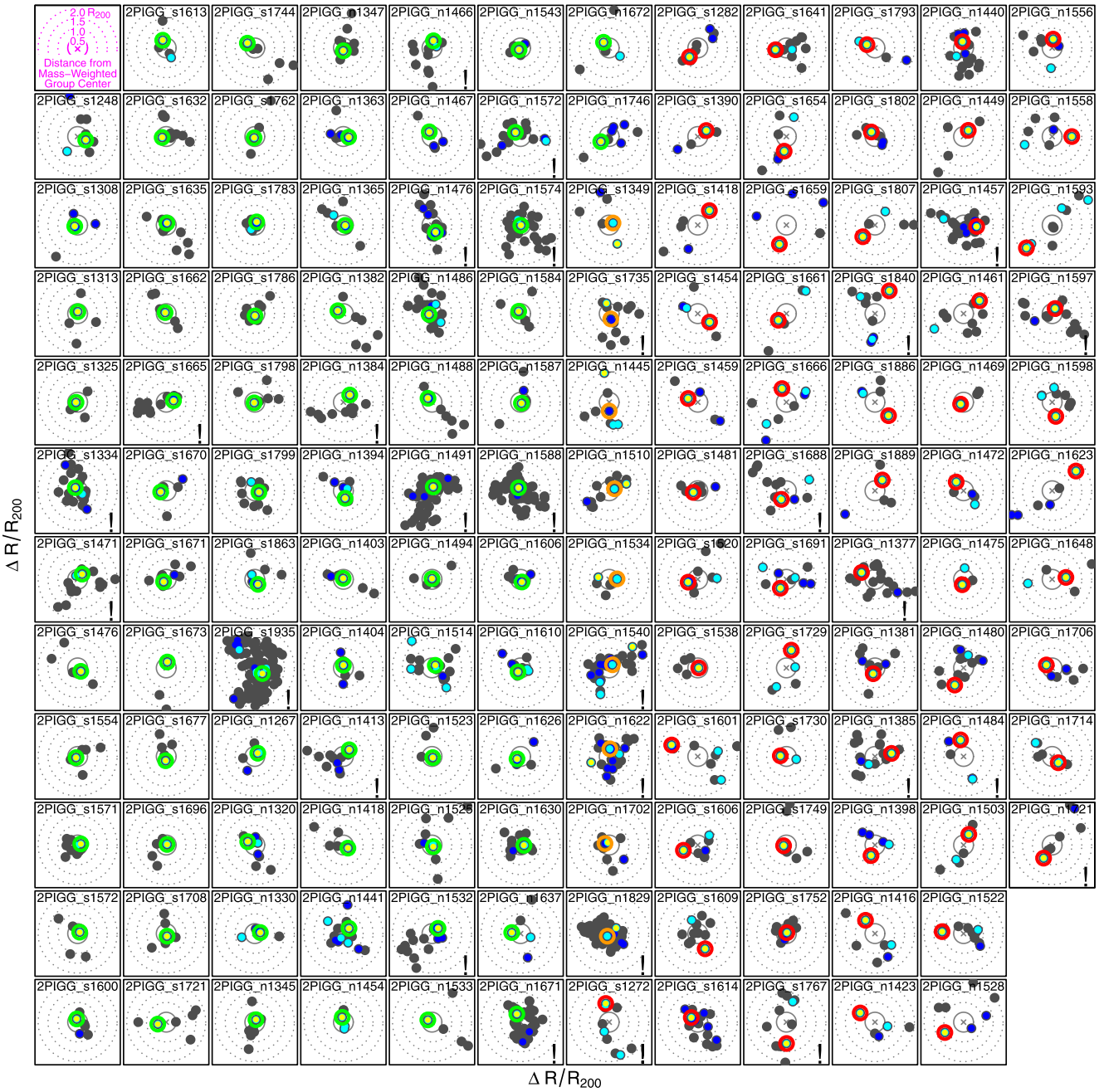

Figure 9. Spatial distributions of galaxies in each of the 141 ZENS groups. Each panel presents the (projected) radial distribution around the mass-weighted geometric center in each group, with the scale set by our estimate of R_{200} for that halo. Concentric circles mark galactocentric distances of 0.5, 1.0, 1.5, and 2.0 R_{200}, respectively, to the mass-weighted center of the groups (marked by gray crosses, not always visible). Yellow symbols indicate the nominal most massive member of each group, based on our fiducial definition of the stellar mass of a galaxy, i.e., the best-fit stellar mass obtained by fitting a large number of synthetic templates, spanning a large range of star formation histories, to the observed galaxy SED. Light and dark blue symbols represent galaxies with nominal stellar masses within a factor of two and four, respectively, from the nominal highest mass in the group. Green and orange circles around the symbols for the galaxies assumed to be the centrals identify groups that we have labeled as "relaxed"; red circles identify "unrelaxed" groups. Green identifies groups in which, based on spatial and velocity considerations, the nominal most massive galaxy in the group is confirmed to be the central galaxy. Orange identifies groups in which the nominal most massive galaxy is not consistent in the spatial and/or velocity domain with being the center of the group, but another galaxy member in the group (1) has an integrated probability $\geqslant$10% of having a stellar mass higher than the nominal most massive galaxy, and (2) also satisfies the spatial and velocity criteria described in the text. These alternative most massive galaxies highlighted in orange, are assumed to be the central galaxies of their host groups. The groups marked with a "!" are those for which the WFI pointings did not cover their entire extent; some galaxy members located at the group outskirts have been missed, but these are low-mass galaxies, unlikely to be the centrals. In general, missed galaxies do not impact the analyses of the central galaxies (see Appendix B for details).

by the overlapping area with the PPD of the most massive member, of exceeding the minimum mass in the PPD of this dominant galaxy. We found nine ZENS groups for which such viable alternative centrals could be identified, which we adopted as the correct central galaxies in these groups. These alternative centrals are highlighted with orange contours around the relevant symbols in Figures 9, 10, and 11.

For the remaining 59 groups, this iterative procedure failed to identify a galaxy member that satisfied the set criteria for being a genuine central galaxy. For these groups, the nominal

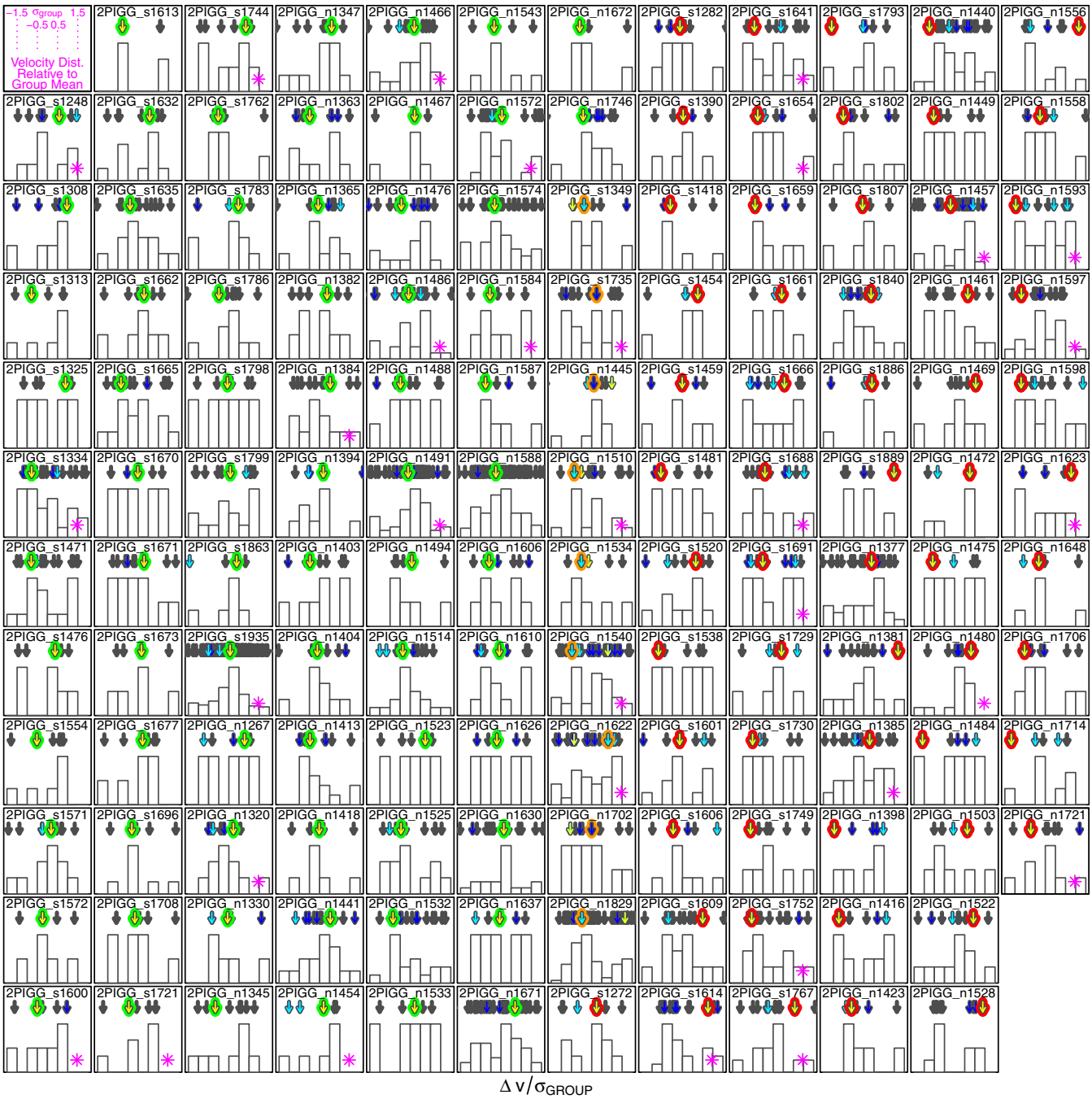

Figure 10. Line-of-sight velocity distributions of galaxies in the 141 ZENS groups. Each panel presents the velocity distribution relative to the median redshift of the group; the eight bins from left to right indicate velocities equal to −2, −1.5, −1.0, −0.5, 0, 0.5, 1, 1.5, and 2 the value of $\sigma_{\rm GROUP}$, respectively (i.e., the velocity scale is normalized to the velocity dispersion of each individual group). Note that only galaxies with velocities between $-1.5\sigma < v < 1.5\sigma$ are plotted here and that arrows showing individual galaxies may be overlapping in some of the panels. This overlap implies that for a few groups, not all galaxy members are visible in this figure. The velocities of individual galaxies are shown with an arrow, using the color coding as in Figure 9. The magenta stars identity those groups that show sub-clustering according to the criteria described in Section 5.1.

most massive galaxy was thus retained as the nominal central, but we flagged these groups so as to be able to estimate the impact of their inclusion in analyses that rely either on a central/satellite separation or the knowledge of the group center. These "dubious" centrals are highlighted with red contours around the symbols in Figures 9, 10, and 11.

In about a third (45) of the ZENS groups, the central galaxy thus identified coincides with the original central galaxy provided by the 2PIGG catalog. In the remaining 96 groups, we find, however, a different solution. The 2PIGG centers were iteratively identified from the galaxies positions, without any knowledge of the galaxy masses. Our approach should thus provide more robust estimates for the group centers, especially for sparse and small groups. We note that a change in the identification of the central galaxy has no impact on the FOF association of the group members and thus on the group identification, which is done prior to the definition of the center itself.

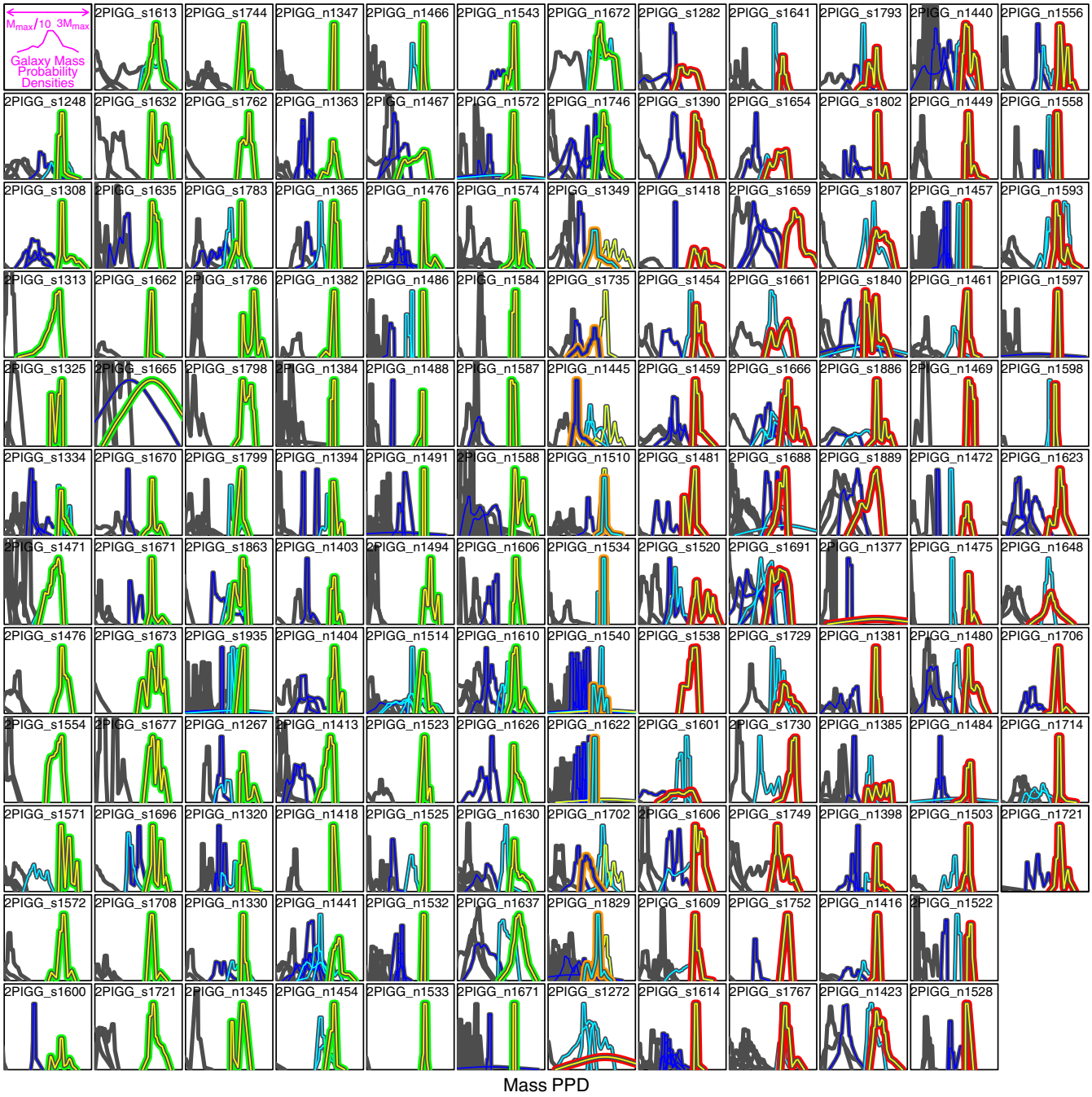

Figure 11. Posterior probability distributions (PPDs) of galaxy stellar masses for the top few most massive galaxies in each ZENS group. The PPDs are derived by connecting 21 sample points spanning the 1%–99% quantiles for the stellar masses obtained by fitting a large set of synthetic templates to the observed galaxy SEDs. The horizontal scale is logarithmic in mass and ranges from one-tenth to three times the nominal (best-fit) mass of the most massive member. The color-coding is as in Figures 9 and 10. Gaussian PPDs are assumed for galaxies that do not have WFI *B*- and *I*-band images (due to the limited coverage of the WFI pointings); for these, the stellar mass is inferred from the r_F −mass relation (see Appendix B.2). The widths of the Gaussian correspond to 1.5 times the observed scatter in this relation.

3.2.2. Sources and Effects of Errors on Our Fiducial Centrals and Group Centers

The fiducial centers and centrals defined above are correct within a certain statistical uncertainty. In addition to introducing uncertainties in the estimates of the total masses of the groups, as discussed in Section 3.1.1.1, the presence of interlopers and the absence of genuine group members from the 2PIGG lists (which define the groups in our sample) can also affect the identification of the central galaxy and thus the identification of the center of the groups. We discuss this issue in more detail in Appendix B. Here, we highlight that, based on our own test of comparison between the 2dFGRS catalog and the SDSS spectroscopic and photometric catalogs (Abazajian et al. 2009), we expect that these effects should lead to the misidentification of the central galaxies in at most ∼10% of cases. The dominant source of error in the identification of centrals and satellites remains the association of galaxies with a given group through the 2PIGG algorithm. We will discuss the impact of such an uncertainty on each individual analysis that relies on either a central-satellite split or the identification of the group centers.

3.3. Environment Number Four: The Backbone Density Field of the Large-scale Structure

A major achievement of recent large spectroscopic redshift surveys, and large multi-wavelength imaging surveys with accurate photometric redshifts, has been enabling the determination of a proxy density field produced by the LSS. The projected overdensity at a position θ in celestial coordinates, at a given redshift z, is defined as $\delta_{\rm LSS} = (\rho(\theta, z) - \rho_m/\rho_m)$, where $\rho(\theta, z)$ is the comoving projected density of the tracers of the density field and ρ_m is the mean projected density calculated over the global survey area at the given redshift. Several approaches have been used to derive LSS density fields, e.g., measuring the density within a fixed volume (e.g., Hogg et al. 2003; Blanton et al. 2005; Wilman et al. 2010), using Voronoi–Delaunay techniques (Schaap & van de Weygaert 2000; Marinoni et al. 2002; Gerke et al. 2005; Romano-Díaz & van de Weygaert 2007; Knobel et al. 2009; Gerke et al. 2012), and adaptive approaches in which the density is calculated out to the distance of a *N*th-nearest neighboring galaxy (e.g., Gómez et al. 2003; Balogh et al. 2004; Baldry et al. 2006; Kovač et al. 2010a).

All of these methods have their virtues and shortfalls, as extensively discussed in the previous literature. The *N*th-nearest galaxy neighbors technique is often preferred to the "fixed volume" approach because the latter washes out information on scales of order of the adopted volume; however, the *N*th-nearest neighbor technique has the strong disadvantage that it shifts its physical meaning from density "within a halo" to density "between halos" for galaxies that reside in groups of richness straddling the chosen value of "*N*" (see also Peng et al. 2012 for a discussion on the correlation between *N*-nearest galaxy neighbor overdensity and group membership). The Voronoi/Delaunay tessellation technique, thanks to its adaptive nature, performs generally better then algorithms based on a fixed aperture, but can be affected by biases related to survey edge effects, redshift-space distortions, and spectroscopic incompleteness (see the discussion in, e.g., Cooper et al. 2005; Kovač et al. 2010a). More generally, as discussed also by Haas et al. (2012), all methods contain a built-in correlation with halo mass, which hampers separating the effects on galaxies of the LSS from those of the host halos. To achieve an environmental LSS that is insensitive to halo mass, these authors construct a density field based on dimensionless galaxy luminosities/masses and distances.

In our study, we opt for an alternative approach both to avoid that the estimator changes meaning (from an intragroup to an intergroup density estimator) with varying group richness, and to minimize the correlation between halo mass and LSS density field that is introduced by construction when using a *N*th-nearest-galaxy method approach. In particular, we adopt an *N*th-nearest-neighbor estimator, but modified so as to use the groups themselves (treated as point masses of mass $M_{\rm GROUP}$) as tracers of the LSS density field, rather than their member galaxies. Thus, $\rho(\theta, z) = \sum_i^N w_i/(\pi d_N^2)$, where N is the chosen number of nearest (point-mass) groups (which we set to 5), d_N is the comoving distance to the Nth neighbor group, and w_i are the weights, which we set equal to $M_{\rm GROUP}$. Note that in our analysis, by construction, all galaxies belonging to a given group are characterized by the same value of LSS overdensity $\delta_{\rm LSS}$.

The entire 2PIGG group catalog, supplemented by all remaining "ungrouped" galaxies in the 2dFGRS (treated as groups with one galaxy member), was used to derive this *N*th-nearest group-neighbors overdensity field $\delta_{\rm LSS}$. Note that by "ungrouped galaxies" we mean the 2dFGRS galaxies that do not belong to any 2PIGG group; this fact does not necessarily imply that such galaxies are located in void regions (see also Appendix C). Halo masses for ungrouped galaxies were calculated following the same procedure adopted for the groups; a correction to total luminosity was applied, which assumes that these ungrouped galaxies have companions fainter than the survey magnitude limit (see Section 3.1). We note that densities calculated at the edges of the 2dFGRS area are biased as a consequence of the limited area of the survey. To correct for this effect, we followed the approach of Kovač et al. (2010a) and divided the computed density for the fraction of the area enclosed within d_N that is covered by the 2dFGRS pointings. For each group, the search for neighboring groups was restricted within a redshift interval of $dz = \pm 0.01$; a minimum luminosity was set for the groups or ungrouped galaxies equal to the total (i.e., integrated to zero) luminosity of a single $b_j = 19.1$ galaxy at redshift $z = 0.07$.

While the fiducial $\delta_{\rm LSS}$ estimates that we use in our analyses are based on the fifth-nearest-neighbor groups, we also computed third- and tenth-nearest-group estimates and checked that our main results do not depend on which of these representations of the LSS density field we use. The comparison between these three estimates is shown in Appendix C, where we also discuss for completeness a comparison of our fiducial $\delta_{\rm LSS}$, which uses the groups as point-mass tracers of the LSS, with the more commonly used density field derived by using the *N*th-nearest individual member galaxies as tracers of the matter density along cosmic filaments.

The final distribution of $\delta_{\rm LSS}$ values for the ZENS groups (and thus galaxies within the groups) is presented in the left panel of Figure 12 as dashed histogram and compared with the complete parent samples of 2PIGG groups in the redshift range $0.035 < z < 0.075$ (solid histogram). Not surprisingly the ZENS sample is shifted toward higher density regions compared with the global distributions of 2PIGG groups, which extend down to smaller associations of two members only (and are in turn shifted to higher densities relative to the whole 2dFGRS catalog, which also includes ungrouped galaxies). Note that our fiducial estimate of $\delta_{\rm LSS}$ does not produce the tail at very high overdensities that is observed when the individual galaxies are used as tracers in *N*th-nearest neighbor calculations of the LSS density field (see Appendix C); this high-density tail is indeed mostly due to small inter-galaxy separations *within* massive halos with richnesses larger than the adopted "*N*" value.

To enable comparisons with the global galaxy population (in addition to relative comparisons within the ZENS sample), we split the distribution of $\delta_{\rm LSS}$ sampled by the entire 2PIGG catalog in four quartiles (one to four in order of increasing density). We adopt the convention that ZENS groups reside in *low* LSS environments if the local overdensity is lower than the value characterizing the first quartile of the global 2PIGG distribution (dashed vertical line in the left panel of Figure 12). Similarly, ZENS groups that reside within local overdensity larger than the threshold defining the fourth quartile (solid line in the left panel of Figure 12) are said to be in a *high* LSS density region. The remaining groups reside in regions of the LSS of *intermediate* density. As indicated in Table 1, applying these criteria results in 8%, 37%, and 55% of ZENS groups being located in low, intermediate, and high density environments, respectively.

Note that, as shown in the right panel of Figure 12, the $\delta_{\rm LSS}$ values that we have adopted to describe the underlying density of the cosmic web do correlate, as expected, with the mass of the groups. Given the approach that we have used to compute $\delta_{\rm LSS}$,

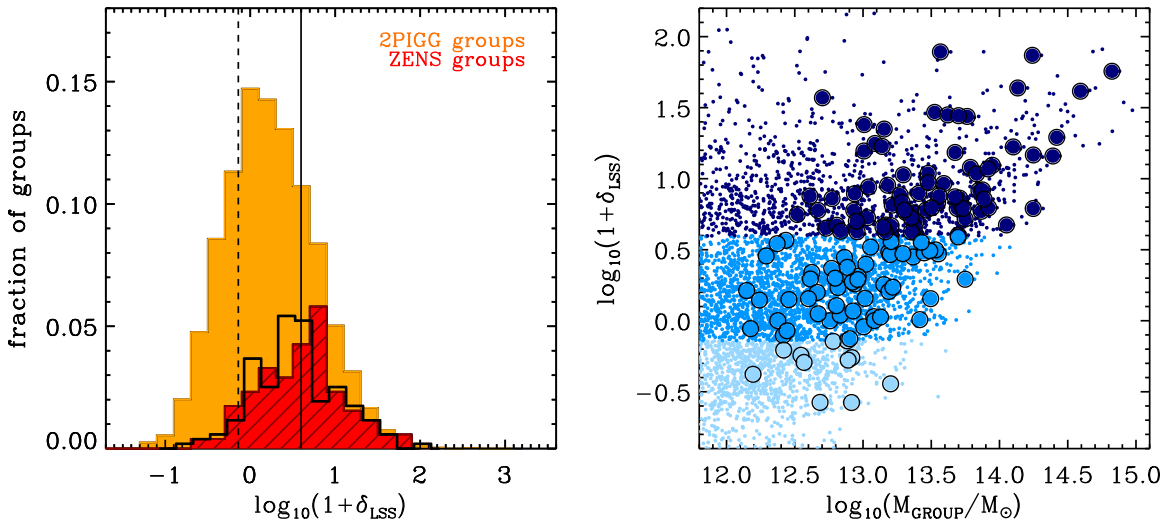

Figure 12. Left: the distribution of the fiducial $\delta_{\rm LSS}$ overdensities calculated with the fifth-nearest *group neighbor* approach described in Section 3.3. All galaxies in a given ZENS group have the same value of LSS overdensity, corresponding to that of their host group. The dashed histogram is for the ZENS sample (normalized to a tenth of the total 2PIGG groups for visual clarity); the solid histogram is for all 2PIGG groups in the redshift range $0.035 < z < 0.075$. The dashed and solid lines highlight the first and fourth quartiles of the latter distribution, respectively. The black empty histogram shows the distribution of $\delta_{\rm LSS}$ for the ZENS groups, which is obtained by excluding the ungrouped galaxies from the sample of groups used in the calculation of $\delta_{\rm LSS}$. The effect of including or removing ungrouped galaxies in the calculation of $\delta_{\rm LSS}$ is minimal. Right: The fiducial LSS overdensity values $\delta_{\rm LSS}$, based on the fifth-nearest *group neighbor* approach described in Section 3.3, as a function of group mass $M_{\rm GROUP}$, calculated as described in Section 3.1. The three shades of blue highlight, from fainter to darker blue, groups in low (lowest quartile), intermediate, and high (highest quartile) LSS densities (relative to the global distribution derived for all 2PIGG groups in the $0.035 < z < 0.075$ redshift range, which are shown as small points with the same color scheme). High-mass groups naturally live in high LSS regions; below $\sim 10^{13.5}\ M_{\odot}$, however, groups with similar masses occupy a wide range of LSS environments (as estimated by the $\delta_{\rm LSS}$ field). At group masses below $\sim 10^{13.5}\ M_{\odot}$ it is thus possible to disentangle the dependence of galaxy properties on halo mass and LSS density.

this fact is however mostly a reflection of the physical truth that the more massive groups inhabit, by definition, high density regions of the universe, which tend to be highly clustered. However, groups with masses below $M \sim 10^{13.5}\ M_{\odot}$ are found over a very wide range of LSS environments (as sampled by our $\delta_{\rm LSS}$ measurements). At these masses, we can therefore compare the properties of groups of similar halo masses that live in different LSS environments and thus identify trends induced by the LSS environment separately from those induced by the group halo mass.

3.3.1. Sources and Effects of Errors on Our LSS (Over)Density Estimates

3.3.1.1. Inclusion or exclusion of ungrouped galaxies in the 2dFGRS. In the calculation of the fiducial $\delta_{\rm LSS}$ values that we adopt in our analysis, we included all 2dFGRS galaxies that are not associated with any of the 2PIGG groups (i.e., also the "ungrouped" galaxies in the 2dFGRS catalog). We checked, however, whether the LSS density field that we measure at the location of the ZENS groups depends on whether these ungrouped galaxies are included or excluded in the computation of the (*N*th-nearest-group-neighbor-based) LSS density field. Figure 12 also shows the distribution of $\delta_{\rm LSS}$ that is obtained when excluding the ungrouped galaxies (black line). We further discuss in Appendix C that the use of one or the other of these two alternative realizations of the LSS densities shifts a group at most to an adjacent density quartile of the global distribution of densities in >90% of the cases, with no major impact on our *comparative* analyses between different environments.

3.3.1.2. The choice of N. We also investigated the impact of the value of "*N*" on the *N*th-nearest group-neighbor algorithm adopted to filter the distribution of the density tracers. In Appendix C, we show that, in contrast with the *N*th-nearest neighbor computations that use the galaxies as tracers of the LSS density field, our adoption of the groups themselves as tracers of the filamentary density distribution results in much weaker differences with the use of $N = 3$, 5, or 10.

4. THE ZENS CATALOG: ENVIRONMENTAL, STRUCTURAL, AND PHOTOMETRIC MEASUREMENTS

For the 1484 galaxies in the 141 ZENS groups, we have measured a number of structural (Paper II) and photometric (Paper III) diagnostics.

In particular, we have quantified galaxy structure both non-parametrically, through measurements of concentration, Gini coefficient, M20, and smoothness (as done in Scarlata et al. 2007), as well as parametrically, through single-Sérsic and double-component (Sérsic bulge plus exponential disk) analytical fits to the two-dimensional surface brightness distributions. We have also used an isophotal analysis to quantify the strength of bars. All structural measurements, including bulge and disk parameters, have been corrected in order to eliminate biases that depend not only on the seeing/PSF, but also on magnitude, size, concentration, and axis ratio. We have furthermore employed the corrected structural measurements, including the bulge-to-total ratios, to define a *quantitative* morphological classification, also validated by visual inspection of each galaxy in the sample, into elliptical, early-, intermediate-, and late-type disks, and irregulars.

The photometric measurements for the galaxies as a whole include colors (total and at various galactocentric distances), radial color gradients from analytical fits to the galaxy surface brightness profiles and the scatter around these gradients, total stellar masses and SFRs (and dust reddening), through fitting synthetic stellar population models to the near-UV to near-IR galaxy SEDs. Furthermore, through inspection of the 2dFGRS spectra, coupled with $(\mathrm{NUV}-I)-(B-I)$ and $(\mathrm{FUV}-\mathrm{NUV})-(\mathrm{NUV}-B)$ color–color diagrams, we have disentangled dust-reddened galaxies from red, quenched galaxies. We have used

this additional information to robustly classify galaxies into strongly star-forming, "moderately" star-forming, or quenched systems. We have also derived estimates for stellar masses separately for the disk and bulge components of galaxies, from the $B-I$ colors of these sub-galactic components derived from the two-component surface brightness fits.

We publish electronically the ZENS catalog[9] containing all structural and spectrophotometric ZENS measurements for these 1484 galaxies, together with the environmental diagnostics discussed above and listed in Table 1. The *readme* file is given for convenience in Appendix E.

5. GROUPS WITH OR WITHOUT A CENTRAL GALAXY: DEFINITION OF "RELAXED" AND "UNRELAXED" GROUPS

In Section 3.2.1, we saw that a total of 82 ZENS groups, whose centrals are highlighted in either green (73) or orange (9) in Figures 9, 10, and 11, host a galaxy member that satisfies simultaneously the three criteria that we require in order to be a genuine central, i.e., it has the largest stellar mass within the errors and it is consistent with being the center of the group in terms of both the spatial and velocity domains. The fact that the most massive galaxies in these groups have been able to establish their rank within their group potentials suggests a state of dynamical relaxation for the host groups. Dynamically "relaxed" systems indeed show a well-defined center for the potential and are a golden sample to extend to low (i.e., smaller than cluster) mass scale studies of galaxy properties as a function of group-centric distance.

In the remaining 59 ZENS groups, no galaxy member in the nominal 2PIGG group associations satisfies simultaneously the three criteria listed above to be a genuine central. For these groups, we highlight in red in Figures 9, 10, and 11 the symbols for their nominal centrals as a reminder that these, adopted as such on the basis of their nominal highest stellar masses, show a "displacement" from the groups' spatial and/or velocity centers. We label these groups as "unrelaxed," to contrast them with the well-behaved, relaxed groups discussed above. Figure 13 shows the distribution of total group masses for these unrelaxed groups, comparatively with the distribution of group masses for the entire ZENS sample; this figure shows that unrelaxed groups span a large range of masses, from low masses to relatively high masses.

We expect a physical origin to contribute to our inability to identify a bulletproof central galaxy in the "unrelaxed" groups in the ZENS sample. Non-physical factors may also however contribute to preventing us from identifying the real central galaxy in some of these groups. The main sources of error are again related to interlopers in group membership, incompleteness in the parent 2dFGRS database, and/or the inherent limitations of the 2PIGG group-finding algorithm (see Sections 2.2 and 3.2.2 and Appendix B). Based on the tests that we have conducted to understand the impact of interlopers and missing galaxies in the identification of central galaxies (Section 3.2.2), we expect that ~20%–25% of groups may appear as "unrelaxed" due to these catalog failures. The fraction that we observed is however substantially higher, of order ~40%. From this fact we estimate that in at least ~10%–15% of groups in the ZENS sample the displaced centrals are a genuine smoking gun for an unsettled dynamical state. This result may stem from the accretion of individual galaxies by the group potential and/or group–group merger events. This rough estimate for the fraction of genuinely unrelaxed groups in the ZENS sample is consistent with the estimate derived from both a comparison with the Yang et al. group sample (Section 3.1.1.2) and with a sub-clustering analysis, which we describe below.

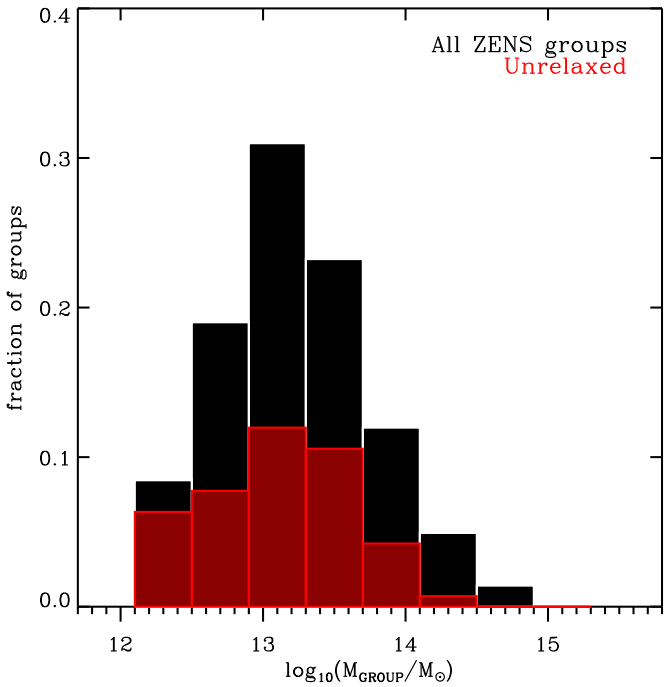

Figure 13. Red histogram shows the distribution of $M_{\rm GROUP}$ for the ZENS groups that are classified as "unrelaxed" according to the criteria described in Sections 3.2.1 and 5. The black histogram is the distribution of the total sample of ZENS groups. Both curves are normalized to the total number of ZENS groups (141).

5.1. Testing the Dynamical State of Groups with a Sub-clustering Analysis

As a complementary method for testing the dynamical state of the ZENS groups, we searched for substructures in position and velocity space, following the approach described in Dressler & Shectman (1988). In the original test, for each group, a local mean velocity ($\bar{v}_{\rm local}$) and velocity dispersion ($\sigma_{\rm local}$) around each member was calculated by using the Nth-nearest neighbors galaxies in the group, plus the galaxy on which the search was centered. The quantity $\delta^2 = ((N+1)/\sigma^2)[(\bar{v}_{\rm local}-\bar{v})^2+(\sigma_{\rm local}-\sigma)^2]$ parameterizes the deviation of this subset of galaxies from the group global velocity and dispersion, with $\bar{v}$ and σ being the group mean velocity and total dispersion, respectively. Under a Gaussian assumption and in the absence of substructures within the groups, the sum of the δ parameters of all galaxies in a group ($\Delta_{\rm tot}$) will be close to the number of its members. As discussed in Dressler & Shectman (1988), a non-Gaussian distribution of galaxies velocities can also bias the result in the absence of real substructures. For these reasons, the test is repeated for a number of Monte Carlo realizations in which the positions of the galaxies are held fixed but the velocities are randomly redistributed between the group members. Any intrinsic correlation among velocities will thus be erased and these Monte Carlo samples can be used to quantify the probability that a value of $\Delta_{\rm tot}$ larger than the one observed can originate from a random distribution.

To optimize the test for the ZENS groups, which have typically much lower richness than the clusters for which the

[9] The ZENS catalog is also downloadable from http://www.astro.ethz.ch/research/Projects/ZENS.

test was devised, we applied the following modification to the original formulation: we chose a value of N that depends to the group richness to calculate $\bar{v}_{\rm local}$ and $\sigma_{\rm local}$; specifically, we adopted $N = 0.4 \times N_{\rm members}$. This procedure accounts for the fact that the ZENS groups span a wide richness range, from $N_{\rm members} = 5$ to $N_{\rm members} \simeq 100$. Following the above prescription, we generated 500 Monte Carlo simulations for each ZENS group and identified groups having significant sub-clustering as those in which fewer than 20% of the Monte Carlo simulations resulted in a $\Delta_{\rm tot}$ larger than the measured value for that given group.

More than 80% of groups that we classify as "relaxed" according to the criteria described in Section 3.2.1 also show no hint for substructure in this clustering analysis; a fraction of about 20% of "unrelaxed" groups show distinct substructure in the Δ statistics analysis. There is therefore a good global agreement between the two approaches in establishing that a group is a relaxed system. These approaches hint at an absolute fraction of order ∼10%–15% of ZENS groups that are genuinely dynamically young.

We briefly investigate below whether and how the central and satellite galaxy populations in "relaxed" and "unrelaxed" groups display differences that can help us to understand the co-evolution of galaxies and their host group halo potentials.

5.2. A Quick Exploration of Central and Satellite Properties in Relaxed and Unrelaxed Groups

To compare the distribution of galactic properties of central or satellite galaxies in relaxed groups with those of similarly ranked galaxies in unrelaxed groups, we limit the sample to groups with $M_{\rm GROUP} < 10^{13.5}\,M_{\odot}$. Up to this halo mass, there is a fair mix of unrelaxed and relaxed groups in our sample; in contrast, the sample at higher group masses is shifted toward relaxed systems. This cut therefore helps avoiding mistakenly attributing differences in the galaxy populations to the dynamical state of the groups. These differences in actuality stem from a different halo mass distribution of the two categories of groups (shown in Figure 13).

We consider two bins of stellar mass, $10^{9.3}\,M_{\odot} < M < 10^{10}\,M_{\odot}$ and $10^{10}\,M_{\odot} < M < 10^{10.7}\,M_{\odot}$. Only satellites populate the "low-mass" bin in our sample; both satellites and centrals are fairly represented in the "high-mass" bin. We use the measurements published in Cibinel et al. (2013a, 2013b) to search for differences in galaxy half-light radii[10] $r_{1/2}$, sSFRs, SFR surface densities ($\Sigma_{\rm SFR}$), and $(B-I)$ colors. As discussed in Paper III, galaxies in which the best-fit template results in a very low SFR $< 10^{-4}\,M_{\odot}\,{\rm yr}^{-1}$ have their SFR and SFR values set to SFR $= 10^{-4}\,M_{\odot}\,{\rm yr}^{-1}$ and sSFR $= 10^{-14}\,M_{\odot}\,{\rm yr}^{-1}$, respectively.

The results are presented in Figure 14. The figure shows, from left to right, the distribution of $r_{1/2}$, sSFR, $\Sigma_{\rm SFR}$, $(B-I)$, and stellar mass for central (red/orange) and satellite (dark/light blue) galaxies in our low stellar mass bin (top panel) and high stellar mass bin (bottom panel).

We find a global similarity between the color and star formation properties of central galaxies in relaxed and unrelaxed groups in our high-mass bin ($10^{10}\,M_{\odot} < M < 10^{10.7}\,M_{\odot}$; see Appendix D). The median half-light radius of central galaxies in relaxed groups is however larger than for (alleged) centrals of similar mass in the non-relaxed groups ($5.30^{+0.40}_{-0.32}$ kpc and $3.77^{+0.69}_{-0.25}$ kpc, respectively, with a K-S-test probability for the size distributions of relaxed and unrelaxed groups being different of about 90%). The fact that no statistically significant effect is seen in either the sSFR or the $\Sigma_{\rm SFR}$ distributions between the two samples of centrals is possibly a reflection of the relatively large errors on these quantities (since the median stellar masses within the mass bin for the relaxed and unrelaxed groups are virtually identical, i.e., $10.50^{+0.04}_{-0.06}\,M_{\odot}$ and $10.50^{+0.02}_{-0.04}\,M_{\odot}$, respectively).

The median size of central galaxies in the high-mass bin matches well the median size of satellite galaxies of similar masses (both in relaxed and unrelaxed groups; $3.27^{+0.31}_{-0.11}$ kpc and $3.41^{+0.31}_{-0.13}$ kpc, respectively). There is a small shift in galaxy mass between centrals and satellites within this mass bin, i.e., $10.30^{+0.03}_{-0.02}\,M_{\odot}$ for satellites in relaxed groups, compared with the corresponding value for centrals given above. This difference is however not sufficient to explain the difference in median size. Once again, this result may well be evidence that, in at least some of the unrelaxed groups, the nominal central galaxy is not a real "central," but a satellite galaxy that has been mistaken for a central due to survey incompleteness issues. This finding may also partly indicate, however, that central galaxies in relaxed group potentials further grow in size relative to (pseudo)centrals in young/merging groups; this process may happen due to accretion of low-mass satellites in a virialized group potential, as shown by numerical simulations (e.g., Hopkins et al. 2008; Feldmann et al. 2010).

A constant stellar mass, satellite galaxies have virtually identical properties independent of whether they inhabit relaxed or unrelaxed groups, with only a hint in our data for low-mass ($10^{9.3}\,M_{\odot} < M < 10^{10}\,M_{\odot}$) satellites in unrelaxed groups to be on average 0.05 mag bluer than galaxies of similar rank and mass in relaxed groups (at the ∼90% probability level). We note that we do not detect a similar effect in the sSFR (or $\Sigma_{\rm SFR}$) diagrams; we again interpret this result as possibly being due to a dilution of signal resulting from intrinsic uncertainties in the SFR values derived from the SED fits. All median values for the histograms of Figure 14 are listed in Appendix D.

5.3. The Stellar Content of Relaxed and Unrelaxed Groups

The fraction of group mass that is in the form of stars is an indication of how efficiently star formation has progressed in a given halo. We thus ask whether there are detectable differences in the relation between total stellar mass and halo mass between relaxed and unrelaxed ZENS groups.

Following a similar approach as the one described in Section 3.1 to calculate the group total luminosity, we derive the total stellar mass that is locked in galaxies within a given halo as follows. We recall here that our group masses are determined using the total luminosities, independent of the dynamical state of the group; thus, by construction, similar relations should be obtained for relaxed and unrelaxed groups if their galaxies had similar stellar populations. We first sum the incompleteness-weighted mass of all member galaxies above the completeness limits, for star-forming and quenched galaxies separately, i.e., $M_{\rm OBS,SF} = \sum_{i, M > M_{\rm lim,SF}} w_{i,\rm SF} M_{i,\rm SF}$ and $M_{\rm OBS,}{}_{Q} = \sum_{i, M > M_{\rm lim,}{}_{Q}} w_{i,Q} M_{i,Q}$. We use $M_{\rm lim,SF} = 10^{9.2}\,M_{\odot}$ and $M_{\rm lim,}{}_{Q} = 10^{10}\,M_{\odot}$ for star-forming and quenched galaxies, respectively, as derived in Paper III. These estimates need to be corrected for the stellar mass in galaxies falling below $M_{\rm lim}$.

[10] Note that we use here the global galactic half-light radii obtained through our double-component, bulge plus disk fits to the two-dimensional galaxy surface brightness distributions; see Paper II for details. Furthermore, we employ semi-major axis measurements for all galaxies, except for elliptical galaxies, for which we use circularized half-light radii.

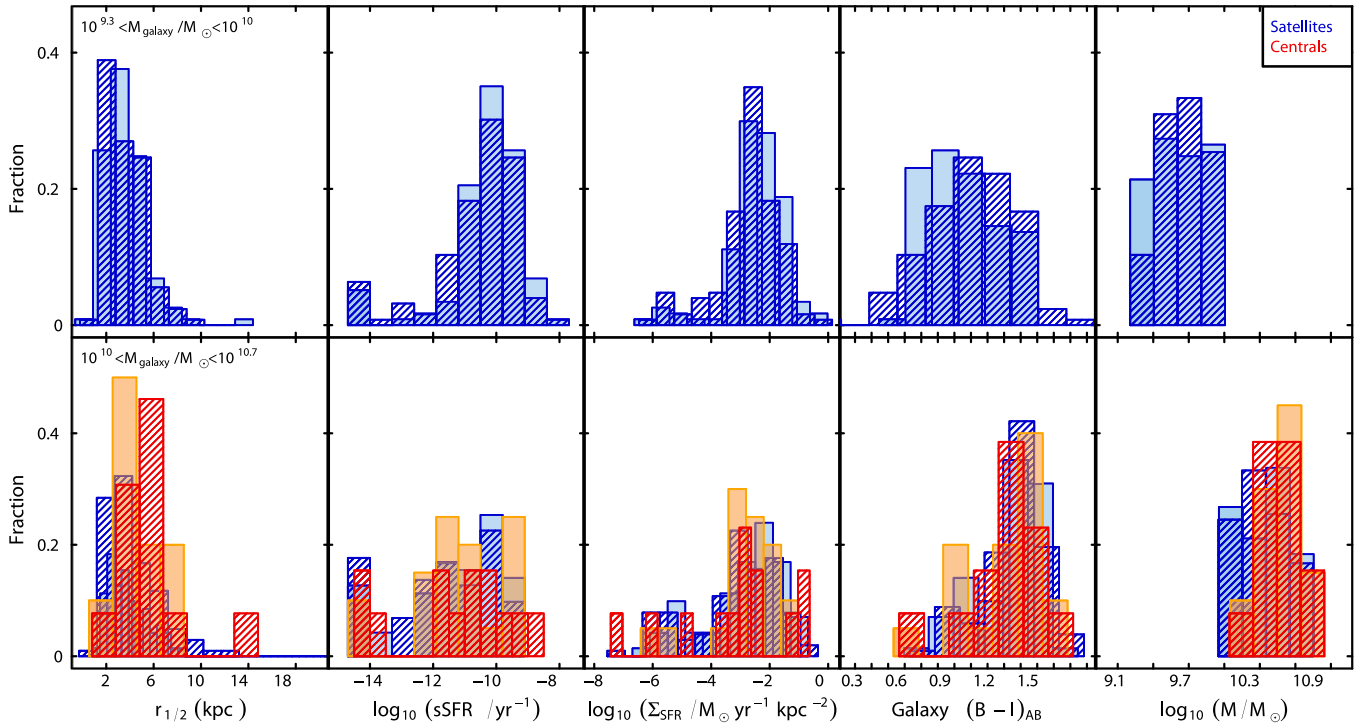

Figure 14. From left to right, the figure shows the distribution of galaxy half-light radii, specific star-formation rates, star-formation rate surface densities, $(B-I)$ colors, and stellar masses for central (red/orange) and satellite (dark-/light-blue) galaxies in two bins of stellar mass (top and bottom rows, as indicated in the figure). Dark hatched histograms show galaxies in relaxed groups; light filled histograms show galaxies in unrelaxed groups. To match the distribution of halo masses of the unrelaxed sample and avoid spurious effects in comparisons between relaxed and unrelaxed groups due to differences in the distributions of group masses between these two families (see Figure 13), only groups with $M_{\rm GROUP} < 10^{13.5}\,M_\odot$ are shown in this figure.

The correction is done by separately integrating the mass functions of star-forming and quenched galaxies, for which we adopt the estimates of the Schechter function parameters for blue and red galaxies, respectively, provided in Table 3(a) of Peng et al. (2010). Although Peng et al. (2010) provide the mass function parameters split in quartiles of high and low environmental density, we utilize the parameters obtained for the global populations, since the one-to-one matching between our group environments and their density definition is not straightforward. In analogy with the computations outlined in Section 3.1, the correction factor, by which we divide $M_{\rm OBS}$, is $\Gamma(\alpha_*+2,\, M_{\rm lim,SF}/M_*)/\Gamma(\alpha_*+2)$ for the star-forming population (characterized by a single Schechter function; Peng et al. 2010). The correction for the quenched population (described by two Schechter functions) is

$$\frac{\Phi_{*,1}\Gamma(\alpha_*+2,\, M_{\rm lim,Q}/M_*)+\Phi_{*,2}\Gamma(\alpha_{*,2}+2,\, M_{\rm lim,Q}/M_*)}{\Phi_{*,1}\Gamma(\alpha_*+2)+\Phi_{*,2}\Gamma(\alpha_{*,2}+2)}.$$

The resulting contribution to the total stellar mass from galaxies below the completeness limits is of order 6% and 15% for quenched and star-forming galaxies, respectively. The total mass in galaxies $M_{\rm tot,galaxies}$ is finally obtained as the sum of the corrected masses for the star-forming and quenched populations, $M_{\rm tot,galaxies} = M_{\rm SF} + M_Q$.

The relation between $M_{\rm GROUP}$ and $M_{\rm tot,galaxies}$ for relaxed and unrelaxed groups is plotted in Figure 15, where we also show the results of other literature studies for groups and clusters. A quantitative comparison between the different samples is made difficult by a number of factors, including differences in the groups' selection criteria and redshift. Furthermore, differences in the assumptions and methodologies used for calculating the total stellar masses (and halo masses) complicated the comparison. These complications are at least in part the cause for the scatter in the relation resulting from the direct comparison of the different studies. Nevertheless, we recover the well-known result that the fraction of halo mass that is in the form of stars

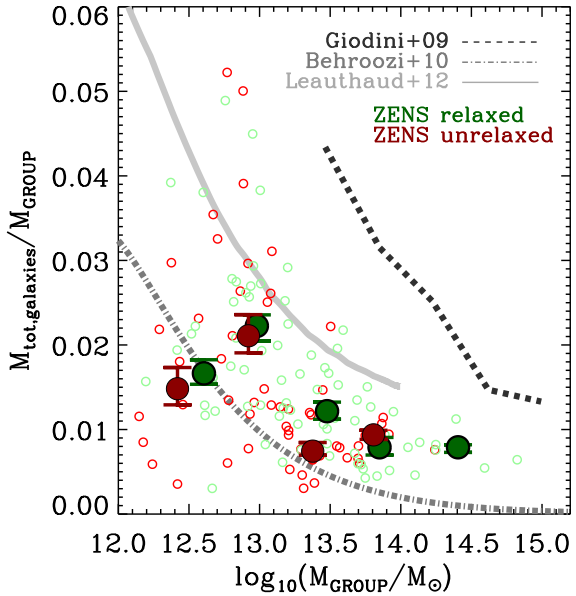

Figure 15. Fraction of group halo mass that is converted into stars within galaxies as a function of group halo mass. Small empty points are the values for the individual ZENS groups: green points show relaxed groups and red points show unrelaxed groups. Large symbols with error bars are the median values for the relaxed and unrelaxed ZENS groups. For a qualitative comparison, estimates from the literature are shown: the Giodini et al. (2009) relation for a sample of X-ray selected groups at $0.1 \leqslant z \leqslant 1$ (dashed line), the Behroozi et al. (2010) relation derived from halo abundance matching at $z = 0.1$ (dash-dotted line), and the halo occupation-based estimate of Leauthaud et al. (2012) at redshift $z = 0.37$ (solid line).

in the ZENS groups generally amounts to about 1%–2% and is a factor of order two higher at group masses $<10^{13}\,M_{\odot}$ (∼2%) than at group masses $>10^{13.5}\,M_{\odot}$ (∼0.8%). This increase in star-formation efficiency in Milky-Way sized halos, i.e., at the low-end of the mass distribution of the ZENS groups, has indeed been previously highlighted as a quite fundamental (and redshift independent) fact of nature (Behroozi et al. 2013). There is no evidence for relaxed and unrelaxed groups having significantly different stellar mass fractions or dependences on halo mass, although, relaxed groups show a hint for marginally higher stellar mass fractions relative to their unrelaxed counterparts. The systematic small increase in stellar mass fraction apparent in Figure 15 is a reflection of the slightly different mass-to-light ratios implied by the somewhat redder colors of the satellites in the relaxed groups, coupled with the adopted uniform luminosity to halo mass calibration. The fact that the stellar populations in relaxed and unrelaxed groups are broadly similar is consistent with an efficiency of conversion of gas into stars that is not affected by the dynamical state of the group.

6. SUMMARY AND CONCLUDING REMARKS

Motivated by the picture that both the mass of a galaxy and its immediate and distant environment may impact how the galaxy evolves and its redshift zero properties and by the uncertainty on which mass and which environment are relevant to galaxies, we undertake the ZENS project, which uses new and archival multi-wavelength data for a statistically complete sample of 1627 galaxies brighter than $b_J = 19.45$ that are members of 141 $\sim 10^{12.5-14.5}\,M_{\odot}$, $0.05 < z < 0.0585$ groups. The aim of ZENS is to explore the dependence of key galactic population diagnostics on large-scale environment, the mass of the host group halo, the location of galaxies within their group halos, and the central/satellite rank of a galaxy within its host group halo. The ZENS sample is extracted from the 2PIGG catalog of the 2dFGRS. We publish the ZENS catalog, which combines the environmental diagnostics computed in this article with the structural and spectrophotometric galactic measurements described in Cibinel et al. (2013a, 2013b).

In this first paper, introducing the project, we have described an improved algorithm adopted to define the group centers, rank galaxies as centrals or satellites in their host groups, and separate the effects on galaxies of groups mass and LSS density. Specifically:

(1) We have introduced a three-faceted self-consistency criterion for identifying central galaxies. These objects must, simultaneously, be the most massive galaxies in the group within the error bars estimated for the galaxy stellar masses and be consistent with being the spatial and dynamical centers of the host groups.

(2) We have adopted an *N*th-nearest *group*-neighbors computation to estimate the LSS density underlying the groups which, especially at group masses $M_{\rm GROUP} < 10^{\sim 13.5}\,M_{\odot}$, and in contrast with the commonly used *N*th-nearest *galaxy*-neighbors approach, is independent of group mass/richness and enables us to study separately the effects of these two distinct environments on galaxy properties.

Furthermore, we have used simulations, also based on semi-analytic models of galaxy evolution, to quantify the intrinsic uncertainties in the trends of galaxy properties with the environmental parameters that are propagated from the random and systematic errors in these parameters.

We have found that at least ∼60% of groups are dynamically relaxed systems with a strongly-identifiable central galaxy that satisfies the stringent criteria above—and thus a well-defined center of the group. These groups enable a robust investigation of galaxy properties with group-centric distance down to the smallest group masses sampled in ZENS. In the remaining ∼40% of groups, there is no galaxy that satisfies the required criteria to be a central galaxy—and thus the center of the group potential well. We estimate that a non-negligible fraction of these groups—up to of order ∼10%–15% of groups in the total ZENS sample—are likely genuinely dynamically young, possibly merging groups.

At a constant stellar mass, central galaxies in relaxed and unrelaxed groups have similar color and star formation properties, although relaxed groups show larger size centrals than unrelaxed groups. Centrals in unrelaxed groups have sizes comparable with satellite galaxies of similar masses. These results may partly arise from the misclassification of satellite galaxies as central galaxies in groups, in our analysis labeled unrelaxed, for which however the identification of their dynamical state and of the central galaxy might be hampered by observational errors. We estimate that in about two-thirds of nominally "unrelaxed" groups, the lack of identification of a self-consistent central galaxy has its roots in the incomplete spectroscopic and photometric coverage of the 2PIGG and 2dFGRS surveys, respectively. Therefore, our use of the term "unrelaxed" should be read as highlighting the important fact that the alleged central galaxies, and thus the centers in these groups, should be handled with care.

Partly, however, the lack of a dependence of central galaxies properties on the nominal dynamical state of the group may be evidence that the properties of central galaxies are shaped by their own mass content and not by their group environment, with the exception of a growth in size in dynamically relaxed halos due to secular accretion of smaller satellites.

Over the whole galaxy mass range of our study, satellites have indistinguishable physical properties (in terms of sizes, optical colors, sSFRs, and $\Sigma_{\rm SFR}$) independent of whether they are hosted by relaxed or unrelaxed groups.

Furthermore, relaxed and unrelated groups appear to have similar stellar populations and thus likely gas-to-star conversion efficiencies, suggesting that the efficiency of conversion of gas into stars within halos may be largely independent of the dynamical state of the group. A more detailed investigation of this important issue is postponed to a future dedicated paper.

The only possible difference between relaxed and unrelaxed potentials is a very modest shift toward redder $(B-I)$ colors for $<10^{10}\,M_{\odot}$ satellites in relaxed compared with unrelaxed groups. A possible explanation is that, at the higher masses, satellites are either unaffected by the group environment or they reach their final state as they first enter the potential of a relatively small group, with subsequent group–group mergers having no further impact on their properties (see also De Lucia et al. 2012 for theoretical support for this scenario).

The marginally redder colors of low-mass satellites in relaxed groups relative to unrelaxed groups may be due to satellites orbiting since longer times within the former relative to the latter, or to quenching of star formation in these systems for processes that are active or at least most efficient in relaxed group potentials. Independent studies also point to low-mass satellite quenching by physical processes acting within virialized halos.

In future ZENS analyses, we will investigate whether and how including or excluding the unrelaxed groups from any given specific diagnostic impacts our main conclusions.

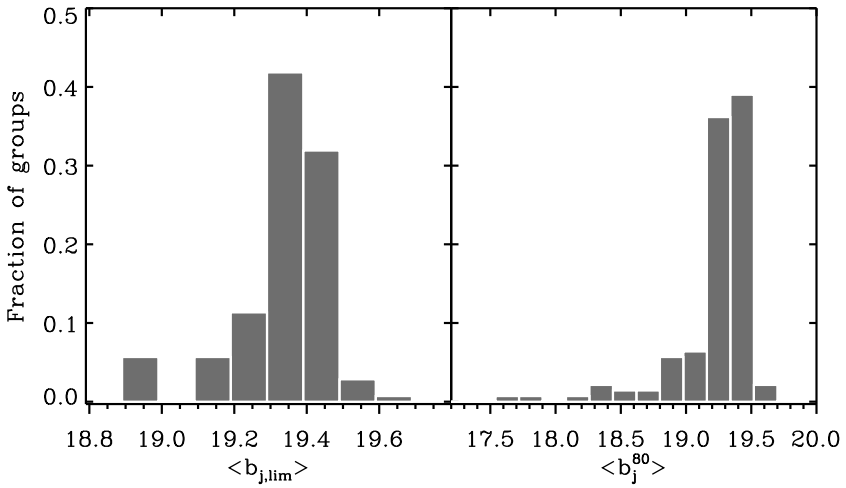

Figure 16. Completeness of the 2dFGRS over the targeted ZENS fields. Left: average value of the limiting magnitude in the 2dFGRS catalog, without constraints on completeness. Right: mean limiting magnitude for the ZENS fields, imposing a 80% completeness level in the 2dFGRS images.

A.C., E.C., and C.R. acknowledge support from the Swiss National Science Foundation. This publication makes use of data from ESO Large Program 177.A-0680 and data products from the Two Micron All Sky Survey, which is a joint project of the University of Massachusetts and the Infrared Processing and Analysis Center/California Institute of Technology, funded by the National Aeronautics and Space Administration and the National Science Foundation. *GALEX* (*Galaxy Evolution Explorer*) is a NASA Small Explorer mission. The Millennium simulation databases used in this paper and the web application providing online access to them were constructed as part of the activities of the German Astrophysical Virtual Observatory.

APPENDIX A

THE IMPACT ON ZENS OF THE ORIGINAL 2DFGRS MAGNITUDE LIMITS

The 2dFGRS team made available three maps that specify a given position on the sky θ: (1) the extinction-corrected magnitude limit of the survey $b_{j,\rm lim}(\theta)$, (2) the redshift completeness $R(\theta)$,—the number of galaxies with measured redshifts relative to the parent APM survey catalog, which is the photometric basis of the 2dFGRS, and (3) the parameter $\mu(\theta)$ that enters the expression for the magnitude-dependent redshift completeness, $c_z(b_j, \mu(\theta)) = \gamma[1 - \exp(b_j - \mu(\theta))]$, with $\gamma = 0.99$ (Colless et al. 2001). The overall redshift completeness around a given set of celestial coordinates is given by $C(\theta, b_j) = R(\theta)c_z(b_j, \mu(\theta))/\bar{c}_z(\mu(\theta))$. The factor $\bar{c}_z(\mu(\theta)$ is a normalization constant derived from the average of $c_z(b_j, \mu)$ over the expected apparent magnitude distribution of the survey galaxies (Colless et al. 2001; Norberg et al. 2002; Cole et al. 2005) and can be calculated using Equation (7) of Colless et al. (2001).

The 2PIGG catalog is constructed only from those fields and sectors of the 2dFGRS that have a high number of measured redshifts. Furthermore, during the selection of the ZENS groups, we restricted the sample to the most complete fields (i.e., those that have galaxy weights from the 2PIGG catalog <1.6). This procedure ensures that the average completeness $R(\theta)$ in a group, defined as the mean of all values at the positions on the sky of the member galaxies, is typically ∼90%. We thus compute the limiting faint magnitude at which the survey is complete at the 80% level ($\langle b_j^{0.80}\rangle$) from mean estimates of the limiting magnitude without constraints on completeness ($\langle b_{j,\rm lim}\rangle$) by inverting the expression for $C(\theta, b_j)$ given above. In calculating the factor $\bar{c}_z(\mu(\theta)$, we use a bright and faint magnitude limit of $b_j = 14$ and $b_{j,\rm lim}(\theta)$, respectively. Figure 16 shows the derived distribution of $\langle b_{j,\rm lim}\rangle$ and $\langle b_j^{0.80}\rangle$. There are small variations among the ZENS groups in the faintest magnitude reached by the original 2dFGRS data. As shown in the figure, the effect is small, however, with only a handful of groups having $\langle b_j^{80}\rangle$ brighter than 19. Most of the ZENS groups are complete down to the ($\langle b_{j,\rm lim}\rangle$) limit. We have checked in all cases that none of our results are affected by this modest field-to-field scatter in completeness in the ZENS fields.

We finally applied corrections for spectroscopic completeness. As done in the 2dFGRS studies, these corrections are obtained by assigning a weight w to each galaxy, defined as $w = 1/C(\theta, b_j)$, such that the complete number of galaxies N (total, or of a given type) is $N = \sum_i 1/w_i$.

APPENDIX B

IMPACT OF "MISSED" GALAXIES ON OUR ANALYSES

B.1. Searching in the SDSS for Galaxies Missed by the 2dFGRS

The ZENS fields lie in regions of the 2dFGRS that have an average redshift completeness of 87%, with some variations: 128 groups have a completeness of at least 80% while 13 groups have a lower completeness between 72% and 80%. Four of these latter groups are in the ZENS unrelaxed class. Comparing the positions of the ZENS groups with respect to the 2dFGRS survey boundaries, we found that nine unrelaxed groups may be close enough to the survey edges/gaps (within 1 Mpc) to have been only partially covered by the 2dFGRS observations.

To understand these and other biases in the ZENS sample introduced by galaxies "missed" by the 2dFGRS,[11] we studied the SDSS DR7 spectroscopic catalog of Abazajian et al. (2009). About a quarter of ZENS groups (43 out of 141) are located in fields that overlap with the SDSS. For each of these 43 groups, the search for missed galaxies was performed on circular projected areas of radius equal to 1.5 times the rms radius of the group, centered on the nominal most massive galaxy.

[11] This approach is similar to the one we adopted in Section 3.1.1.1 to search for suitable galaxies in the 2dFGRS that had not been associated with a given group by the 2PIGG algorithm.

Table 2
ZENS Groups with Extra Candidate Galaxy Members in the SDSS

Name	Nominal Members	SDSS Candidates	Below $b_{j,\mathrm{lim}}$	M_{GROUP}
2PIGG_m1363	8	2	···	7.781×10^{12}
2PIGG_m1377	23	1	···	7.506×10^{13}
2PIGG_m1381	10	3	···	1.223×10^{13}
2PIGG_m1384	11	1	1	5.796×10^{13}
2PIGG_m1418	5	1	···	8.660×10^{12}
2PIGG_m1457	30	9	1	1.741×10^{14}
2PIGG_m1469	6	1	···	2.051×10^{13}
2PIGG_m1472	5	1	···	2.446×10^{13}
2PIGG_m1486	23	4	···	8.869×10^{13}
2PIGG_m1522[a]	10	2	···	3.189×10^{13}
2PIGG_m1523	5	1	···	1.035×10^{13}
2PIGG_m1525	11	2	···	1.381×10^{13}
2PIGG_m1532	15	1	···	7.710×10^{13}
2PIGG_m1540	32	10	2	1.766×10^{14}
2PIGG_m1543	6	1	···	8.449×10^{12}
2PIGG_m1572	19	1	···	4.717×10^{13}
2PIGG_m1584	6	1	···	8.936×10^{12}
2PIGG_m1597	16	4	···	8.237×10^{13}
2PIGG_m1598	9	2	1	2.671×10^{13}
2PIGG_m1622	27	10	···	1.261×10^{14}

Notes. The ZENS groups for which candidate "extra galaxy members" were found in the SDSS DR7 spectroscopic sample, according to the criteria described in Appendix B.1. For each group, we specify the number of original 2PIGG members (Column 2), the number of SDSS galaxies that are not in the 2dFGRS (Column 3), and, among these, the number of galaxies whose magnitudes lie below the 2dFGRS selection limits (Column 4). In Column 5, we list the fiducial group masses based on the extrapolation of the luminosity function (in units of $M_{\odot}$), as sampled by the 2PIGG galaxies (see Section 3.1).

[a] The entry for m1522 refers to the group center fixed on the nominal most massive galaxy, which was rejected as the central by our test described in Section 3.2.1; centering the search for extra galaxies on the newly assigned central galaxy results in no extra galaxies potentially associated with this group according to the search criteria in the SDSS catalog that are detailed in Appendix B.1.

To set an operational definition, we considered as plausible missed galaxies in each of these groups galaxies with coordinates within these circular areas, and with redshifts between $z_{\mathrm{min}} - \delta < z < z_{\mathrm{max}} + \delta$. Here, z_{min} and z_{max} are the minimum and maximum redshift of the galaxies in the given 2PIGG group; a δ value from 10% up to 30% of the redshift interval spanned by the nominal 2PIGG galaxy members of that group was explored.

With $\delta = 30\%$, we found a total of 56 "extra" galaxies in the SDSS that satisfied these criteria in 19 of the total 43 ZENS groups with SDSS pointings, compared with a total of 267 nominal 2PIGG members in these groups. A summary of the fields with these "extra" galaxies is given in Table 2. As indicated in this table, only a small fraction of these galaxies have magnitudes below the nominal selection limit of the 2dFGRS (for 26 galaxies, we could not find information on the b_j magnitude; for these galaxies we used the relation between b_j and SDSS g magnitudes when both measurements were available). An analysis of the images shows that fiber collisions should not be a primarily responsible for the absence of these galaxies from the 2dFGRS catalog. Although ultra-compact galaxies could be missed due to a star/galaxy misclassification, generally these galaxies seem simply casualties of the 2dFGRS statistical sampling.

The statistics above suggest that of order ∼40%–50% of the ZENS groups and in general of the 2PIGG groups are potentially missing some member galaxies above the 2dFGRS magnitude limit, due to the absence of these galaxies from the parent 2dFGRS catalog. We use this information to assess an order of magnitude estimate for the impact of the plausible extra members on our analyses, including group mass estimates as well as the definition of centrals and satellites.

In Table 2, we show the nominal group masses for these 19 groups; even assuming that all missed SDSS galaxies are additional members of the relevant ZENS groups changes the group masses by less than 30% in 85% of the groups. In two groups the change in mass would be ∼60% and in one group the mass would change by a factor of two.

We then ran the algorithm described in Section 3.2.1 on these 19 groups in order to identify the central and satellite galaxies, this time also including the 56 extra galaxies (using the total stellar masses provided in the MPA/JHU value added catalog for the masses of the extra SDSS galaxies; in Paper III we use a sample in common to show that there are no severe systematics between our estimates for galaxy stellar masses and those in this catalog). Since we do not have information on the full PPDs for the stellar masses of the extra SDSS galaxies, we generated artificial Gaussian PPDs, centered on the galaxy MPA/JHU stellar mass, with a standard deviation of 0.3 dex. Only in four of these 19 groups (2PIGG-n1363, 2PIGG-n1457, 2PIGG-n1469, and 2PIGG-n1540) did the inclusion of the extra SDSS galaxies result in a possible change in the identification of the central galaxy. Three of these four potential "SDSS centrals" have structural, morphological, stellar mass, and star formation properties very similar to those of the nominal ZENS central. In the remaining case, the "SDSS central" is a quenched

E/S0 galaxy, in contrast with the nominal ZENS central, which had an intermediate disk morphology and an intermediate SFR (see Paper III for our definitions of quenched, moderately star-forming, and strongly star-forming). While in principle such situation may lead to uncertainties in the analysis of the central and satellite galaxy populations, the global statistics are comforting.

We estimate the incompleteness relative to the SDSS as follows. We first assumed that all missed SDSS galaxies are physically associated with the 19 groups in question and that the true central galaxies in the four aforementioned groups, for which the inclusion of the SDSS extra sample leads to a change in the identification of the central, are indeed the newly added SDSS galaxies rather than the nominal ZENS centrals. Considering all 43 groups for which we know whether they are (or are not) missing SDSS galaxies, we then defined (1) the number of centrals that we should have observed, $n_{\rm centrals} = 43$, (2) the number of centrals that we have correctly identified, $n_{\rm centrals,obs} = 39$, (3) the number of satellites that we should have observed, $n_{\rm sats} = 505$ (i.e., the total sample of 492 2PIGG members of the 43 groups in question, plus the 56 extra SDSS galaxies found in total for this sample, minus 43, the number of their centrals), (4) the number of satellites that are misclassified as centrals, $n_{\rm false\text{-}cen} = 4$, and, finally, (5) the number of correctly identified satellites $n_{\rm sats,obs} = 449$ (i.e., the total sample of 492 2PIGG members, minus 43 centrals). We then estimate the level of incompleteness due to missing SDSS galaxies in the 2dFGRS sample as, for the central galaxies, $1 - n_{\rm centrals,obs}/n_{\rm central} \sim 10\%$ and, for the satellites, $1 - n_{\rm sats,obs}/n_{\rm sats} \sim 10\%$. These results imply a 10% contamination of satellites incorrectly identified as centrals. All of these values are upper limits to the fraction of misidentifications, since not all "extra" galaxies identified as described above will be missed group members. We therefore conclude that this specific source of uncertainty in the identification of the central (and thus satellite) galaxy populations is not a dominant one. The identification remains mostly affected by other factors such as the global impact of the FOF clustering algorithm used for the identification of bound galaxy groups.

For the four groups with a candidate "missed" central galaxy, we had to decide to which galaxy we would assign the rank of central. We maintained the identification of the central galaxies in these groups with the original centrals found among the nominal 2PIGG group members and checked that this choice did not affect any of our conclusions.

The above checks imply virtually no effect of these missed potential galaxy group members on any of our studies of the group environment based on our group mass estimates, galaxy membership, and central/satellite ranking.

B.2. ZENS Galaxies Missed by ZENS Pointings

Another possible source of error in the estimate of group mass and identification of centrals and satellites are galaxies missed in the WFI observations. For 28 of the 141 groups, the WFI pointings did not cover their entire extent, resulting in a total of 172 members for which no B- and I-band imaging was available. These groups are indicated with an exclamation mark in Figure 9. For 20 groups, the fraction of missing members is $<20\%$ of the original 2PIGG group richness; for six other groups the fraction is between 20% and 30%. For only two massive groups (2PIGG-s1935 and 2PIGG-n1377) is the fraction as high as 40%–45%. We include in the ZENS catalog these galaxies that are beyond the WFI field; we set to null all entries relating to quantities that rely on the WFI photometry, except for the galaxy mass. A mass estimate for these galaxies was in fact obtained from the linear relation between the SuperCOSMOS Survey r_F magnitude (provided in the 2dFGRS data release and corrected for galactic extinction) and the SED-inferred galaxy mass, as derived for the ZENS galaxies with available B- and I-band observations. For the mass probability distribution of these galaxies, we assumed a Gaussian centered on the mass predicted by the $r_F - M$ relation, with a standard deviation equal to 1.5 times the observed scatter of the $r_F - M$ relation.

We again asked whether these "missed" galaxies could be the true central galaxies in groups for which we failed to find a self-consistent solution in Section 3.2.1. In the majority of cases, such galaxies that lie beyond the WFI pointings are small satellites in the outskirts of the groups ($R > 0.5\,R_{200}$). In fact, 85% of the galaxies that fall outside the WFI pointings are substantially more than a factor of four less massive than the most massive group member; about 60% of these "missed" galaxies have masses below the mass completeness limit of quenched galaxies in our study ($10^{10}\,M_{\odot}$). Only for three groups, 2PIGG-s1272, 2PIGG-s1665, and 2PIGG-n1377, does our scheme for the definition of the group center identify one of the galaxies with no B- and I-band WFI imaging as a possible candidate central galaxy. From a statistical perspective, these objects are again negligible contributors to the misidentification of central and satellite galaxies in our sample.

For these three groups, we adopted as central the "missed" galaxy that suitably satisfied all criteria. However, given that the uncertainties on the masses for these "missed" galaxies are substantially larger than for the rest of the sample, we flag these groups in the ZENS catalog; this procedure gives us the chance to check whether any of our results change when these groups are included/excluded from our analyses and/or when we adopt as the central galaxy the galaxy that satisfies these criteria from within the pool of objects with WFI B- and I-band observations. As expected, given that only three groups are involved, these groups do not affect any of our conclusions in any of our studies so far.

B.3. Search in the 2dFGRS for Potential Missed Members of the ZENS-2PIGG Groups

As mentioned in Section 3.1.1.1, the search for 2dFGRS galaxies not included in a given ZENS (i.e., 2PIGG) group but with magnitudes, coordinates, and redshifts within the ranges that could possibly make them members of this group (according to the criteria listed in Section 3.1.1.1), resulted in a total of 52 galaxies distributed over 24 of the ZENS groups. Figure 17 shows the spatial (left panels) and velocity (right panels) distributions for these possible candidate members, in relation to the galaxies that compose the ZENS group extracted from the 2PIGG catalog. Note that these possible candidate members often cluster both spatially and in velocity space. While statistically their identification with independent groups is validated by comparisons with mock catalogs, it is clear that, on a group-to-group basis, it is not possible to exclude the fact that at least some of these galaxies may be missed members of the 2PIGG groups that we study in ZENS. The velocity dispersions and masses of these groups would, however, not change substantially if the potential extra candidate members were added to them, as these groups have already relatively high total masses, as shown in Figure 18 (see also Section 3.1.1.1). Furthermore, none of these extra galaxies would qualify as being the central galaxies within their respective ZENS groups.

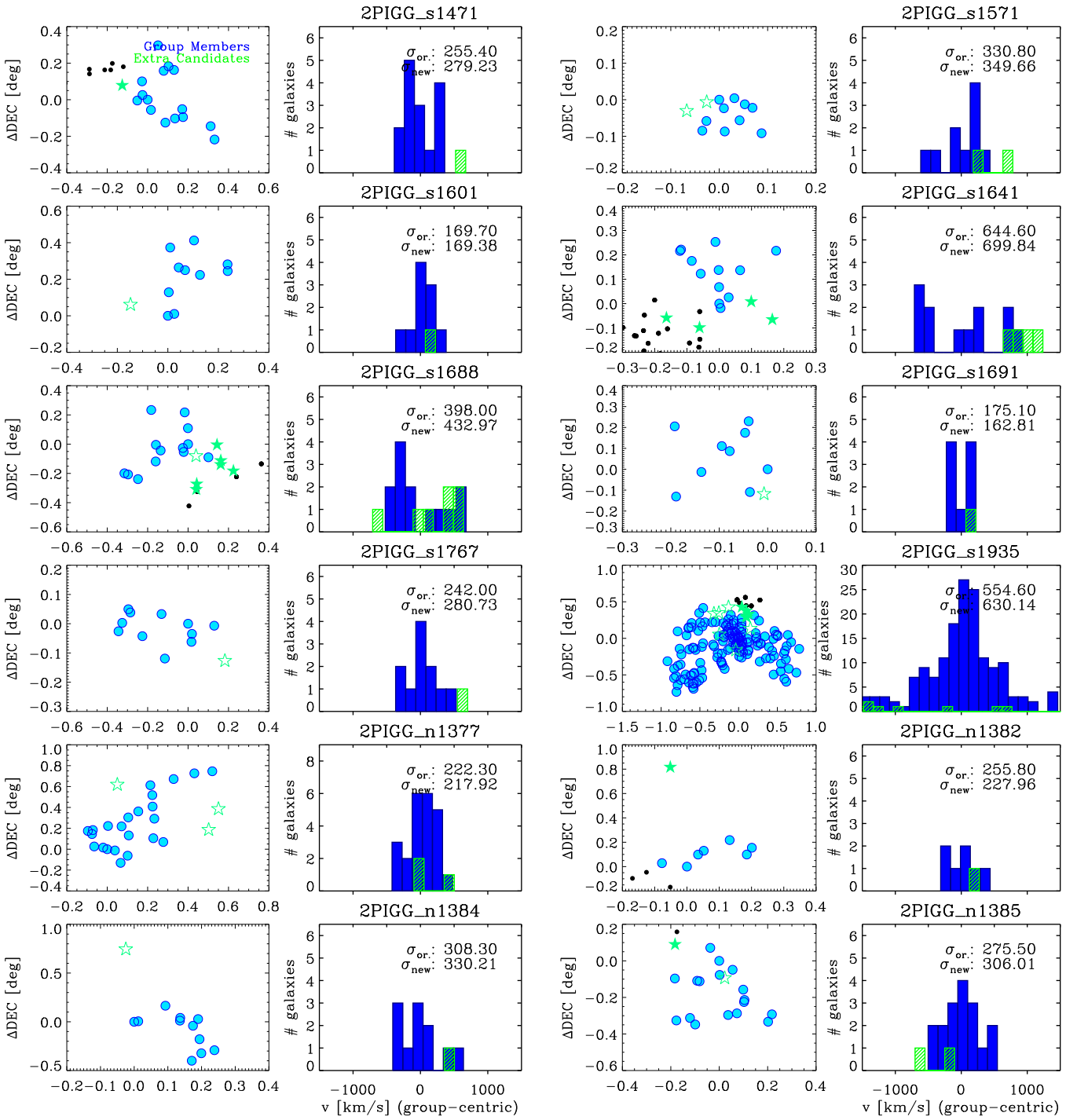

Figure 17. Left: the projected-spatial distribution, relative to the group central galaxy as defined in Section 3.2.1 (placed at the (0,0) position) of potential group member galaxies in the 2dFGRS catalog, which are not listed as members of the 2PIGG groups that we use in ZENS. The nominal 2PIGG member galaxies are shown as filled circles, and the potential extra group members are shown as stars. Among these potential "extra" candidate members for a given 2PIGG group, we identify with empty stars galaxies that are not associated with any other 2PIGG group. We identify with filled-stars galaxies that are associated with a different 2PIGG group. We also show as black dots the remaining galaxy members of these other 2PIGG groups to which the filled-star galaxies belong, although the galaxies represented with black dots do not qualify to be potential extra members of our ZENS groups, according to the definition discussed in Section 3.1.1.1. Right: the corresponding distribution of relative velocities of galaxies with respect to the mean redshift of the group. Solid histograms show the velocities for the original 2PIGG group members and dashed histograms show the relative velocities of the potential "extra" candidate members. The values of the velocity dispersion of the groups, computed before and after the inclusion of these potential extra members, are given in the top-right corners of the plots. These velocity dispersions are calculated with the gapper estimator as in Eke et al. (2004a).

With respect to the satellite population, the 2dFGRS extra galaxies with masses above the passive ("quenched") mass completeness limit of $>10^{10}\,M_{\odot}$ (22 in total), not included in the 2PIGG catalog, would add a contribution of only 4% to the ZENS satellite sample with similar properties. A similar fraction of order 4% applies for star-forming galaxies above the mass completeness threshold of $10^{9.2}\,M_{\odot}$. We therefore do not consider these extra galaxies in any of our analyses and we

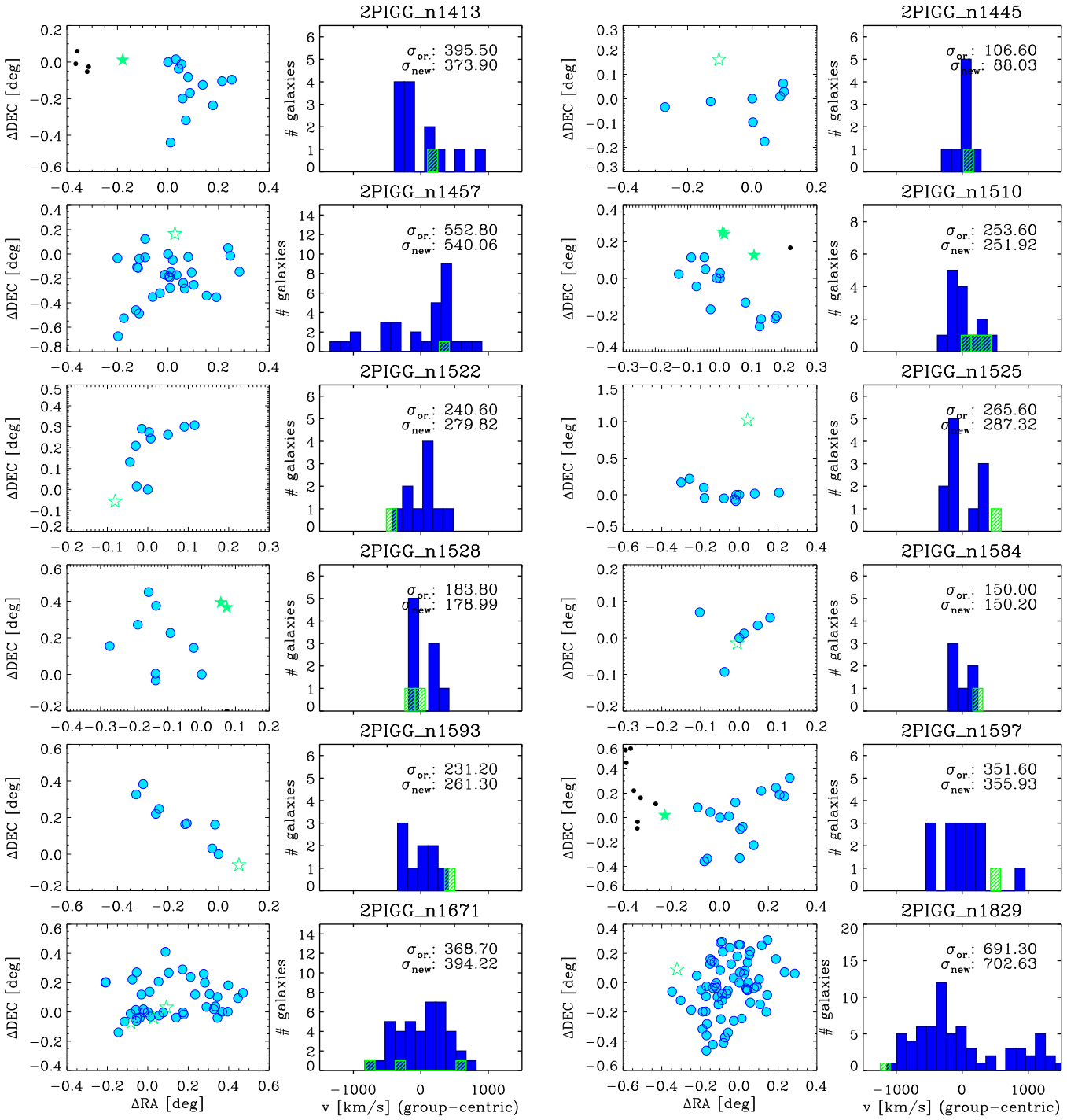

Figure 17. (Continued).

instead we adopt the nominal galaxy membership in the ZENS groups of the 2PIGG catalog.

APPENDIX C

TEST OF THE ROBUSTNESS OF THE FIDUCIAL LSS DENSITY ESTIMATES

As discussed in Section 3.3, we adopted a *N*th-nearest *group* neighbor algorithm to compute our fiducial LSS densities at the location of the ZENS fields. The volume-limited sample of 2PIGG *groups* used in the construction of the density field and the imposed minimum luminosity are plotted in Figure 19.

C.1. The Role of "Ungrouped" Galaxies

As explained in the main text, we investigated whether the fiducial LSS density values for the ZENS groups are significantly affected by the addition or removal of galaxies in the 2dFGRS that were not identified as members of any group in the 2PIGG catalog. The results of this investigation are shown in Figure 20. There is a good correlation between the two measurements of LSS density: in only ∼10% of the cases is the difference between the overdensities derived with and without the ungrouped galaxies larger than 0.5 dex.

We note that, as evident from the left panel of Figure 12, the exclusion of the "ungrouped" galaxies moves the peak of

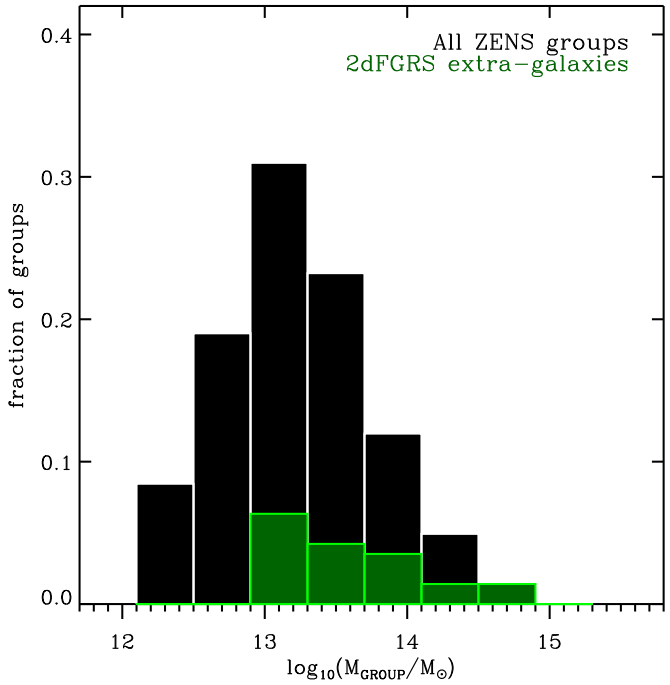

Figure 18. Green histogram shows the distribution of fiducial group masses for the 24 ZENS groups for which we have found, in the 2dFGRS catalog, galaxies that are consistent with being additional group members (according to the definition given in Section 3.1.1.1). For comparison, the black histogram shows the distribution of fiducial group masses for the entire ZENS sample. The green histogram is normalized to the total number of groups in the ZENS sample.

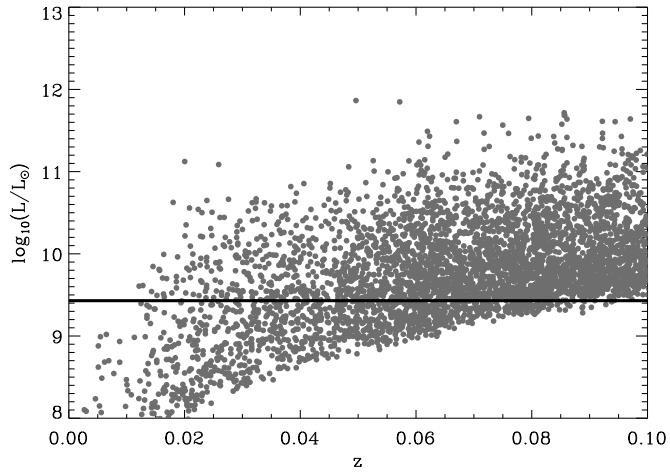

Figure 19. Luminosity of the 2PIGG groups and ungrouped galaxies used to derive the *N*th-group-neighbor LSS density field (see Section 3.3). The solid line shows the minimum group luminosity considered in the computation, i.e., $L = 10^{9.43}\ L_{\odot}$, corresponding to the total (i.e., integrated to zero) luminosity of $b_j = 19.1$ individual galaxies at $z = 0.07$. Densities at each group location are calculated considering all other groups in the 2PIGG catalog, plus the remaining ungrouped galaxies in the 2dFGRS, within a redshift range of $\Delta z = \pm 0.1$ from the given group. Only a tenth of the points are plotted for clarity.

the $\delta_{\rm LSS}$ distribution toward slightly lower values. This result is a consequence of a ∼40% increase in the typical distance to the fifth-nearest-neighbor when the "ungrouped" galaxies are excluded. As also emphasized in Section 3.3, this result is evidence that the "ungrouped" galaxies may not be isolated systems in void regions. For our purposes, the key point is that including or excluding these "ungrouped" galaxies does not alter

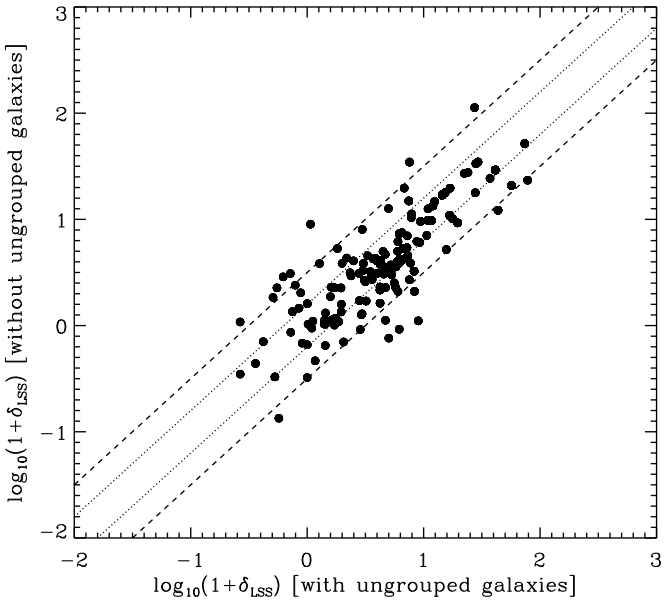

Figure 20. Comparison between the fiducial *N*th-group-neighbor LSS overdensities for the ZENS groups and those obtained by excluding the ungrouped galaxies in the 2dFGRS. The dotted and dashed lines highlight differences of 0.2 dex and 0.5 dex, respectively.

significantly either our LSS density measurements, or the trends with density that we investigate in our study.

C.2. A Comparison with Standard Nth-nearest Galaxy Neighbor Density Estimates

Many studies in the past several years have adopted a *N*th-nearest *galaxy* neighbor approach to derive an estimate for the LSS density field. In our case, we opted instead for the use of the groups as the density tracers, rather than the galaxies, to avoid the drawback of switching from a density within the groups, for groups with richness $>N$, to a density outside of the groups, for groups with richness $<N$. We highlight below this shortfall of the *N*th-nearest galaxy neighbor density field, which we also computed (but never used in our analyses, for the reason outlined above).

Similarly to what is customarily done (e.g., Gómez et al. 2003; Balogh et al. 2004; Baldry et al. 2006; Kovač et al. 2010a), we computed the *N*th-nearest *galaxy* field using a volume-limited sample of galaxies; in our case, with $M_{b_j} < -18.3 - z$ in the Vega system. This brightness limit corresponds to the absolute magnitude of a galaxy having $b_j = 19.1$ at the maximum redshift of the ZENS sample. This limit was chosen to ensure a uniform depth/completeness over the bulk of the ZENS groups (see Figure 16) and also provide an adequate number of tracers. Neighbor galaxies were searched within a velocity range of ± 1000 km s^{-1} centered at the given galaxy redshift; galaxies were weighted for spectroscopic incompleteness during the computation.

The distributions of typical distances to the *N*th-nearest galaxy neighbor, with $N = 3$, 5, or 10 are shown in the left panel of Figure 21. The distances to the third- and fifth-nearest galaxy neighbors peak at ∼0.5–1 Mpc, a separation that is comparable to the typical radius of many of the ZENS groups. This result is not surprising given that the ZENS groups have at least five members; at these distance scales, the *N*th-nearest galaxy neighbor density estimates mostly probe the variation of density within the groups themselves. Also, the

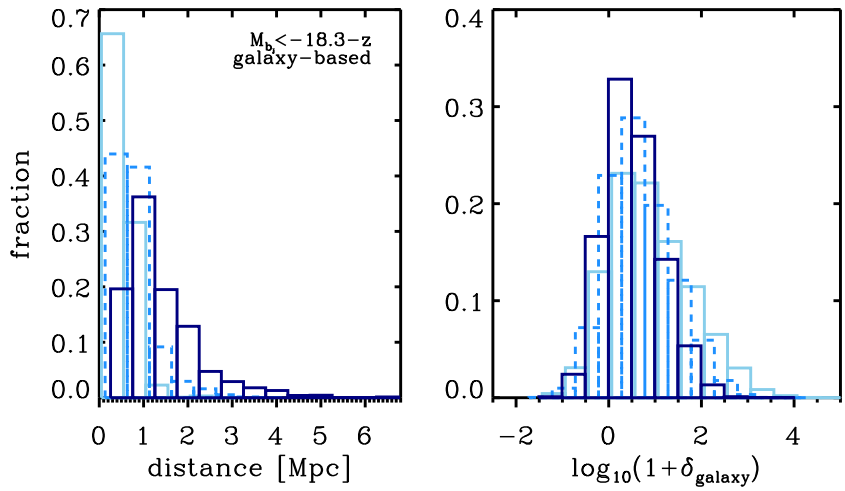

Figure 21. Distribution of distances (left) and densities (right) resulting from a third (solid light blue line), fifth (dashed blue line), and tenth (solid dark blue line) nearest *galaxy* neighbor computation of the LSS field. We stress that we do not use these density values in our analysis, since we prefer to adopt the fiducial LSS density estimates that are based on using the groups instead of the group member galaxies as tracers of the LSS density field.

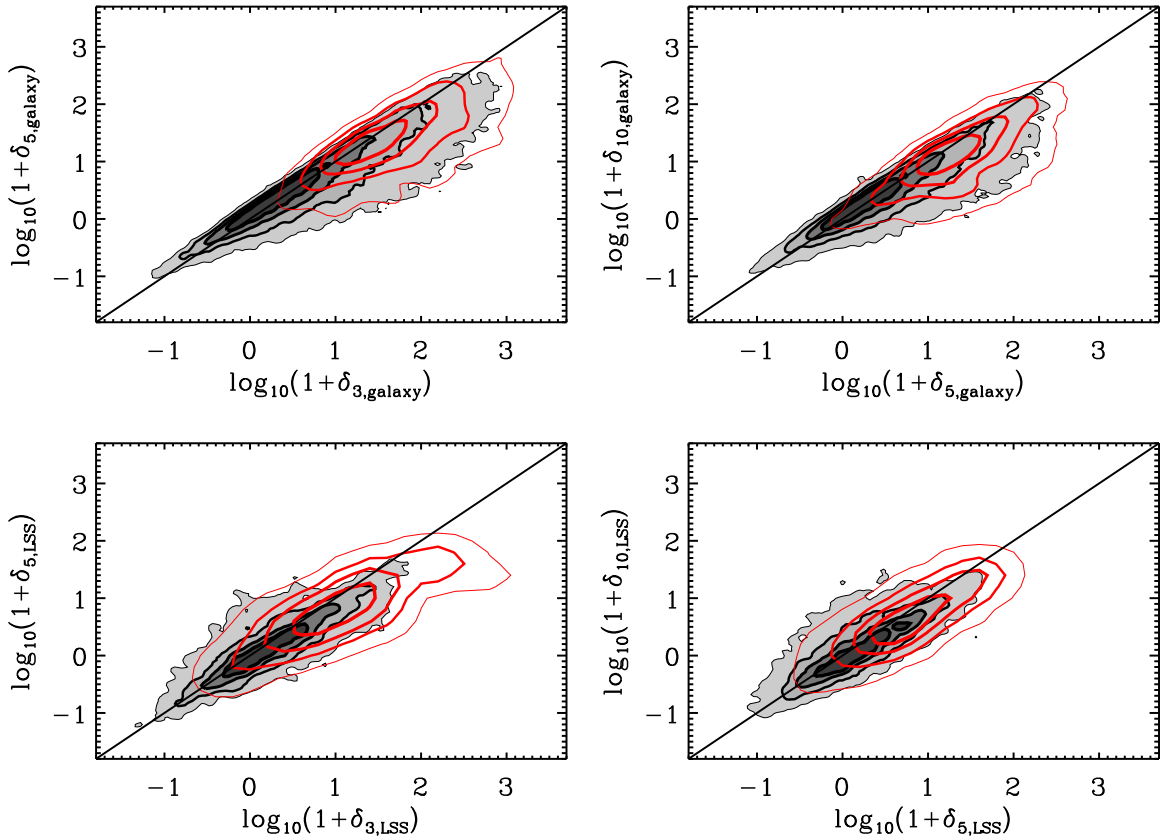

Figure 22. Top: comparison between the overdensities calculated using the distance to the third- (δ_3), fifth- (δ_5), or tenth- (δ_{10}) nearest *group* neighbor. The upper panels are for the density calculated using the volume-limited sample of galaxies from the 2dFGRS with $M_{b_j} < -18.3 - z$ as tracers; the lower panels show the densities obtained using the groups in the 2PIGG catalog with $L > 10^{9.43} L_{\odot}$ as tracers. The gray areas show the values for all the galaxies or groups in the 2dFGRS with $0.035 < z < 0.075$; the red contours show the ZENS sample.

10th-nearest galaxy neighbor densities, at high richness values, will probe the environment inside massive groups rather than being a genuine proxy for the LSS density field. We note that, given the luminosity limit discussed above to ensure a uniform completeness and depth, the density field that we calculate using the Nth-nearest galaxy neighbor density field uses a sub-sample of the 2PIGG galaxies (and hence a sub-sample of the galaxies used for the definition of the ZENS groups). Thus, also for the ZENS groups with five members, a partial contamination from interlopers is in principle possible when using the fifth-nearest galaxy neighbor approach. From the number of galaxies in the ZENS sample that are below the limit of $M_{b_j} < -18.3 - z$, we estimate this contamination to be about 20%–25%. The corresponding distributions of overdensities for the Nth-nearest galaxy neighbor realizations with $N = 3$, 5, or 10 are shown in the right panel of Figure 21. As discussed in the main text, and as a consequence of galaxy–galaxy "clustering" within the groups, a tail at high densities is observed, which is not present

Table 3
Median Properties of Galaxies in Relaxed and Unrelaxed Groups

Quantity	Relaxed	Unrelaxed
$9.3 < \log_{10}(M/M_\odot) < 10$		
Satellites		
$r_{1/2}$(kpc)	$3.28^{+0.17}_{-0.12}$	$3.29^{+0.15}_{-0.12}$
$\log_{10}$(sSFR yr^{-1})	$-10.25^{+0.07}_{-0.11}$	$-10.10^{+0.06}_{-0.08}$
$\log_{10}(\Sigma_{\rm SFR}\ M_\odot\ {\rm yr}^{-1}\ {\rm kpc}^{-2})$	$-2.59^{+0.07}_{-0.08}$	$-2.39^{+0.07}_{-0.06}$
$(B-I)$	$0.99^{+0.02}_{-0.02}$	$0.93^{+0.03}_{-0.02}$
$10 < \log_{10}(M/M_\odot) < 10.7$		
Satellites		
$r_{1/2}$(kpc)	$3.27^{+0.31}_{-0.11}$	$3.41^{+0.31}_{-0.13}$
$\log_{10}$(sSFR yr^{-1})	$-11.38^{+0.13}_{-0.26}$	$-11.01^{+0.12}_{-0.29}$
$\log_{10}(\Sigma_{\rm SFR}\ M_\odot\ {\rm yr}^{-1}\ {\rm kpc}^{-2})$	$-3.00^{+0.11}_{-0.22}$	$-2.63^{+0.12}_{-0.26}$
$(B-I)$	$1.31^{+0.01}_{-0.02}$	$1.30^{+0.01}_{-0.03}$
Centrals		
$r_{1/2}$(kpc)	$5.30^{+0.40}_{-0.32}$	$3.77^{+0.69}_{-0.25}$
$\log_{10}$(sSFR yr^{-1})	$-10.92^{+0.35}_{-0.83}$	$-11.16^{+0.32}_{-0.23}$
$\log_{10}(\Sigma_{\rm SFR}\ M_\odot\ {\rm yr}^{-1}\ {\rm kpc}^{-2})$	$-2.70^{+0.38}_{-0.59}$	$-2.66^{+0.20}_{-0.14}$
$(B-I)$	$1.24^{+0.04}_{-0.03}$	$1.28^{+0.03}_{-0.07}$

Notes. The table lists the median values derived from the histograms of Figure 14, for central and satellite galaxies in two bins of stellar mass, for relaxed and unrelaxed groups with $M_{\rm GROUP} < 10^{13.5}\ M_\odot$.

in our fiducial fifth-nearest *group* neighbor computation of the LSS density field.

C.3. The Negligible Impact of the Choice of N When Using Groups as Density Tracers

In Figure 22, we show the comparison between the LSS (over)densities calculated using the distances to *N*th-nearest galaxy or group neighbors. In particular, we compare the cases of $N = 3$, 5, and 10. The upper and lower panels show the densities calculated using the volume-limited sample of $M_{b_j} < -18.3 - z$ *galaxies* in the entire 2dFGRS catalog as tracers, and the densities obtained using the *groups* in the 2PIGG catalog with $L > 10^{9.43}\ L_\odot$ as tracers, respectively. The gray areas show the values for all the galaxies or groups in the 2dFGRS with $0.035 < z < 0.075$; the red contours show galaxies or groups in the ZENS sample. The ZENS galaxies and groups are slightly shifted toward higher density, reflecting the selection of our ZENS sample. The figure shows (again) that the density field traced by the *galaxies* shows an extended tail below the identity line at $\log(1+\delta) \sim 2$, which is the signature that galaxy-based densities obtained with small apertures tend to be biased by local density peaks within group halos. The figure also shows that our adopted LSS density estimates, that use the groups themselves as tracers of the LSS density field are less sensitive to the choice of "N" than estimates based on the *N*th-nearest individual galaxies.

APPENDIX D

MEDIAN PROPERTIES OF CENTRALS AND SATELLITES IN RELAXED AND UNRELAXED GROUPS

We discuss the classification of groups in dynamically "relaxed" and "unrelaxed" systems in Table 3.

APPENDIX E

THE README FILE OF THE ENCLOSED ZENS CATALOG

We list, for each galaxy in the sample, the structural and photometric measurements presented in Papers II and III and the environmental diagnostics discussed in this paper. Table 4 matches the *readme* file that accompanies the ZENS catalog, which we publish in this paper.

Table 4
The Readme File for the ZENS Catalog of Structural, Photometric, and Environmental Properties for the Sample Galaxies

Column	Format	Units	Label	Comments
1	a11	···	GroupID	Group identification (1)
2	a10	···	2dFID	Galaxy 2dFGRS identification
3	a17	···	ZENSID	Galaxy identification in ZENS
4	f7.5	···	groupz	Group redshift
5	f11.6	deg	RAdeg	Right Ascension in decimal degrees (J2000)
6	f11.6	deg	DEdeg	Declination in decimal degrees (J2000)
7	f7.5	···	galz	Galaxy 2dFGRS heliocentric redshift
8	f5.3	···	wComp	Galaxy completeness weight (2)
9	f5.3	Mpc	RmsRad	Group rms radius from 2PIGG catalog
10	f5.3	Mpc	R200	Group R_{200} radius (3)
11	f6.1	km s^{-1}	Sigma	Group velocity dispersion from 2PIGG catalog
12	e10.4	$L_\odot$	Lgroup	Group luminosity as in Eke et al. 2004
13	i3	···	Nmemb	Group richness from 2PIGG catalog
14	e10.4	$M_\odot$	Mgroup	Group mass $M_{\rm GROUP}$
15	f6.3	···	DeltaLSS	Large scale overdensity $\delta_{\rm LSS}$ (4)
16	i1	···	qLSS	Quartile large scale overdensity (5)
17	i1	···	relaxFlag	Group dynamical status (6)
18	i1	···	cenFlag	Flag identifying central galaxy and group center (7)
19	f6.3	R_{200}	dR200	Galaxy distance from group center in units of R200
20	e11.4	$M_\odot$	MassBest	Galaxy mass from ZEBRA+ best-fit template (8)
21	e11.4	$M_\odot$	erMassBest	Lower limit on MassBest (9)
22	e11.4	$M_\odot$	ErMassBest	Upper limit on MassBest (9)
23	e11.4	$M_\odot$	MassMedian	ZEBRA+ median likelihood galaxy mass
24	e11.4	$M_\odot$	MassP16	The 16th percent. of galaxy stellar mass likelihood distribution

Table 4
(Continued)

Column	Format	Units	Label	Comments
25	e11.4	$M_\odot$	MassP84	The 84th percent. of galaxy stellar mass likelihood distribution
26	e11.4	$M_\odot$	maxLMass	ZEBRA+ maximum likelihood galaxy mass
27	i3	···	MType	Morphological type (10)
28	i3	···	MergerFlag	Merger flag (11)
29	f6.2	···	nI	Galaxy GIM2D *I*-band raw Sérsic index from single Sérsic fit
30	f6.2	···	ernI	GIM2D formal 99% confidence lower error on nI
31	f6.2	···	ErnI	GIM2D formal 99% confidence upper error on nI
32	f6.2	···	nB	Galaxy GIM2D *B*-band raw Sérsic index from single Sérsic fit
33	f6.2	···	ernB	GIM2D formal 99% confidence lower error on nB
34	f6.2	···	ErnB	GIM2D formal 99% confidence upper error on nB
35	f6.2	···	nIcorr	Galaxy GIM2D *I*-band corrected Sérsic index from single Sérsic fit (12)
36	f6.2	···	nBcorr	Galaxy GIM2D *B*-band corrected Sérsic index from single Sérsic fit (12)
37	f7.3	kpc	gReI	Galaxy GIM2D *I*-band raw half-light radius from single Sérsic fit; semi-major axis
38	f7.3	kpc	ergReI	GIM2D formal 99% confidence lower error on gReI
39	f7.3	kpc	ErgReI	GIM2D formal 99% confidence upper error on gReI
40	f7.3	kpc	Delta-gReI	Single vs. double component scatter on *I*-band half-light semi-major axis (12)
41	f7.3	kpc	gReB	Galaxy GIM2D *B*-band raw half-light radius from single Sérsic fit; semi-major axis
42	f7.3	kpc	ergReB	GIM2D formal 99% confidence lower error on gReB
43	f7.3	kpc	ErgReB	GIM2D formal 99% confidence upper error on gReB
44	f7.3	kpc	Delta-gReB	Single vs. double component scatter on *B*-band half-light semi-major axis (12)
45	f7.3	kpc	gReIcorr	Galaxy GIM2D *I*-band corrected half-light radius from single Sérsic fit; semi-major axis (11)
46	f7.3	kpc	gReBcorr	Galaxy GIM2D *B*-band corrected half-light radius from single Sérsic fit; semi-major axis (11)
47	f7.3	···	gEllipI	Galaxy GIM2D *I*-band raw ellipticity from single Sérsic fit
48	f7.3	···	ergEllipI	GIM2D formal 99% confidence lower error on gEllipI
49	f7.3	···	ErgEllipI	GIM2D formal 99% confidence upper error on gEllipI
50	f7.3	···	gEllipB	Galaxy GIM2D *B*-band raw ellipticity from single Sérsic fit
51	f7.3	···	ergEllipB	GIM2D formal 99% confidence lower error on gEllipB
52	f7.3	···	ErgEllipB	GIM2D formal 99% confidence upper error on gEllipB
53	f7.3	···	gEllipIcorr	Galaxy GIM2D *I*-band corrected ellipticity from single Sérsic fit (12)
54	f7.3	···	gEllipBcorr	Galaxy GIM2D *B*-band corrected ellipticity from single Sérsic fit (12)
55	f7.3	kpc	diskhI-tot	Galaxy GIM2D *I*-band disk scale-length from pure exponential fit; semi-major axis (14)
56	f7.3	kpc	erdiskhI-tot	GIM2D formal 99% confidence lower error on diskhI-tot
57	f7.3	kpc	ErdiskhI-tot	GIM2D formal 99% confidence upper error on diskhI-tot
58	f7.3	kpc	diskhB-tot	Galaxy GIM2D *B*-band disk scale-length from pure exponential fit; semi-major axis (14)
59	f7.3	kpc	erdiskhB-tot	GIM2D formal 99% confidence lower error on diskhB-tot
60	f7.3	kpc	ErdiskhB-tot	GIM2D formal 99% confidence upper error on diskhB-tot
61	i3	···	tDecompI	GIM2D vs. Galfit Flag for *I*-band bulge+disk decomposition (15)
62	i3	···	tDecompB	GIM2D vs. Galfit Flag for *B*-band bulge+disk decomposition (15)
63	f8.4	···	BTI	*I*-band bulge-to-total ratio from bulge+disk decomposition (16)
64	f8.4	···	erBTI	Formal 99% confidence lower error on BTI
65	f8.4	···	ErBTI	Formal 99% confidence upper error on BTI
66	f8.4	···	BTB	*B*-band bulge-to-total ratio from bulge+disk decomposition (16)
67	f8.4	···	erBTB	Formal 99% confidence lower error on BTB
68	f8.4	···	ErBTB	Formal 99% confidence upper error on BTB
69	f7.3	kpc	bulgeRe-I	*I*-band bulge half-light radius from bulge+disk decomposition; semi-major axis (16)
70	f7.3	kpc	erbulgeRe-I	Formal 99% confidence lower error on bulgeRe-I
71	f7.3	kpc	ErbulgeRe-I	Formal 99% confidence upper error on bulgeRe-I
72	f7.3	kpc	bulgeRe-B	*B*-band bulge half-light radius from bulge+disk decomposition; semi-major axis (16)
73	f7.3	kpc	erbulgeRe-B	Formal 99% confidence lower error on bulgeRe-B
74	f7.3	kpc	ErbulgeRe-B	Formal 99% confidence upper error on bulgeRe-B
75	f7.3	kpc	diskh-I	*I*-band disk scale-length from bulge+disk decomposition; semi-major axis (16)
76	f7.3	kpc	erdiskh-I	Formal 99% confidence lower error on diskh-I
77	f7.3	kpc	Erdiskh-I	Formal 99% confidence upper error on diskh-I
78	f7.3	kpc	diskh-B	*B*-band disk scale-length from bulge+disk decomposition; semi-major axis (16)
79	f7.3	kpc	erdiskh-B	Formal 99% confidence lower error on diskh-B
80	f7.3	kpc	Erdiskh-B	Formal 99% confidence upper error on diskh-B
81	f7.3	···	nBulge-I	*I*-band bulge Sersic index from bulge+disk decomposition (16)
82	f7.3	···	ernBulge-I	Formal 99% confidence lower error on nBulge-I
83	f7.3	···	ErnBulge-I	Formal 99% confidence upper error on nBulge-I
84	f7.3	···	nBulge-B	*B*-band bulge Sersic index from bulge+disk decomposition (16)
85	f7.3	···	ernBulge-B	Formal 99% confidence lower error on nBulge-B
86	f7.3	···	ErnBulge-B	Formal 99% confidence upper error on nBulge-B
87	f7.3	···	ellBulge-I	*I*-band bulge ellipticity from bulge+disk decomposition (16)
88	f7.3	···	erellBulge-I	Formal 99% confidence lower error on ellBulge-I
89	f7.3	···	ErellBulge-I	Formal 99% confidence upper error on ellBulge-I
90	f7.3	···	ellBulge-B	*B*-band bulge ellipticity from bulge+disk decomposition (16)

Table 4
(Continued)

Column	Format	Units	Label	Comments
91	f7.3	···	erellBulge-B	Formal 99% confidence lower error on ellBulge-B
92	f7.3	···	ErellBulge-B	Formal 99% confidence upper error on ellBulge-B
93	f7.3	deg	diskInc-I	*I*-band disk inclination from bulge+disk decomposition (16)
94	f7.3	deg	erdiskInc-I	Formal 99% confidence lower error on diskInc-I
95	f7.3	deg	ErdiskInc-I	Formal 99% confidence upper error on diskInc-I
96	f7.3	deg	diskInc-B	*B*-band disk inclination from bulge+disk decomposition (16)
97	f7.3	deg	erdiskInc-B	Formal 99% confidence lower error on diskInc-B
98	f7.3	deg	ErdiskInc-B	Formal 99% confidence upper error on diskInc-B
99	f7.3	kpc	ReI-decomp	*I*-band global galaxy half-light radius from bulge+disk decomposition; semi-major axis (17)
100	f7.3	kpc	ReB-decomp	*B*-band global galaxy half-light radius from bulge+disk decomposition; semi-major axis (17)
101	f7.3	kpc	zReI	ZEST+ *I*-band raw half-light radius; semi-major axis
102	f7.3	kpc	zReB	ZEST+ *B*-band raw half-light radius; semi-major axis
103	f7.3	kpc	zReIcorr	ZEST+ *I*-band corrected half-light radius; semi-major axis (12)
104	f7.3	kpc	zReBcorr	ZEST+ *B*-band corrected half-light radius; semi-major axis (12)
105	f7.3	···	zEllipI	SExtractor/ZEST+ *I*-band raw ellipticity
106	f7.3	···	zEllipB	SExtractor/ZEST+ *B*-band raw ellipticity
107	f7.3	···	zEllipIcorr	SExtractor/ZEST+ *I*-band corrected ellipticity (12)
108	f7.3	···	zEllipBcorr	SExtractor/ZEST+ *B*-band corrected ellipticity (12)
109	f7.3	···	CI	ZEST+ *I*-band raw Concentration index
110	f7.3	···	CB	ZEST+ *B*-band raw Concentration index
111	f7.3	···	CIcorr	ZEST+ *I*-band corrected Concentration index (18)
112	f7.3	···	CBcorr	ZEST+ *B*-band corrected Concentration index (18)
113	f7.3	···	GiniI	ZEST+ *I*-band raw Gini index
114	f7.3	···	GiniB	ZEST+ *B*-band raw Gini index
115	f7.3	···	GiniIcorr	ZEST+ *I*-band corrected Gini index (18)
116	f7.3	···	GiniBcorr	ZEST+ *B*-band corrected Gini index (18)
117	f7.3	···	M20I	ZEST+ *I*-band raw M_{20} index
118	f7.3	···	M20B	ZEST+ *B*-band raw M_{20} index
119	f7.3	···	M20Icorr	ZEST+ *I*-band corrected M_{20} index (18)
120	f7.3	···	M20Bcorr	ZEST+ *B*-band corrected M_{20} index (18)
121	f8.4	···	AsymI	ZEST+ *I*-band raw asymmetry index
122	f8.4	···	AsymB	ZEST+ *B*-band raw asymmetry index
123	f8.4	···	SI	ZEST+ *I*-band raw smoothness index
124	f8.4	···	SB	ZEST+ *B*-band raw smoothness index
125	f7.3	kpc	RpI	SExtractor *I*-Band petrosian radius; semi-major axis (19)
126	f7.3	kpc	RpB	SExtractor *B*-Band petrosian radius; semi-major axis (19)
127	f7.3	kpc	RkI	SExtractor *I*-band Kron aperture; semi-major axis (20)
128	f7.3	kpc	RkB	SExtractor *B*-band Kron aperture; semi-major axis (20)
129	i3	···	BarType	Bar Flag (21)
130	f7.3	kpc	aBar	Bar semi-major axis
131	f6.2	···	fBar	Bar strength
132	i3	···	SpType	Spectral type (22)
133	i3	···	Dust-SBFlag	Dusty, star-forming or post starburst flag (23)
134	f8.4	$M_\odot$ yr^{-1}	SFRBest	Star-formation rate from ZEBRA+ best-fit template (24)
135	f8.4	$M_\odot$ yr^{-1}	erSFRBest	Lower limit on SFRBest (9)
136	f8.4	$M_\odot$ yr^{-1}	ErSFRBest	Upper limit on SFRBest (9)
137	f8.4	$M_\odot$ yr^{-1}	SFRMedian	ZEBRA+ median likelihood SFR
138	f8.4	$M_\odot$ yr^{-1}	SFRP16	The 16th percentile of the ZEBRA+ SFR likelihood distribution
139	f8.4	$M_\odot$ yr^{-1}	SFRP84	The 84th percentile of the ZEBRA+ SFR likelihood distribution
140	f8.4	$M_\odot$ yr^{-1}	maxLSFR	ZEBRA+ maximum likelihood SFR
141	e11.4	yr^{-1}	sSFRBest	Specific star-formation rate from ZEBRA+ best-fit template (24)
142	e11.4	yr^{-1}	ersSFRBest	Lower limit on sSFRBest (9)
143	e11.4	yr^{-1}	ErsSFRBest	Upper limit on sSFRBest (9)
144	e11.4	yr^{-1}	sSFRMedian	ZEBRA+ median likelihood specific star-formation rate
145	e11.4	yr^{-1}	sSFRP16	The 16th percentile of the ZEBRA+ sSFR likelihood distribution
146	e11.4	yr^{-1}	sSFRP84	The 84th percentile of the ZEBRA+ sSFR likelihood distribution
147	e11.4	yr^{-1}	maxLsSFR	ZEBRA+ maximum likelihood sSFR
148	f8.4	mag	kcorr-B	ZEBRA+ *B*-band k-correction
149	f8.4	mag	kcorr-I	ZEBRA+ *I*-band k-correction
150	f8.3	mag	oBmag	Galaxy Petrosian apparent *B*-band magnitude; observer-frame (25)
151	f8.3	mag	rBmag	Galaxy Petrosian apparent *B*-band magnitude; rest-frame (25)
152	f8.3	mag	errBmag	Error on rBmag
153	f8.3	mag	BMag	Absolute galaxy Petrosian *B*-band magnitude
154	f8.3	mag	oImag	Galaxy Petrosian apparent *I*-band magnitude; observer-frame (25)
155	f8.3	mag	rImag	Galaxy Petrosian apparent *I*-band magnitude; rest-frame (25)
156	f8.3	mag	errImag	Error on rImag

Table 4
(Continued)

Column	Format	Units	Label	Comments
157	f8.3	mag	IMag	Absolute galaxy Petrosian *I*-band magnitude
158	f8.3	mag	BmagKron	Galaxy Kron apparent *B*-band magnitude; rest-frame (26)
159	f8.3	mag	erBmagKron	Error on BmagKron
160	f8.3	mag	ImagKron	Galaxy Kron apparent *I*-band magnitude; rest-frame (26)
161	f8.3	mag	erImagKron	Error on ImagKron
162	f8.3	mag	$B-I$	Galaxy Petrosian rest-frame ($B-I$) color
163	f8.3	mag	bjmag	Galaxy 2dFGRS b_j Vega magnitude (27)
164	f8.3	mag	rFmag	Galaxy 2dFGRS/SCOS r_F Vega magnitude (27)
165	f8.3	mag	FUVmag	Galaxy apparent FUV magnitude; rest-frame (25,28)
166	f8.3	mag	erFUVmag	Error on FUVmag
167	f8.3	mag	NUVmag	Galaxy apparent NUV magnitude; rest-frame (25,28)
168	f8.3	mag	erNUVmag	Error on NUVmag
169	f8.3	mag	NUV-I	NUV-I color; rest-frame
170	f8.3	mag	NUV-B	NUV-B color; rest-frame
171	f8.3	mag	FUV-NUV	FUV-NUV color; rest-frame
172	f8.3	mag	umag	Galaxy apparent SDSS u magnitude; rest-frame (25,28)
173	f8.3	mag	erumag	Error on umag
174	f8.3	mag	gmag	Galaxy apparent SDSS g magnitude; rest-frame (25,28)
175	f8.3	mag	ergmag	Error on gmag
176	f8.3	mag	rmag	Galaxy apparent SDSS r-magnitude; rest-frame (25,28)
177	f8.3	mag	errmag	Error on rmag
178	f8.3	mag	imag	Galaxy apparent SDSS i-magnitude; rest-frame (25,28)
179	f8.3	mag	erimag	Error on imag
180	f8.3	mag	zmag	Galaxy apparent SDSS z-magnitude; rest-frame (25,28)
181	f8.3	mag	erzmag	Error on zmag
182	f8.3	mag	Jmag	Galaxy apparent 2MASS J-magnitude; rest-frame (25,28)
183	f8.3	mag	erJmag	Error on Jmag
184	f8.3	mag	Hmag	Galaxy apparent 2MASS H-magnitude; rest-frame (25,28)
185	f8.3	mag	erHmag	Error on Hmag
186	f8.3	mag	Kmag	Galaxy apparent 2MASS K-magnitude; rest-frame (25,28)
187	f8.3	mag	erKmag	Error on Kmag
188	f7.3	mag	BmagSer	Total galaxy *B*-band magnitude from GIM2D single Sérsic fit; rest-frame
189	f7.3	mag	erBmagSer	GIM2D formal 99% confidence lower error on BmagSer
190	f7.3	mag	ErBmagSer	GIM2D formal 99% confidence upper error on BmagSer
191	f7.3	mag	ImagSer	Total galaxy *I*-band magnitude from GIM2D single Sérsic fit; rest-frame
192	f7.3	mag	erImagSer	GIM2D formal 99% confidence lower error on ImagSer
193	f7.3	mag	ErImagSer	GIM2D formal 99% confidence upper error on ImagSer
194	f7.3	mag	BmagSercorr	Corrected total galaxy *B* mag from single Sérsic fit; rest-frame (12)
195	f7.3	mag	ImagSercorr	Corrected total galaxy *I* mag from single Sérsic fit; rest-frame (12)
196	f7.3	mag	BmagExp	Total galaxy *B*-band magnitude from GIM2D pure exponential fit; rest-frame
197	f7.3	mag	erBmagExp	GIM2D formal 99% confidence lower error on BmagExp
198	f7.3	mag	ErBmagExp	GIM2D formal 99% confidence upper error on BmagExp
199	f7.3	mag	ImagExp	Total galaxy *I*-band magnitude from GIM2D pure exponential fit; rest-frame
200	f7.3	mag	erImagExp	GIM2D formal 99% confidence lower error on ImagExp
201	f7.3	mag	ErImagExp	GIM2D formal 99% confidence upper error on ImagExp
202	f7.3	mag	oBmagBulge	Bulge *B*-band magnitude from bulge+disk decomposition; observer-frame
203	f7.3	mag	eroBmagBulge	Formal 99% confidence lower error on oBmagBulge (29)
204	f7.3	mag	EroBmagBulge	Formal 99% confidence upper error on oBmagBulge (29)
205	f7.3	mag	oImagBulge	Bulge *I*-band magnitude from bulge+disk decomposition; observer-frame
206	f7.3	mag	eroImagBulge	Formal 99% confidence lower error on oImagBulge (29)
207	f7.3	mag	EroImagBulge	Formal 99% confidence upper error on oImagBulge (29)
208	f7.3	mag	rBmagBulge	Bulge *B*-band magnitude from bulge+disk decomposition; rest-frame (30)
209	f7.3	mag	rImagBulge	Bulge *I*-band magnitude from bulge+disk decomposition; rest-frame (30)
210	f7.3	mag	oBmagDisk	Disk *B*-band magnitude from bulge+disk decomposition; observer-frame
211	f7.3	mag	eroBmagDisk	Formal 99% confidence lower error on oBmagDisk (29)
212	f7.3	mag	EroBmagDisk	Formal 99% confidence upper error on oBmagDisk (29)
213	f7.3	mag	oImagDisk	Disk *I*-band magnitude from bulge+disk decomposition; observer-frame
214	f7.3	mag	eroBmagIulge	Formal 99% confidence lower error on oImagDisk (29)
215	f7.3	mag	EroImagDisk	Formal 99% confidence upper error on oImagDisk (29)
216	f7.3	mag	rBmagDisk	Disk *B*-band magnitude from bulge+disk decomposition; rest-frame (30)
217	f7.3	mag	rImagDisk	Disk *I*-band magnitude from bulge+disk decomposition; rest-frame (30)
218	e11.4	$M_\odot$	BulgeMass	Bulge stellar mass (31)
219	e11.4	$M_\odot$	BulgeMassP16	The 16th percentile bulge mass (31)
220	e11.4	$M_\odot$	BulgeMassP84	The 84th percentile bulge mass (31)
221	e11.4	$M_\odot$	DiskMass	Disk stellar mass (31)
222	e11.4	$M_\odot$	DiskMassP16	The 16th percentile disk mass (31)

Table 4
(Continued)

Column	Format	Units	Label	Comments
223	e11.4	$M_\odot$	DiskMassP84	The 84th percentile disk mass (31)
224	f7.3	mag	d($B-I$)/dlogrVor	The ($B-I$) color gradient from Voronoi tessellated color maps
225	f7.3	mag	erd($B-I$)/dlogrVor	Error on ($B-I$)gradVor
226	f7.3	mag	corr_d($B-I$)/dlogrVor	Corrected ($B-I$) color gradient from Voronoi tessellated color maps (32)
227	f7.3	mag	($B-I$)ReVor	The ($B-I$) color at half-light radius from Voronoi tessellated color maps; rest-frame
228	f7.3	mag	er($B-I$)ReVor	Error on ($B-I$)ReVor (33)
229	f7.3	mag	corr($B-I$)ReVor	Corrected ($B-I$) color at $r_{1/2}$ from Voronoi color maps; rest-frame (32)
230	f7.3	mag	($B-I$)rms	Dispersion around best fit color profile from Voronoi color maps
231	f7.3	mag	d($B-I$)/dlogrGim	The ($B-I$) color gradient from GIM2D best fits
232	f7.3	mag	erd($B-I$)/dlogrGim	Error on ($B-I$)gradGim
233	f7.3	mag	($B-I$)ReGim	The ($B-I$) color at half-light radius from GIM2D best fits; rest-frame
234	f7.3	mag	er($B-I$)ReGim	Error on ($B-I$)ReGim (34)
235	e11.4	$M_\odot$	FlagBadSFR	Flag for ZEBRA+ template limited to a star-forming model (35)
236	i3	···	cFlag	Contamination flag (36)
237	f7.3	mag	BmagKroncorr	Corrected galaxy Kron B-band magnitude; rest-frame (18)
238	f7.3	mag	ImagKroncorr	Corrected galaxy Kron I-band magnitude; rest-frame (18)
239	f6.3	···	zCompl	2dFGRS redshift completeness at galaxy position (37)
240	f6.3	mag	dFmagLim	Extinction corrected magnitude limit of 2dFGRS at galaxy position (37)
241	f6.3	···	muVal	2dFGRS completeness μ factor at galaxy position (37)
242	i1	···	PIGGCen	Original 2PIGG central galaxy flag (38)
243	f7.3	deg	diskInc-tot-I	I-band disk inclination from pure exponential fit
244	f7.3	deg	erdiskInc-tot-I	Formal 99% confidence lower error on diskInc-tot-I
245	f7.3	deg	ErdiskInc-tot-I	Formal 99% confidence upper error on diskInc-tot-I
246	f7.3	deg	diskInc-tot-B	B-band disk inclination from pure exponential fit
247	f7.3	deg	erdiskInc-tot-B	Formal 99% confidence lower error on diskInc-tot-B
248	f7.3	deg	ErdiskInc-tot-B	Formal 99% confidence upper error on diskInc-tot-B
249	i3	···	GalfitDev	Flag indicating deviations between GIM2D and GALFIT parameters (39)
250	f5.1	···	SpecClass	Flag indicating type of galaxy spectrum (40)

Notes. Note 1: Projected sizes are converted into physical units assuming the following cosmological parameters: $h = 0.7$, $\Omega_m = 0.3$, $\Omega_\Lambda = 0.7$. Parameters that are not available are listed as: −99 entries for definite positive parameters and +99 for definite negative parameters. For merging galaxy pairs, we list parameters for both the primary and secondary galaxy, when available. Unless otherwise specified, all magnitudes and colors are in the AB system. For galaxies outside the WFI field of view, all galactic parameters, except stellar masses, are given as −99 entries.
Note 2: Galaxy weight accounting for 2dFGRS redshift incompleteness, calculated as described in Appendix A.
Note 3: R_{200} radius derived from the group mass (see text).
Note 4: Defined as $\log(1+\delta_{\rm LSS})$, where $\delta_{\rm LSS}$ is calculated to the fifth-nearest 2PIGG *group* (see text).
Note 5: 1 = group located in first quartile of the distribution of $\log(1+\delta_{\rm LSS})$; 2 = second quartile; 3 = third quartile; 4 = fourth quartile.
Note 6: 0 = relaxed, nominal best-fit most massive galaxy is identified as "central" (and group center); 1 = relaxed, a central galaxy satisfying criteria of Section 3.2.1 is identified, but it is not the nominal best-fit most massive galaxy; 2 = unrelaxed, no galaxy in the group satisfies the criteria of Section 3.2.1 to be a central, but nevertheless the nominal best-fit most massive galaxy is labeled as "central" and used as the group center.
Note 7: 0 = satellite, 1 = central, 2 = central if considering only galaxies with WFI B- and I-band imaging.
Note 8: For galaxies outside the WFI field of view, the masses are inferred from the mass vs. r_F magnitude relation as described in the text.
Note 9: Lower and upper limits corresponding to an increase of 50% of the best-fit χ^2, derived from the distribution of χ^2 for all templates used in the ZEBRA+ SED fitting.
Note 10: 0 = elliptical, 1 = S0, 2 = bulge-dominated spiral, 3 = intermediate disk, 4 = late-type disk, 5 = irregular.
Note 11: 0 = not merging; 1 = plausible merger, no spectroscopic or photo-z confirmation; 1.5 = same as flag 1, but visible tidal tails; 2 = merger, spectroscopic or photo-z confirmation; 3 = close pair among group members; 4 = disturbed morphology. Close pairs are identified as those galaxies that have a velocity difference with respect to another group member of $\Delta v < 500$ km s^{-1} and lie at a projected distance from the same member, $D_{\rm max} \leqslant 48\farcs368$ (equal to the maximum separation between merging galaxies type = 1 or type = 2. This distance is about 50 kpc at the typical ZENS redshift).
Note 12: The parameter is corrected for observational biases, as described in Paper II.
Note 13: Together with the formal GIM2D errors, we also provide an additional error that is obtained by the half difference between the single- and double-component half-light radii.
Note 14: Disk scale length from pure exponential GIM2D fit for the entire galaxy. This scale length is only available for late-type disks (Mtype = 4).
Note 15: GIM2D failed to provide some decompositions, which were successfully re-computed using GALFIT. For the I-band: 0 = GIM2D, 1 = GALFIT. For the B-band: 0 = GIM2D unconstrained; 1 = GALFIT; 2 = average of GIM2D unconstrained and GIM2D with ellipticity/position angle (PA) fixed to the I-band; 3 = GIM2D with ellipticity/PA fixed to the I-band; 4 = GIM2D with ellipticity/PA/bulge parameters fixed to the I-band; 5 = GIM2D with ellipticity/PA/bulge/disk parameters fixed to the I-band.
Note 16: −99 if no reliable decomposition is available; −98 if galaxy has a late-type morphology and is described by a single-component Sérsic fit with $n < 1.5$. No bulge+disk decomposition is performed on galaxies classified as ellipticals, however we set bulge-to-total ratio (B/T) = 1 in this catalog for this morphological type. All other bulge and disk parameters are set to −99 for elliptical galaxies.
Note 17: Obtained by integration to infinity of the bulge+disk surface brightness profiles.
Note 18: Non-parametric structural index corrected for PSF and observational biases, as described in Paper II.
Note 19: Actual Petrosian radius, not the default SExtractor Petrosian aperture, which is 2.5 the Petrosian radius.
Note 20: Default SExtractor Kron aperture equal to 2.5 times $R_{\rm Kron}$.
Note 21: 0 = not barred, 1 = barred.

Table 4
(Continued)

Note 22: 0 = quenched, 1 = moderately star-forming, 2 = strongly star-forming.
Note 23: 0 = the galaxy satisfies color–color and spectral criteria; 1 = the galaxy has an actively star-forming spectrum but has red optical–UV colors; 2 = the galaxy has a quenched spectrum but has blue optical–UV colors and strong H_δ absorption; 3 = the galaxy has a quenched spectrum, has blue optical–UV colors but no strong H_δ absorption (see Paper III for details).
Note 24: The sSFR for galaxies for which the best-fit SED results in a SFR $< 10^{-4}\ M_\odot\ \mathrm{yr}^{-1}$ is set equal to sSFR $= 10^{-14}\ \mathrm{yr}^{-1}$. Likewise, for SFR $< 10^{-4}\ M_\odot\ \mathrm{yr}^{-1}$, these values are set to SFR $= 10^{-4}\ M_\odot\ \mathrm{yr}^{-1}$.
Note 25: Magnitude computed in an elliptical aperture equal to two times the largest Petrosian radius in either the *B* and *I* band. These data are used in the derivation of stellar masses.
Note 26: SExtractor MAG_AUTO.
Note 27: Original b_j and r_F magnitudes, as released by the 2dFGRS team. The b_j magnitude is corrected for Galactic extinction, but is not in the rest frame. The r_F in not corrected for galactic extinction and is not in the rest frame. Both the r_F and b_j magnitudes are in the Vega system.
Note 28: 999 = undetected, −99 = not available.
Note 29: Sum in quadrature of the magnitude errors deriving from the formal GIM2D uncertainty on the flux and the bulge-to-total ratio. Bulge lower magnitude errors are set to 99 if erBT = 0. Disk upper magnitude errors are set to 99 if ErBT = 1.
Note 30: For the bulge and disk components, the *k*-corrections are obtained from the observed colors and the relation between the *k*-correction and color as derived for the entire galaxies (see Paper III).
Note 31: −99 if no reliable B+D decompositions are available in both the *B* and *I* bands or the color cannot be reproduced by a synthetic spectral library.
Note 32: Color gradients and color at the half-light radius corrected for observational biases, as described in Paper III.
Note 33: This error reflects the signal-to-noise ratio obtained in the Voronoi bins at the galaxy half-light radius. It is set to 99 if the tessellated map does not reach the half-light radius.
Note 34: Quadratic sum of the *B*- and *I*-band surface brightness errors on a single pixel at the galaxy half-light radius. It is set to 99 if surface brightness in one of the two bands is below the rms value of the sky.
Note 35: For a few galaxies classified as moderately or strongly star-forming from their spectral features or location on the NUV–optical color–color diagram, the unconstrained ZEBRA+ fits give inconsistently low SFR and sSFR values. For these galaxies, ZEBRA+ was re-run imposing a star-forming template model. The flag in this column identifies such galaxies and is set equal to the "incorrect" galaxy stellar mass from the unconstrained ZEBRA+ fits for the re-fitted galaxies and to −99 for all other galaxies (see Paper III for details).
Note 36: 0 = no bright star/companion within Petrosian radius; 1 = galaxy lies close to a bright star, the parameters for this galaxy may be subject to large uncertainties; 2 = companion within the galaxy Petrosian radius; 3 = bright clump/star clusters within Petrosian radius.
Note 37: These parameters are used to calculate the magnitude- and position-dependent 2dFGRS redshift completeness at the ZENS galaxy positions. See Section 8 of Colless et al. (2001) and Appendix A.
Note 38: This flag is equal to 1 if the given galaxy corresponds to the original 2PIGG group center, and otherwise equal to 0. For merging pairs/triplets, which have a single entry in the 2PIGG catalog, the flag is set equal for all merger members.
Note 39: 0 = GIM2D and GALFIT *I*-band parameters agree within a factor of two; 1 = at least one parameter differs more than a factor of two between the GIM2D and GALFIT *I*-band fits; −99 = if either the GALFIT or GIM2D decomposition is not reliable/available (see Paper II).
Note 40: The spectroscopic flag used, together with the color criteria described in Paper III, to classify galaxies as strongly star-forming, moderately star forming, and quenched systems (see also Figure 4 of Paper III). Specifically, 1 = no emission lines (in particular Hα and Hβ); 2 = Hα and [O III] or [O II] in emission, but no Hβ ; 3 = strong emission in Hα, Hβ, [O II] and [O III]. The flag is negative (from −1 to −3) if the spectrum is probing only the galaxy central region (i.e., a "nuclear spectrum").

(This table is also available in a machine-readable form in the online journal.)

REFERENCES

Abazajian, K. N., Adelman-McCarthy, J. K., Agüeros, M. A., et al. 2009, ApJS, 182, 543
Arnouts, S., Walcher, C. J., Le Fèvre, O., et al. 2007, A&A, 476, 137
Baldry, I. K., Balogh, M. L., Bower, R. G., et al. 2006, MNRAS, 373, 469
Balogh, M., Eke, V., Miller, C., et al. 2004, MNRAS, 348, 1355
Balogh, M. L., & Morris, S. L. 2000, MNRAS, 318, 703
Balogh, M. L., Morris, S. L., Yee, H. K. C., Carlberg, R. G., & Ellingson, E. 1999, ApJ, 527, 54
Behroozi, P. S., Conroy, C., & Wechsler, R. H. 2010, ApJ, 717, 379
Behroozi, P. S., Wechsler, R. H., & Conroy, C. 2013, ApJL, 762, L31
Berlind, A. A., Frieman, J., Weinberg, D. H., et al. 2006, ApJS, 167, 1
Blanton, M. R., Eisenstein, D., Hogg, D. W., Schlegel, D. J., & Brinkmann, J. 2005, ApJ, 629, 143
Bolzonella, M., Kovač, K., Pozzetti, L., et al. 2010, A&A, 524, A76
Brinchmann, J., & Ellis, R. S. 2000, ApJL, 536, L77
Bundy, K., Ellis, R. S., Conselice, C. J., et al. 2006, ApJ, 651, 120
Bundy, K., Scarlata, C., Carollo, C. M., et al. 2010, ApJ, 719, 1969
Calvi, R., Poggianti, B. M., Fasano, G., & Vulcani, B. 2012, MNRAS, 419, L14
Calvi, R., Poggianti, B. M., & Vulcani, B. 2011, MNRAS, 416, 727
Carollo, C. M. 1999, ApJ, 523, 566
Carollo, C. M., & Danziger, I. J. 1994, MNRAS, 270, 523
Carollo, C. M., Danziger, I. J., & Buson, L. 1993, MNRAS, 265, 553
Carollo, C. M., Franx, M., Illingworth, G. D., & Forbes, D. A. 1997, ApJ, 481, 710
Carollo, C. M., Scarlata, C., Stiavelli, M., Wyse, R. F. G., & Mayer, L. 2007, ApJ, 658, 960
Carollo, C. M., Stiavelli, M., & Mack, J. 1998, AJ, 116, 68
Chary, R., & Elbaz, D. 2001, ApJ, 556, 562
Cibinel, A., Carollo, C. M., Lilly, S. J., et al. 2013a, ApJ, in press (arXiv:1206.6108) (Paper II)
Cibinel, A., Carollo, C. M., Lilly, S. J., et al. 2013b, ApJ, in press (arXiv:1206.6496) (Paper III)
Cole, S., Percival, W. J., Peacock, J. A., et al. 2005, MNRAS, 362, 505
Colless, M., Dalton, G., Maddox, S., et al. 2001, MNRAS, 328, 1039
Cooper, M. C., Coil, A. L., Gerke, B. F., et al. 2010, MNRAS, 409, 337
Cooper, M. C., Griffith, R. L., Newman, J. A., et al. 2012, MNRAS, 419, 3018
Cooper, M. C., Newman, J. A., Madgwick, D. S., et al. 2005, ApJ, 634, 833
Croton, D. J., Farrar, G. R., Norberg, P., et al. 2005, MNRAS, 356, 1155
Croton, D. J., Springel, V., White, S. D. M., et al. 2006, MNRAS, 365, 11
De Lucia, G., & Blaizot, J. 2007, MNRAS, 375, 2
De Lucia, G., Weinmann, S., Poggianti, B. M., Aragón-Salamanca, A., & Zaritsky, D. 2012, MNRAS, 423, 1277
Di Matteo, P., Combes, F., Melchior, A.-L., & Semelin, B. 2007, A&A, 468, 61
Dressler, A. 1980, ApJ, 236, 351
Dressler, A., & Shectman, S. A. 1988, AJ, 95, 985
Eke, V. R., Baugh, C. M., Cole, S., et al. 2004a, MNRAS, 348, 866
Eke, V. R., Frenk, C. S., Baugh, C. M., et al. 2004b, MNRAS, 355, 769
Faber, S. M., Willmer, C. N. A., Wolf, C., et al. 2007, ApJ, 665, 265
Feldmann, R., Carollo, C. M., & Mayer, L. 2011, ApJ, 736, 88
Feldmann, R., Carollo, C. M., Mayer, L., et al. 2010, ApJ, 709, 218
Feldmann, R., Carollo, C. M., Porciani, C., et al. 2006, MNRAS, 372, 565

Font, A. S., Bower, R. G., McCarthy, I. G., et al. 2008, MNRAS, 389, 1619
Genzel, R., Lutz, D., Sturm, E., et al. 1998, ApJ, 498, 579
Gerke, B. F., Newman, J. A., Davis, M., et al. 2005, ApJ, 625, 6
Gerke, B. F., Newman, J. A., Davis, M., et al. 2012, ApJ, 751, 50
Giodini, S., Pierini, D., Finoguenov, A., et al. 2009, ApJ, 703, 982
Gómez, P. L., Nichol, R. C., Miller, C. J., et al. 2003, ApJ, 584, 210
Goto, T., Yamauchi, C., Fujita, Y., et al. 2003, MNRAS, 346, 601
Gunn, J. E., & Gott, J. R., III. 1972, ApJ, 176, 1
Guo, Y., McIntosh, D. H., Mo, H. J., et al. 2009, MNRAS, 398, 1129
Haas, M. R., Schaye, J., & Jeeson-Daniel, A. 2012, MNRAS, 419, 2133
Hambly, N. C., MacGillivray, H. T., Read, M. A., et al. 2001, MNRAS, 326, 1279
Hansen, S. M., Sheldon, E. S., Wechsler, R. H., & Koester, B. P. 2009, ApJ, 699, 1333
Harrison, C. D., Miller, C. J., Richards, J. W., et al. 2012, ApJ, 752, 12
Hogg, D. W., Blanton, M. R., Eisenstein, D. J., et al. 2003, ApJL, 585, L5
Hopkins, P. F., Hernquist, L., Cox, T. J., & Kereš, D. 2008, ApJS, 175, 356
Huchra, J. P., & Geller, M. J. 1982, ApJ, 257, 423
Jones, L. R., Ponman, T. J., Horton, A., et al. 2003, MNRAS, 343, 627
Kauffmann, G., Heckman, T. M., White, S. D. M., et al. 2003, MNRAS, 341, 33
Kewley, L. J., Geller, M. J., & Barton, E. J. 2006, AJ, 131, 2004
Khosroshahi, H. G., Jones, L. R., & Ponman, T. J. 2004, MNRAS, 349, 1240
Kimm, T., Somerville, R. S., Yi, S. K., et al. 2009, MNRAS, 394, 1131
Knobel, C., Lilly, S. J., Iovino, A., et al. 2009, ApJ, 697, 1842
Kovač, K., Lilly, S. J., Cucciati, O., et al. 2010a, ApJ, 708, 505
Kovač, K., Lilly, S. J., Knobel, C., et al. 2010b, ApJ, 718, 86
Labbé, I., Huang, J., Franx, M., et al. 2005, ApJL, 624, L81
Larson, R. 1980, ApJ, 237, 692
Leauthaud, A., George, M. R., Behroozi, P. S., et al. 2012, ApJ, 746, 95
Lee, B. C., Allam, S. S., Tucker, D. L., et al. 2004, AJ, 127, 1811
Lemson, G., & Virgo Consortium, t. 2006, arXiv:astro-ph/0608019
Lilly, S. J., Le Fevre, O., Hammer, F., & Crampton, D. 1996, ApJL, 460, L1
Madau, P., Ferguson, H. C., Dickinson, M. E., et al. 1996, MNRAS, 283, 1388
Maddox, S. J., Efstathiou, G., Sutherland, W. J., & Loveday, J. 1990, MNRAS, 243, 692
Marinoni, C., Davis, M., Newman, J. A., & Coil, A. L. 2002, ApJ, 580, 122
Masters, K. L., Mosleh, M., Romer, A. K., et al. 2010, MNRAS, 405, 783
McConnachie, A. W., Patton, D. R., Ellison, S. L., & Simard, L. 2009, MNRAS, 395, 255
Merchán, M., & Zandivarez, A. 2002, MNRAS, 335, 216
Muldrew, S. I., Croton, D. J., Skibba, R. A., et al. 2012, MNRAS, 419, 2670
Navarro, J. F., Frenk, C. S., & White, S. D. M. 1997, ApJ, 490, 493
Norberg, P., Cole, S., Baugh, C. M., et al. 2002, MNRAS, 336, 907
Oemler, A., Jr. 1974, ApJ, 194, 1
Oesch, P. A., Carollo, C. M., Feldmann, R., et al. 2010, ApJL, 714, L47
Park, C., Choi, Y.-Y., Vogeley, M. S., et al. 2007, ApJ, 658, 898
Peng, Y.-j., Lilly, S. J., Kovač, K., et al. 2010, ApJ, 721, 193
Peng, Y.-j., Lilly, S. J., Renzini, A., & Carollo, M. 2012, ApJ, 757, 4
Ponman, T. J., Allan, D. J., Jones, L. R., et al. 1994, Natur, 369, 462
Postman, M., & Geller, M. J. 1984, ApJ, 281, 95
Pozzetti, L., Bolzonella, M., Zucca, E., et al. 2010, A&A, 523, A13
Raichoor, A., Mei, S., Stanford, S. A., et al. 2012, ApJ, 745, 130
Rasmussen, J., Bai, X.-N., Mulchaey, J. S., et al. 2012, ApJ, 747, 31
Rasmussen, J., Ponman, T. J., & Mulchaey, J. S. 2006, MNRAS, 370, 453
Rasmussen, J., Ponman, T. J., Verdes-Montenegro, L., Yun, M. S., & Borthakur, S. 2008, MNRAS, 388, 1245
Robotham, A. S. G., Norberg, P., Driver, S. P., et al. 2011, MNRAS, 416, 2640
Rodighiero, G., Vaccari, M., Franceschini, A., et al. 2010, A&A, 515, A8
Romano-Díaz, E., & van de Weygaert, R. 2007, MNRAS, 382, 2
Romer, A. K., Nichol, R. C., Holden, B. P., et al. 2000, ApJS, 126, 209
Scarlata, C., Carollo, C. M., Lilly, S., et al. 2007, ApJS, 172, 406
Schaap, W. E., & van de Weygaert, R. 2000, A&A, 363, L29
Silverman, J. D., Kampczyk, P., Jahnke, K., et al. 2011, ApJ, 743, 2
Simha, V., Weinberg, D. H., Davé, R., et al. 2009, MNRAS, 399, 650
Skibba, R. A. 2009, MNRAS, 392, 1467
Skibba, R. A., Masters, K. L., Nichol, R. C., et al. 2012, MNRAS, 423, 1485
Skibba, R. A., van den Bosch, F. C., Yang, X., et al. 2011, MNRAS, 410, 417
Skrutskie, M. L., Cutri, R. M., Stiening, R., et al. 2006, AJ, 131, 1163
Smith, B. J., Struck, C., Hancock, M., et al. 2007, AJ, 133, 791
Somerville, R. S., & Primack, J. R. 1999, MNRAS, 310, 1087
Springel, V., & Hernquist, L. 2005, ApJL, 622, L9
Springel, V., White, S. D. M., Jenkins, A., et al. 2005b, Natur, 435, 629
Strateva, I., Ivezić, Ž., Knapp, G. R., et al. 2001, AJ, 122, 1861
Tago, E., Einasto, J., Saar, E., et al. 2008, A&A, 479, 927
Tago, E., Saar, E., Tempel, E., et al. 2010, A&A, 514, A102
Tempel, E., Tago, E., & Liivamägi, L. J. 2012, A&A, 540, A106
van den Bosch, F. C., Aquino, D., Yang, X., et al. 2008, MNRAS, 387, 79
van den Bosch, F. C., Yang, X., Mo, H. J., et al. 2007, MNRAS, 376, 841
Weinmann, S. M., Kauffmann, G., van den Bosch, F. C., et al. 2009, MNRAS, 394, 1213
Weinmann, S. M., van den Bosch, F. C., Yang, X., & Mo, H. J. 2006b, MNRAS, 366, 2
Wetzel, A. R., Tinker, J. L., & Conroy, C. 2012, MNRAS, 424, 232
Williams, R. J., Quadri, R. F., Franx, M., van Dokkum, P., & Labbé, I. 2009, ApJ, 691, 1879
Wilman, D. J., Zibetti, S., & Budavári, T. 2010, MNRAS, 406, 1701
Wolf, C., Aragón-Salamanca, A., Balogh, M., et al. 2009, MNRAS, 393, 1302
Woo, J., Dekel, A., Faber, S. M., et al. 2013, MNRAS, 428, 3306
Yang, X., Mo, H. J., & van den Bosch, F. C. 2008, ApJ, 676, 248
Yang, X., Mo, H. J., van den Bosch, F. C., & Jing, Y. P. 2005, MNRAS, 356, 1293
Yang, X., Mo, H. J., van den Bosch, F. C., et al. 2007, ApJ, 671, 153
York, D. G., Adelman, J., Anderson, J. E., Jr., et al. 2000, AJ, 120, 1579
Zehavi, I., Blanton, M. R., Frieman, J. A., et al. 2002, ApJ, 571, 172